REPORT DOCUMENTATION PAGE

Form Approved OMB NO. 0704-0188

1. REPORT DATE (DD-MM-YYYY)	2. REPORT TYPE	3. DATES COVERED (From - To)
13-11-2009	Final Report	1-Sep-2008 - 31-May-2009

4. TITLE AND SUBTITLE
Advanced Physiological Estimation of Cognitive Status (APECS) Final Report

5a. CONTRACT NUMBER

5b. GRANT NUMBER
W911NF-08-C-0121

5c. PROGRAM ELEMENT NUMBER
8620AQ

6. AUTHORS
Leonard J. Trejo, Roman Rosipal, and Paul L. Nunez

5d. PROJECT NUMBER

5e. TASK NUMBER

5f. WORK UNIT NUMBER

7. PERFORMING ORGANIZATION NAMES AND ADDRESSES
Pacific Development and Technology LLC
999 Commercial St.
Palo Alto, CA 94303 -

8. PERFORMING ORGANIZATION REPORT NUMBER

9. SPONSORING/MONITORING AGENCY NAME(S) AND ADDRESS(ES)
U.S. Army Research Office
P.O. Box 12211
Research Triangle Park, NC 27709-2211

10. SPONSOR/MONITOR'S ACRONYM(S)
ARO

11. SPONSOR/MONITOR'S REPORT NUMBER(S)
55044-LS-II.2

12. DISTRIBUTION AVAILIBILITY STATEMENT
Approved for Public Release; Distribution Unlimited

13. SUPPLEMENTARY NOTES
The views, opinions and/or findings contained in this report are those of the author(s) and should not contrued as an official Department of the Army position, policy or decision, unless so designated by other documentation.

14. ABSTRACT
EEG (electroencephalogram) recorded in human participants as they performed tasks that induced different mental states, including engagement, mental workload, and mental fatigue. We tested two types of atomic decomposition, each of which identifies unique EEG sources simultaneously in three dimensions: 1) atoms with dimensions of power spectral density, space (electrode position), and time (time on task or task conditions), or 2) atoms with dimensions of magnitude squared coherence, spatial relationships (electrode pairs), and time. For tasks that induced

15. SUBJECT TERMS
mental state estimation, mental workload, mental fatigue, EEG, atomic decomposition, multiway analysis

16. SECURITY CLASSIFICATION OF:			17. LIMITATION OF ABSTRACT	15. NUMBER OF PAGES	19a. NAME OF RESPONSIBLE PERSON
a. REPORT	b. ABSTRACT	c. THIS PAGE			Leonard Trejo
UU	UU	UU	UU		19b. TELEPHONE NUMBER: 650-248-3318

Report Title

Advanced Physiological Estimation of Cognitive Status (APECS) Final Report

ABSTRACT

EEG (electroencephalogram) recorded in human participants as they performed tasks that induced different mental states, including engagement, mental workload, and mental fatigue. We tested two types of atomic decomposition, each of which identifies unique EEG sources simultaneously in three dimensions: 1) atoms with dimensions of power spectral density, space (electrode position), and time (time on task or task conditions), or 2) atoms with dimensions of magnitude squared coherence, spatial relationships (electrode pairs), and time. For tasks that induced mental workload, we found atoms that combine sources in the theta (4-8 Hz) and alpha (8-12 Hz) EEG frequency bands consistently in individual participants at different times of day and on different days. The temporal variations of the atoms clearly reflected the levels of mental workload induced by varying task conditions. For a task that induced mental fatigue, we found atoms that tracked the development of mental fatigue in individual participants over time, while reflecting underlying changes in power or coherence of primarily theta-band EEG. Our results show that atomic decomposition is a valuable new approach to the identification and measurement of EEG sources for monitoring cognitive status. By comparing these results with results of prior analyses using the same data sets, we observed that atomic decomposition can supplement or overcome existing approaches based on conventional two-dimensional space-time or frequency-time decomposition of EEG.

List of papers submitted or published that acknowledge ARO support during this reporting period. List the papers, including journal references, in the following categories:

(a) Papers published in peer-reviewed journals (N/A for none)

Number of Papers published in peer-reviewed journals: 0.00

(b) Papers published in non-peer-reviewed journals or in conference proceedings (N/A for none)

Number of Papers published in non peer-reviewed journals: 0.00

(c) Presentations

Number of Presentations: 0.00

Non Peer-Reviewed Conference Proceeding publications (other than abstracts):

Number of Non Peer-Reviewed Conference Proceeding publications (other than abstracts): 0

Peer-Reviewed Conference Proceeding publications (other than abstracts):

Rosipal, R., Trejo, L.J. & Nunez, P.L. (2009). Application of Multi-way EEG Decomposition for Cognitive Workload Monitoring. In Vinzi V.E, Tenenhaus M., Guan R. (eds.), Proceedings of the 6th International Conference on Partial Least Squares and Related Methods, Beijing, China, pp. 145-149.

Number of Peer-Reviewed Conference Proceeding publications (other than abstracts): 1

(d) Manuscripts

Number of Manuscripts: 0.00

Number of Inventions:

Graduate Students

NAME	PERCENT_SUPPORTED

FTE Equivalent:
Total Number:

Names of Post Doctorates

NAME	PERCENT_SUPPORTED

FTE Equivalent:
Total Number:

Names of Faculty Supported

NAME	PERCENT_SUPPORTED

FTE Equivalent:
Total Number:

Names of Under Graduate students supported

NAME	PERCENT_SUPPORTED

FTE Equivalent:
Total Number:

Student Metrics

This section only applies to graduating undergraduates supported by this agreement in this reporting period

The number of undergraduates funded by this agreement who graduated during this period:	0.00
The number of undergraduates funded by this agreement who graduated during this period with a degree in science, mathematics, engineering, or technology fields:.....	0.00
The number of undergraduates funded by your agreement who graduated during this period and will continue to pursue a graduate or Ph.D. degree in science, mathematics, engineering, or technology fields:.....	0.00
Number of graduating undergraduates who achieved a 3.5 GPA to 4.0 (4.0 max scale):	0.00
Number of graduating undergraduates funded by a DoD funded Center of Excellence grant for Education, Research and Engineering:	0.00
The number of undergraduates funded by your agreement who graduated during this period and intend to work for the Department of Defense	0.00
The number of undergraduates funded by your agreement who graduated during this period and will receive scholarships or fellowships for further studies in science, mathematics, engineering or technology fields:	0.00

Names of Personnel receiving masters degrees

NAME

Total Number:

Names of personnel receiving PHDs

NAME
Total Number:

Names of other research staff

NAME	PERCENT SUPPORTED	
LEONARD TREJO	0.18	No
ROMAN RIOSIPAL	0.18	No
PAUL NUNEZ	0.05	No
FTE Equivalent:	**0.41**	
Total Number:	**3**	

Sub Contractors (DD882)

Inventions (DD882)

Advanced Physiological Estimation of Cognitive Status (APECS)

Final Report

ARO Contract No. W911NF08CO121
PDT Report No. UA01BF0636B131
September 15, 2009

Leonard J. Trejo, Roman Rosipal, and Paul L. Nunez

Pacific Development and Technology, LLC
999 Commercial Street, Suite 205, Palo Alto, Ca 94303

TABLE OF CONTENTS

Advanced Physiological Estimation of Cognitive Status (APECS): Final Report

Leonard J. Trejo, Roman Rosipal, and Paul L. Nunez

Pacific Development and Technology, LLC
999 Commercial Street, Suite 205, Palo Alto, Ca 94303
ltrejo@pacdel.com

1 Introduction

Impairment of cognitive performance in individual warfighters during a mission poses a high risk for procedural errors, for which the Army currently lacks real-time countermeasures. Such cognitive impairment has been documented in previous missions, and attributed to several factors, including time on duty, sleep loss, extended time on single tasks, unusually high workload, psychosocial or combat stress, exposure to neurotoxins and vestibular dysfunction. To address this problem, the Army, DARPA, and other DOD agencies have been developing, testing and refining systems that automatically monitor the physiological and cognitive status of individual soldiers.[1,2,3] These systems use physiological sensors to track soldiers' health and mental fitness and transmit data to command and control systems.

Some of the signals that the physiological sensors measure are readily interpreted, such as estimation of the heart rate or heart-rate variability from the electrocardiogram (ECG). However, the estimation of cognitive workload from the electroencephalogram (EEG) and other signals requires a complex series of mathematical transformations or algorithms. Overall, research on algorithms for estimation of cognitive status has made remarkable progress. For example, certain *kernel partial least squares* (KPLS) algorithms classified physiological states corresponding to states of mental engagement or cognitive fatigue using a few seconds of EEG and other signals with 90-100% accuracy and good test-retest reliability.[4,5,6] However, algorithms to estimate cognitive workload are typically only about 60-70% accurate under realistic test conditions.[7,8]

For example, Pacific Development and Technology (PDT) recently applied a KPLS algorithm to estimate engagement and workload for the US Army Toxins II SBIR program.[1] We found that the EEG features that previously worked for classification of engagement or fatigue failed to classify workload.[8] However, due to limitations in the scope of that program, we could not study several promising avenues for adaptation of the algorithm to workload. In particular, we identified two innovations that have the potential for isolating and measuring neurophysiological mechanisms important for cognitive workload. The first innovation is to apply a biophysical model of EEG coherence among neuronal networks that participate in cognitive processes.[9] The second innovation is to apply new multi-way analyses that more accurately model the interaction of interdependent processes than previous two-way methods. [10,11]

2 Objective

This project addressed two requirements described in ARO BAA W911NF-07-R-0003:

> *3.1.4. Human Cognitive and Behavioral Modeling. Quantitative, analytical models of cognition and behavior are required for training, simulation … and mission planning.*
>
> *8.4 Neurophysiology and Cognitive Neuroscience. Research in the perception and cognition subfields of neurophysiology and the cognitive neurosciences, ... physiological, … and/or cortical/cognitive mechanisms underlying successful completion of complex task behaviors applicable to non-laboratory environments under non-ideal conditions, to include both*

amelioration of induced losses as well as enhancement in defined perceptual, cognitive and/or motor abilities.

In service of these requirements we developed new algorithms for *Advanced Physiological Estimation of Cognitive Status* (APECS), which significantly improved the estimation of cognitive workload and shed new light on the estimation of mental fatigue. More specifically, we used *atomic decomposition* to identify unique sources of brain electrical activity as measured by the EEG recorded in human participants as they performed tasks that induced different mental states, including engagement, mental workload, and mental fatigue. We tested two types of atomic decomposition, each of which identifies unique EEG sources simultaneously in three dimensions: 1) atoms with dimensions of power spectral density, space (electrode position), and time (time on task or task conditions), or 2) atoms with dimensions of magnitude squared coherence, spatial relationships (electrode pairs), and time. For tasks that induced mental workload, we found atoms that combine sources in the theta (4-8 Hz) and alpha (8-12 Hz) EEG frequency bands consistently in individual participants at different times of day and on different days. The temporal variations of the atoms clearly reflected the levels of mental workload induced by varying task conditions. For a task that induced mental fatigue, we found atoms that tracked the development of mental fatigue in individual participants over time, while reflecting underlying changes in power or coherence of primarily theta-band EEG.

Our results show that atomic decomposition is a valuable new approach to the identification and measurement of EEG sources for monitoring cognitive status. By comparing these results with results of prior analyses using the same data sets, we observed that atomic decomposition can supplement or overcome existing approaches based on conventional two-dimensional space-time or frequency-time decomposition of EEG.

We foresee the future development of APECS algorithms for occupational use or performance optimization as comprising several stages. Initially, we must evaluate the APECS algorithms in a wider range of experimental contexts, and over a much wider range of individual participants. In parallel, APECS algorithms may be embedded in wearable systems that use advanced sensors and intelligent software to gather preliminary field estimates of cognitive status of individual warfighters in operational settings. The interplay of these parallel efforts – one laboratory based and the other field based – will allow us to "harden" the algorithms, both in terms of scientific accuracy and operational utility. Ultimately, through the use of interactive simulations, such as immersive virtual reality, the APECS algorithms may be adapted to provide continuous feedback of cognitive status that can serve to enhance or sustain cognitive performance. Prior research has shown that such feedback may enhance situational awareness, sustain cognitive engagement in supervisory control tasks and lower the risk of errors associated with fatigue, inattention, or overload. [12,13,14]

The APECS algorithms are presently specified in high-level MATLAB code that can readily be cross-compiled to run on different hardware systems. Thus, ultimately the APECS algorithms may serve as "plug-ins" for biosensor or feedback systems from different vendors and serve to ensure and enhance warfighter performance as part of the Army's future command and control systems.

3 Background

Recently, prototype systems for real-time estimation of cognitive states have been developed by academic, industrial, and government participants in the DARPA Augmented Cognition Program,[15] NASA, and other, focused DOD programs. These systems can use changes in human behavioral and physiological patterns to detect hazardous states such as cognitive fatigue, disengagement (inattention), or cognitive overload. Recent NASA studies have shown that with as little as 3.5

seconds of EEG data, a robust multivariate algorithm correctly identified 90 to 100% of periods during which individuals performing a demanding 3-hour task experienced cognitive fatigue.[5,6] A PDT variant of this algorithm accurately classified fatigue in Air Force pilots over a 37-hr vigil and proved to be resistant to noise and reduced sensor density.[16] Other NASA research had shown that real-time feedback derived from physiological measures of mental engagement prolonged or enhanced human performance during supervisory control of automated systems.[12,13,14] Currently, scientists at the Institute for Human and Machine Cognition (IHMC), Honeywell, and elsewhere are integrating physiological real-time "cognitive gauges" with C^3I tasks.[3,17,18] As PI, co-I or advisor for projects in all of these programs, Dr. Trejo personally directed the development and testing of algorithms for estimation of cognitive status, and contributed to significant technology advancements. His direct experience in these programs also allows him to frankly assess the current limitations and the promise of new research directions.

The ARO now has a timely opportunity to build on existing results and take a significant step forward in the estimation of cognitive workload. Four factors contribute to this opportunity: 1) progress in robust algorithm development, 2) advances in the theory of EEG coherence and its relationship to neurocognitive processes, 3) advances in multi-way methods for neuroimaging, and 4) the availability of multiple databases for algorithm development and validation.

Robust Algorithm Development. First, at PDT we have made substantial progress in formalizing a process of robust algorithm development. We now have a library of unique high-dimensional feature extraction methods and robust linear and nonlinear classifiers specifically for processing neurocognitive data. Our design for the APECS algorithms builds on 12 years of cutting-edge research on modeling, signal processing, and machine learning methods for human physiology and cognition. Drs. Rosipal and Trejo published the seminal article in the field of KPLS regression, and extended this to cognitive task analysis,[19] estimation of cognitive fatigue, [6] and brain-computer interfaces.[20] KPLS finds robust mappings between high-dimensional inputs, such as multimodal physiology, and low-dimensional outputs, such as cognitive states. KPLS also uses non-linear "kernels," to transform high-dimensional features and allow for mapping of nonlinear relationships. When coupled with classifiers, such as Fisher's discriminant or support vector classifiers, KPLS yields robust classification, with fast computation as needed for real-time learning or processing.[21]

Short- and Long-Range EEG Coherence. The theory of short- and long-range coherence is an important development in modeling the macroscopic properties of brain function that reflect cognitive processes,[9] which has yet to be rigorously applied to cognitive workload estimation. However, some simple experiments have shown that the frequency bandwidth, spatial range, and spatial direction of EEG coherence functions can discriminate different cognitive states.[22] Specific processes that are associated with coherence include: selective attention, transfer of information among different but coherent networks, binding of neuronal groups for unitary processing, such as object perception or working memory, and plasticity subserving learning and memory.

As described in the Results (Section 05), we have confirmed that the inclusion of short and long-range EEG coherence features in algorithms for estimating cognitive workload improves on algorithms that rely on the EEG power spectrum alone. One of the problems that have plagued cognitive workload estimation is that changes in EEG band power can mean different things in different contexts, leading to inconsistency of the feature weights used to classify EEG segments. For example it is widely known that alpha band power decreases with engagement and cognitive workload,[23] but in other cases increases in alpha power and coherence may reflect specific memory processes.[24] Without due consideration of the scale and direction of coherence changes, EEG measurements can have an inconsistent connection to cognition. However, the conflicting results of these studies are reconciled by a short/long-range coherence model in which local oscillatory

dynamics interact with global modulations of synaptic action in multiple frequency bands to produce observed EEG.[22]

Multi-way Methods. Another important development is the successful application of multi-way methods such as *N-way Partial Least Squares* (N-PLS) or *parallel factor analysis* (PARAFAC) to brain activity such as EEG or fMRI.[10,25] N-PLS is multi-way extension of PLS which combines the class-specific feature extraction power of PLS while preserving the multi-way structure of the variance sources (supervised learning). PARAFAC is a multi-way extension of factor analysis that extracts features without respect to class criteria (unsupervised learning). In theory, multi-way methods can disambiguate neurocognitive processes that may be confounded by two-way methods such as principal components analysis (PCA), independent components analysis (ICA), or ordinary PLS. For example, the standard approach to EEG analysis for estimation of cognitive state is to analyze the frequency spectrum and location, or *frequency×channel* where a *channel* is an electrode or electrode pair. When a third dimension such as time on task (or conditions) is added, the formal model becomes a matrix of *frequency* × *channel* × *time*. Two-way methods can only decompose the three-way interaction by collapsing frequency and channel into one dimension, resulting in a two-way matrix of (*frequency-channel)* × *time.* The result is a series of frequency-channel components mixed in different proportions for each sample time. Such mixing of dimensions obscures the correct interpretation of a component, or even worse, can fail to identify phenomena that are specific to one of the arbitrarily mixed dimensions. Furthermore, components so obtained are not uniquely determined, and must be constrained artificially by criteria such as orthogonality, which are not likely to fit neurocognitive processes. Multi-way methods, on the other hand, yield a unique decomposition that preserves the uniqueness of each dimension of the measurement matrix.[26] In this way multi-way methods represent EEG sources corresponding to a neurocognitive process with an *atomic* structure, where each *atom* represents a unique source of variance in the multi-way matrix. The N-PLS and PARAFAC methods have been used to identify EEG alpha-, theta-, and gamma-band "atoms" that coincide with simultaneous fMRI estimates of spatial location, with similar degrees of efficacy.[27]

Neurocognitive Databases. We now have access to five databases from controlled studies of physiology and human performance, including four studies that focused on estimation of cognitive workload and detection of cognitive overload. Drs. Trejo and Rosipal directed experiments, wrote algorithms or analyzed data from each of these studies and are uniquely familiar with the databases. We used three of these databases to develop and test APECS algorithms. All data from these studies were collected with informed consent and approved IRB protocols. The data were coded such that the identities of the participants will be unknown to PDT analysts. The three databases used in the present project included:

- USAF-C: C2ISR Multimodal Study of UAV Operator Readiness (6 multi-test participants[17])
- USA-T: *Army Toxins II Multimodal Study of Cognitive Overload* (8 test-retest participants[4])
- NASA-C: *NASA Cognitive Fatigue Database* (16 participants, public domain[6])

Two additional databases, which manipulated cognitive workload, may be used in future research:

- USN-B: *Navy Biopsychometric Assessment Program Database* (8 test-retest participants[28])
- NASA-E: *NASA ERTAS Database* (8 test-retest participants[13])

4 Methods and Procedures

4.1 Task 1. Analysis of Tasks, Workload Metrics, and Physiological Data

The aim of this task was to decompose each experimental database to define workload, time resolution, and physiological metrics. For each database, we followed a three-step process of algorithm adaptation and testing (Figure 1). First, we analyzed each task from a neurocognitive standpoint to guide our selection of workload and physiological metrics and time resolution. For example, the USAF-C database includes visual signal-detection, working memory, and executive control tasks. Perceptual tasks, such as signal detection, would activate visual-spatial processing networks located in occipital, parietal, and inferotemporal cortex, which will modulate alpha 1 and alpha 2 powers and coherence. The working memory demands of the USAF-C task would activate the anterior cingulate and dorsolateral prefrontal cortex, producing increased midline frontal theta rhythms. [24,29] This prior knowledge of functional specialization guided our selection of EEG electrode sites, frequency bands, and spatial / temporal resolution for power and coherence estimates.

The temporal resolution of EEG analysis for each task was long enough to reliably estimate parameters but short enough to detect changes related to task conditions. By applying these principles to each task, we produced a set of analysis parameters (Table 1).

Task Code	Perceptual & Cognitive Processing Demands	Neural Sources	EEG Bandwidth	Range Of Temporal Resolution	Minimum Frequency Resolution
USAF-C	Visual signal detection	Parietal-occipital	8-25 Hz	2-3.5 s	1.0 Hz
	Working memory & executive control	Fronto central	4-8 Hz	2-3.5s	1.0 Hz
			8-12 Hz	2-8 s	0.5 Hz
USA-T	Visual signal detection	Parietal-occipital	8-20 Hz	2-3.5 s	1.0 Hz
	Auditory language processing	Temporal-central	8-20 Hz	2-3.5s	1.0 Hz
	Working memory & executive control	Fronto central	4-12 Hz	2-8s	1.0 Hz
NASA-C	Working memory & executive control	Fronto central	4-18 Hz	2-13 s	0.5 Hz

Table 1. Spatial, frequency, and temporal analysis parameters for the three task databases.

4.2 Task 2. APECS-W Algorithm Adaptation

As suggested by a current theory of local/global EEG coherence[9] and experiments on EEG and cognitive function,[22] we hypothesize that cognitive workload is reflected by the desynchronization of a parietal alpha atom defined by long-range coherence with frontal regions and the synchronization of a frontal midline theta atom defined by local coherence with neighboring frontal regions. Using this guiding hypothesis and the analyses from Task 1, we structured two APECS-W algorithms for each database. In the first algorithm, or APECS-Wp, aimed at power spectral density effects, the three-way input matrix consisted of EEG power spectral densities for frequency bins from 1-25 Hz, electrode position, and time of measurement (which reflected task-induced workload transitions). In

the second algorithm, or APECS-Wc, aimed at spectral coherence effects, the three-way input matrix consisted of multi-scale EEG coherence spectra, electrode-pair (all unique pairs of electrodes excluding self-pairing), and time. For the NASA-C database we structure two similar algorithms, APECS-Fp and APECS-Fc, using similar principles, but different constraints (see below).

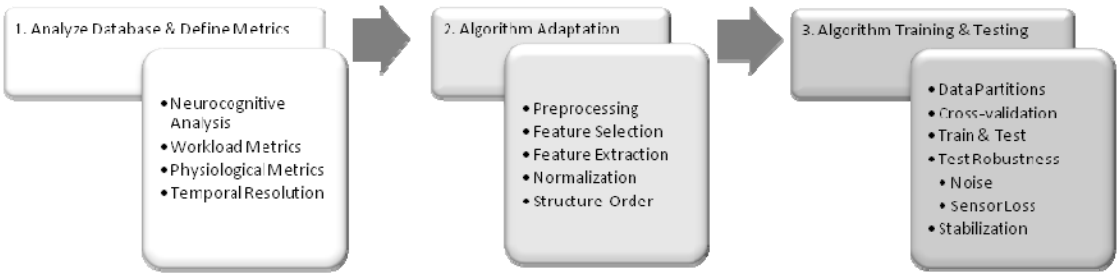

Figure 1. Three-step process of APECS-W algorithm adaptation and testing. In Step 1, we use neurocognitive theory and data to analyze tasks to define workload, time, and physiological metrics. In Step 2, we will define preprocessing, feature selection/extraction, normalization methods and adapt the APECS structure and order to the features. In Step 3 we will select random training, cross-validation, and testing partitions then train and test the algorithm. In future studies we may also test the resulting algorithm for tolerance of noise and sensor loss, and then apply optional stabilization methods to improve test-retest reliability.

In the present analyses the outputs consisted of unique atoms for which we obtained the loadings using PARAFAC decomposition with the following constraints:

- We corrected EEG records for ocular artifacts and segmented them into non-overlapping contiguous epochs of 2-s duration, providing frequency resolution of 0.5 Hz. This resolution was satisfactory for all task requirements (Table 1).
- We performed outlier detection by removing points with unduly high leverage. For this we did an initial PARAFAC decomposition and then clipped data points for which individual loadings in any one dimension exceeded a fixed percentile of the populations of loadings for that dimension in the given experiment. The percentiles we used ranged from 90 to 99%. After removing such points we did a second decomposition and retained the loadings as results.
- We imposed a constraint of non-negativity for loadings on all dimensions of the PARAFAC decompositions. In addition, for the NASA-C dataset, coherence analysis, we used an additional constraint of unimodality on the frequency dimension.
- We did not rescale or normalize data for any dimension. However, for display purposes only, we scaled loadings for the *time* dimension for comparing atoms with very different loading means and variances within experiments.
- Units of power spectral density were $dB/\sqrt{Hz}$. Units of coherence were the conventional dimensionless units of magnitude squared coherence ranging in value from 0 to 1, where 0 means no coherence and 1 means perfect coherence at a given frequency.

Two approaches were used to assign initial values to the loadings before iterating solutions to the PARAFAC decompositions. For both APECS-W algorithms we used a method of performing several small runs then averaging the resulting loadings and using the averages to initialize the loadings for complete decompositions. For the APECS-F algorithm, we used singular value decompositions in each dimension to estimate the initial loadings.

For APECS-W we used a uniform convergence criterion of 1.0×10^{-6} for iterating the algorithm, i.e., iteration ceased when the change in total variance explained was less than $1/10{,}000^{th}$ of one percent. For APECS-F the convergence criterion was 0.001 or an improvement in the model fit of less than $1/10^{th}$ of one percent.

After preprocessing all EEG records to remove EOG artifacts we performed three-way unsupervised PARAFAC decompositions to identify the atoms (multidimensional components of variance) in the three-way input matrices. For the APECS-Wp and APECS-Fp algorithms, the EEG atoms, *A*, are defined as three-way sources with dimensions of frequency, *f*, electrode, *e*, and time, *t* (Eq. 1). Each atom is estimated by two normalized vectors (*a, b*), a score vector *c* and a noise term, ε_{eft}.

$$\hat{A}_{eft} = \sum_{k=1}^{N_k} a_{ek} b_{fk} c_{tk} + \varepsilon_{eft} \qquad \text{(Eq. 1)}$$

4.3 Task 3. Algorithm Training and Testing

The structure of the APECS-W algorithm was similar for each database, but we adapted the variable inputs, outputs, and preprocessing requirements of each database to a format that was suited for cross-study validation. Since all of the decompositions we did were unsupervised, there was no need for formal training, testing, and validation sets. However, for the USAF-C and USA-T datasets we used sessions performed at different times of day and on different days for this purpose. For example, we used session data from Day 1 to estimate the atoms and then projected the EEG data for Day 2 using the weight vectors for each atom to reproduce the time course of each atom across workload conditions. No test-retest validations were performed as of yet for the NASA-C data set.

5 Results

5.1 Synopsis of Results

In this project we designed and tested an APECS workload algorithm (APECS-W), to increase the accuracy and reliability of estimated cognitive workload and detect periods of cognitive overload. We aimed for a 20% increase in accuracy and test-retest reliability. Our minimally successful criterion was 10%. Our prior simulations showed that even a 10% improvement will move estimation of workload near the lower range of accuracy now possible for estimation of engagement or fatigue (Figure 2). We considered distinguishing engagement from workload, but our focus was on discriminating workload states pertaining to active task engagements. We tested the APECS-W algorithm using two databases (USAF-C, USA-T) described above. A formal classification analysis was outside the scope of this STIR project, so we made informal estimates of accuracy based on inspection of the data and comparisons with prior results. We will perform formal classification analyses in our future development of the APECS algorithms. For now, our experience with all of the data sets examined here suggests that there was an improvement of more than 20% in the estimation of cognitive workload using atomic decomposition, as compared to our prior methods using two-way analyses. For the fatigue data, we estimated a lower level of improvement, which is to be expected from the already-high accuracies of prior classifications.

We designed the APECS algorithm to be adaptable to a wide range of tasks that require human performance or supervision. In particular, we adapted the algorithm to the estimation of mental

fatigue, and will refer to this algorithm variant as APECS-F. Although we did not set out to compare APECS-F quantitatively with prior results, we report below that APECS-F was highly successful in identifying EEG atoms that track the development of mental fatigue in individual participants.

5.2 Detailed Results

5.2.1 USAF-C Database – Initial Published Results

We presented results of our initial analyses using two participants from the USAF-C database at the recent PLS09 conference and published a corresponding full-length paper in the edited book of the conference proceedings.[30] Here we present a summary of the results in that paper and we attach the complete paper in Appendix 1.

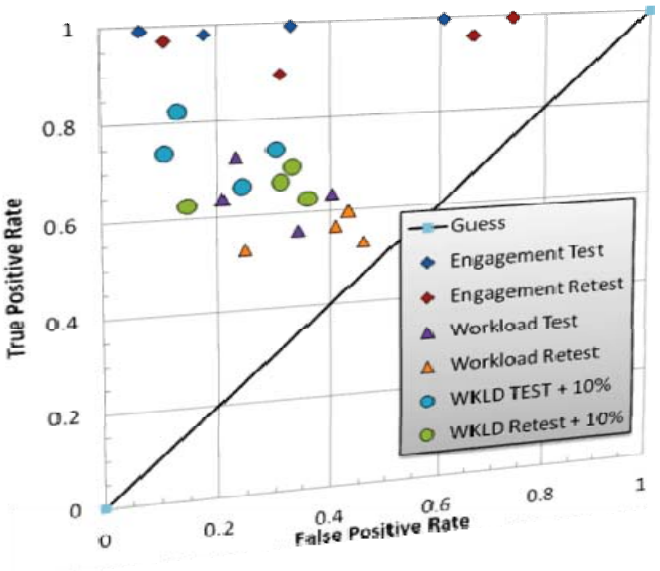

Figure 2. Each group of symbols plots the ROC points for four participants in USA-T Study 2 and for one EEG-classifier type. Engagement test and retest classifiers were much more accurate than corresponding workload classifiers. We simulated the effects of increasing test and re-test accuracy of the workload classifier by 10% (blue and green circles vs. purple and orange triangles).

The paper describes the use of multi-way decomposition methods to efficiently summarize EEG data. A space-frequency-time atomic decomposition was applied to EEG data recorded while participants performed tasks associated with varying levels of cognitive performance. The new atomic decomposition of cognitive workload data revealed alpha and theta EEG oscillations which agree with observations reported in the brain research literature. The temporal signature of the atoms discriminated between different levels of cognitive activity. The results and analysis confirmed the utility of the multi-way decomposition method to construct new models and algorithms for monitoring cognitive status, which can supplement or overcome existing approaches based on conventional two-dimensional space-time or frequency-time data decomposition.

The results showed that mental workload may be tracked by EEG components isolated using PARAFAC. Components or atoms of the PARAFAC decomposition had high loadings in the frequency spectrum and across electrodes, which reflected alpha, theta, and broad-band EEG processes. Unlike other approaches to isolate EEG factors related to mental workload, our application of PARAFAC begins with a truly three-dimensional model of EEG variance observed during

performance of a cognitive task. This model is fit to the EEG simultaneously in frequency, space, and time. The time dimension in the present study reflects imposed task demands that produced calibrated states of low-or high mental workload. For an unsupervised method of decomposition, these PARAFAC results are remarkable. Using a small number of electrodes, the loadings of several PARAFAC atoms in time, co-varied with task demands and mental workload. Admittedly, these results are based on a small sample of two participants. However, the task performances were long, providing about 30 minutes of EEG recordings for analysis. In our extensive experience with similar experiments, the discovery of EEG atoms that track workload and have meaningful spectral and spatial propertied from recordings of these durations is not likely to arise from chance.

5.2.2 USAF-C Database –Unpublished Results

5.2.2.1 Methods

The data were collected from six additional participants in the USAF-C study (denoted 'B', 'C', 'E', 'G', "I', and 'K'), each of whom completed three sessions (trial repetitions). Participants were trained to stable performance on a simulated Unmanned Air Vehicle (UAV) task. The task consisted of monitoring the progress of four UAVs as they flew a preplanned mission, monitoring UAV resources, and classifying synthetic aperture radar images acquired by sensors in each UAV. For additional details concerning the experimental design, methods and procedures, please refer to Appendix 1. Each run contained six different indicators of mental states assigned by the experimenters; however, indicators for only two workload levels (low and high) were provided to us due to a security restriction. Therefore, we used only the data from the two periods designated as high- and low workload. Nineteen channels of EEG (placed according to the International 10-20 System[31] with a linked mastoid reference) were available in this study. One-channel ECG and two channels of bipolar EOG (vertical and horizontal) were also recorded.

First, the EEG data were down-sampled to 128 Hz sampling rate from the original sampling rate of 256 Hz. Next, data were segmented into non-overlapping consecutive windows of 2-s duration. As in the initial analyses[30] (Appendix 1), the power spectral density (PSD) was computed for each segment using the Thomson Multi-taper method.[32] Initial analyses revealed a high level of power at frequencies below 6 Hz. Power at these frequencies often arose from motion artifacts and confounded the PARAFAC analyses of EEG. Therefore, only the frequencies in the range of 6 to 25 Hz were considered in this study. We repeated this procedure for each EEG channel separately and constructed a three-dimensional matrix, $\mathbf{A}(\mathbf{E} \times \mathbf{F} \times \mathbf{T})$, with **E** time segments, **F** electrodes and PSD estimates at **T** frequencies (Eq. 1).

5.2.2.2 Results

5.2.2.2.1 Spectral Representation

The PARAFAC model has been run two times. After the convergence of the first run the points with high values of the residual variance and leverage, that is, points indicating noisy samples, were inspecting. The points exceeding 95 percentile of the residual variance and leverage distribution were removed and the PARAFAC model was run again. In general, this procedure removed points with very high values of temporal loadings (signatures). The core consistency[10] of these final models was in all cases greater than 85% indicating a good model fit.

5.2.2.2.2 Participants B, K

First, the PARAFAC model was run using the full set of 19 EEG electrodes. The results of the three-atom PARAFAC model for Participant B are depicted in Figure 3. It can be observed that the

temporal signatures of the second and third atoms separate the periods of the high and low workload. However, high values of the loadings vectors at frequencies above 20 Hz indicate that this can be due to the movement components superimposed to EEG. To investigate this effect the spatial loading vectors for Atom 2 and 3 are plotted in Figure 4.

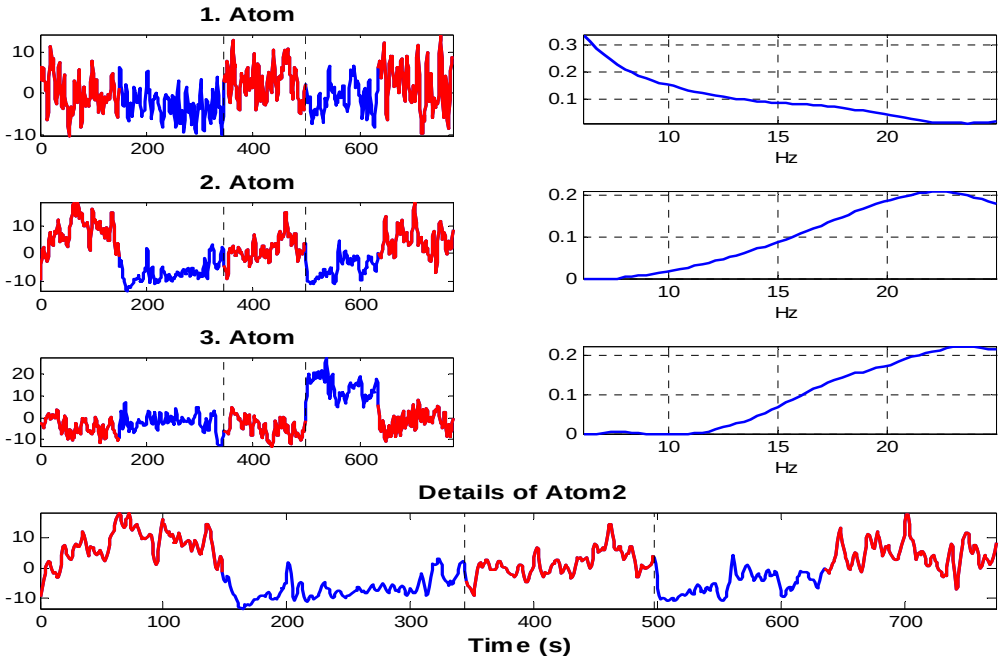

Figure 3. Loadings of three PARAFAC atoms extracted from EEG recordings of Participant B using 19 electrodes. Left panel: Temporal signatures of the EEG atoms. Red marks indicate periods of high workload, blue line marks the low workload periods. Vertical dotted lines separate three distinct experimental sessions. Bottom panel: Detailed plot of temporal loadings of Atom 2. Right panel: Spectral signatures corresponding to atoms numbered in the left panel.

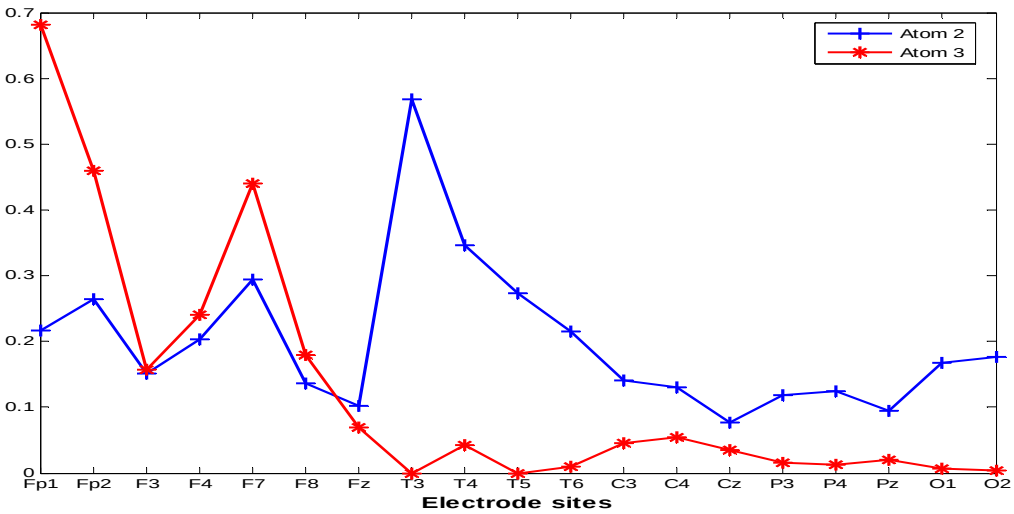

Figure 4. Participant B. Comparison of the spatial signatures corresponding to Atom 2 and Atom 3 plotted in Figure 3.

High spatial loading values can be observed at T3, T4, F7 and Fp2 sites (Atom 2) and at the electrode sites Fp1, Fp2, T5, T6 and F7 for Atom 3. These electrodes are generally known to be susceptible to the movement artifact. Therefore in the next step we have removed these electrodes and run the PARAFAC model again. The results with the reduced set of electrodes are depicted in Figure 5.

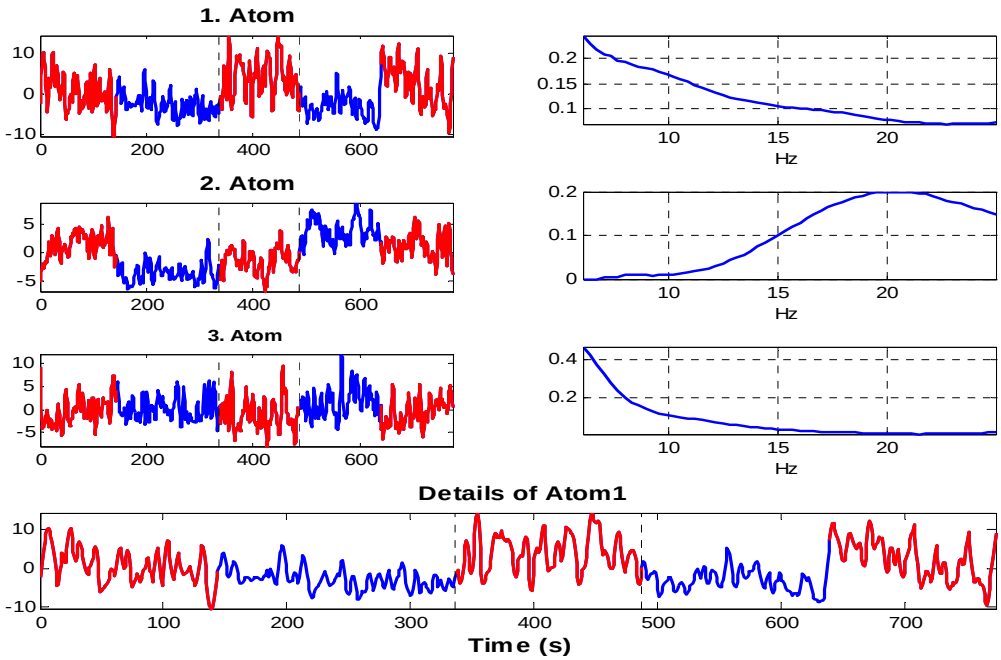

Figure 5. Loadings of the three PARAFAC atoms extracted from EEG recordings of Participant B using the reduced set of 12 electrodes. Left panel: Temporal signatures of the EEG atoms. Red marks indicate periods of high workload, blue line marks the low workload periods. Vertical dotted lines separate three distinct experimental sessions. Bottom panel: Detailed plot of the temporal loadings of Atom 2. Right panel: Spectral signatures corresponding to the atoms numbered in the left panel.

Now three distinct atoms can be observed. While the third atom seems to represent overall EEG power indicating 1/f trend, the first and the second atom seem to be two spectrally complimentary atoms which when applied together discriminate periods of low and high workload. However, although the spectral concentration of the second atom around 20 Hz and its decay at higher frequencies indicate that this atom may represent the beta component in EEG, the spatial distribution shows high influence of the frontal F3, F4 and F8 sites. Therefore the influence of movement artifact in this atom cannot be ruled out. Note that using the reduced set of electrodes increased the core consistency to 87% indicating good fit of the model to data. This is in contrast when the full set of electrodes was used and the core consistency value below 20% indicated poor fit. Similar three atoms to the ones plotted in Figure 5 were observed in Participant K, however, using the full set of electrodes. While two atoms resemble Atoms 1 and 3 in Figure 5, the third extracted atom in this participant resemble the movement atom depicted in Figure 3. This atom was spatially concentrated on Fp1, Fp2, F8 and T4 electrode sites. Removal of these sites and also additional to noise susceptible sites (F3, F4, F7, F8, T3, T5 and T6) did not change the structure of the extracted atoms, indicating that the observed movement related artifact globally influences EEG recordings at all sites.

5.2.2.2.3 Participant C

The three-component PARAFAC model was run using the full set of 19 electrodes. Two distinct workload related atoms (Atom 1 & 3) can be observed in Figure 6. While the spectral signature of the

first atom indicates the importance of lower (below 8Hz) and higher alpha (around 12 Hz) frequencies, the third atom shows spectral concentration somehow complimentary and peaked around 10 Hz. Note clear separation of the low and high workload levels using these two atoms.

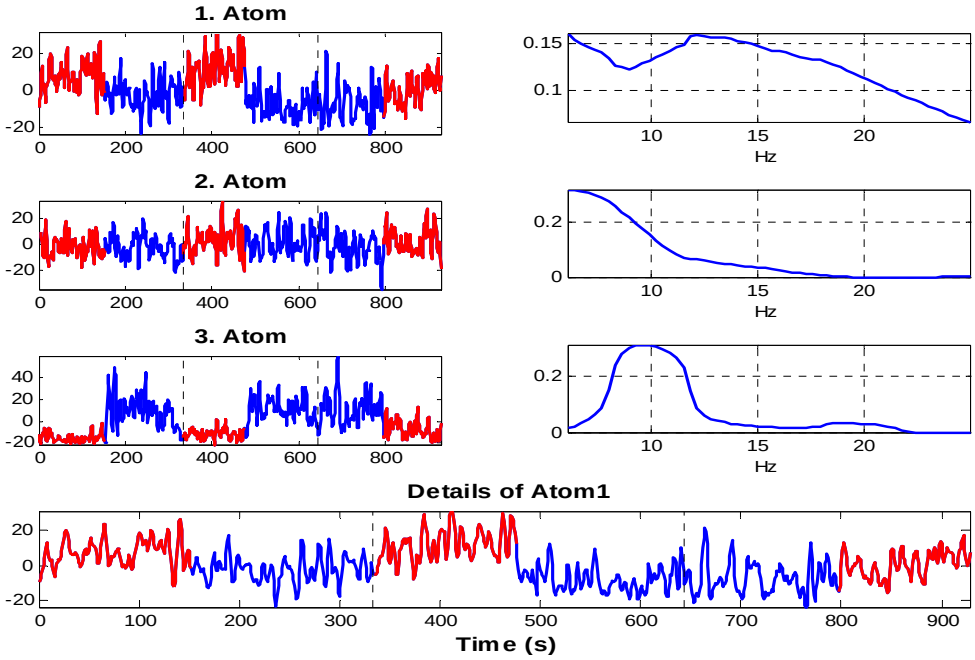

Figure 6. Loadings of the three PARAFAC atoms extracted from EEG of Participant C using 19 electrodes. Left panel: Temporal signatures of the EEG atoms. Red marks indicate periods of high workload, blue line marks the low workload periods. Vertical dotted lines separate three distinct experimental sessions. Bottom panel: The detailed plot of the temporal loadings of Atom 1. Right panel: Spectral signatures corresponding to the atoms numbered in the left panel.

Spatial signatures of these two atoms are plotted in Figure 7. It can be observed that while the third atom is more centro-parietal located, the first atom indicates higher importance of the fronto-central sites. Finally, the second atom exhibits a typical background EEG spectrum with exponential decay of frequencies and no discrimination of the high and low workload periods can be observed in the corresponding temporal signature plot.

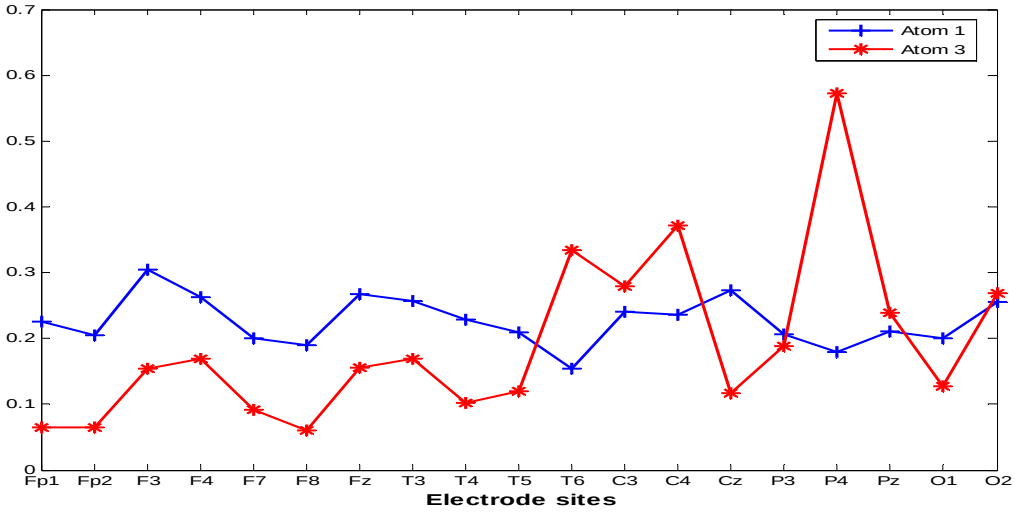

Figure 7. Participant C. Comparison of the spatial signatures corresponding to Atom 1 and Atom 3 plotted in Figure 4.

5.2.2.2.4 Participants E, G, I

The three-component PARAFAC model atomic decomposition has revealed almost identical spatial, spectral and temporal structure of the loading vectors in these three participants. The loading vectors are very similar the ones plotted in Figure 5, but in this case the full set of 19 electrodes was used. Three distinct atoms observed in these participants are plotted in Figure 8 (Participant E).

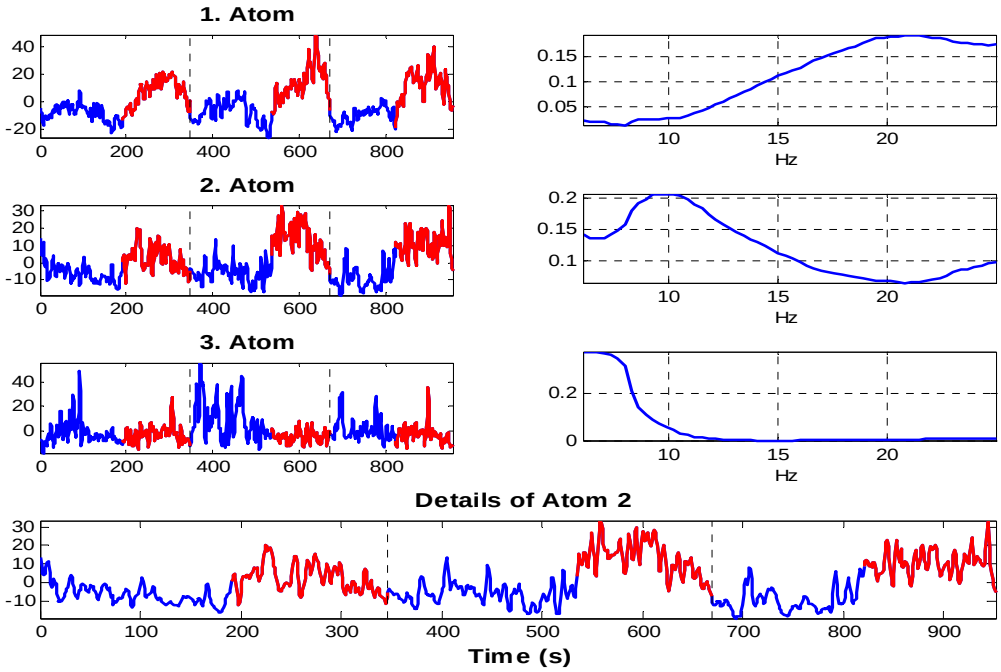

Figure 8. Loadings of the three PARAFAC atoms extracted from EEG recordings of Participant E using the full set of 19 electrodes. Left panel: Temporal signatures of the EEG atoms. Red marks indicate periods of high workload, blue line marks the low workload periods. Vertical dotted lines separate three distinct experimental sessions. Bottom panel: The detailed plot of the temporal loadings of Atom 2. Right panel: Spectral signatures corresponding to the atoms numbered in the left panel.

While the first atom resembles the movement related atom (Atom 2) already observed in Participant B (spatially concentrated around T3 and T4 sites), the spectral distribution of the second atom resembles Atom 3 observed in Participant C. However, the spatial distribution of this atom is different and high loading values are concentrated in occipital sites O1 and O2 (clearly visible in Figure 9 for Participants E and I). This spatial distribution was similar for all three Participants E, G and I. However, the spectral peak in Participants G and I was concentrated a bit higher at 11 Hz. Note the opposite pattern in the temporal signature of Atom 2 in comparison to Atom 3 in Participant C. Now, the values of high workload periods are above the values indicating the low workload periods. The third atom seems to represents the mixture of a typical background EEG spectrum with increased concentration in lower than 8 Hz frequencies. In Participants G and I this concentration of higher loadings values on lower frequencies was not observed and a clear 1/f spectral pattern could be observed. Partial separation of the high and low workload periods can be also observed in the temporal signature of this atom for Participant E. This was not rue for Participants G and I where this background EEG atom has shown no discrimination abilities.

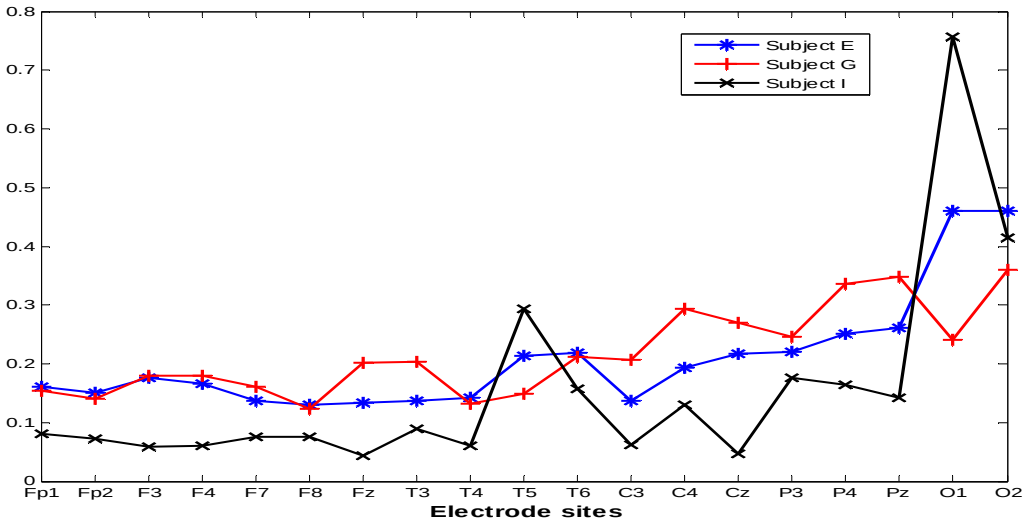

Figure 9. Comparison of the spatial signatures corresponding to the workload atom (Atom 2 in Figure 6) for participant E, G and I.

5.2.2.2.5 Coherence Representation

From the PSDs we also computed three measures of coherence the *magnitude squared coherence*, or C_{xy}, the cross-*spectral power density* via Welch's method, or P_{xy}, and *the transfer function estimate* using Welch's averaged periodogram method, or T_{xy}:

$$C_{xy}(f) = \frac{\left|P_{xy}(f)\right|^2}{P_{xx}(f)P_{yy}(f)} \qquad \text{(Eq. 1)}$$

$$P_{xy}(\omega) = \sum_{m=-\infty}^{\infty} R_{xy}(m)\, e^{-ij\omega m} \qquad \text{(Eq. 2)}$$

$$T_{xy}(f) = \frac{P_{xy}(f)}{P_{xx}(f)} \qquad \text{(Eq. 3)}$$

Where R_{xy} is the cross-correlation sequence of the EEG segments from channels x and y, or

$$R_{xy}(m) = E\left\{ x_{n+m} y_n^* \right\} = E\left\{ x_n y_{n-m}^* \right\} \qquad \text{(Eq. 4)}$$

A three-component PARAFAC model has shown a good fit to data. For individual participants the same EEG electrodes were used as in the case of spectral representation. Coherence among all possible electrode pairs was computed and used in the model.

5.2.2.2.6 Participants B, E, G, I, K

Interestingly, the PARAFAC model trained on data using the fullest of 19 electrodes provided the results without two movement related atoms in contrast to the case when the spectral representation was used (Figure 3). The extracted atoms using the C_{xy} coherence representation are plotted in Figure 10. P_{xy} and T_{xy} representation resulted in atoms with similar spectral signatures but temporal signatures were less discriminative regarding the two different periods of low and high workload.

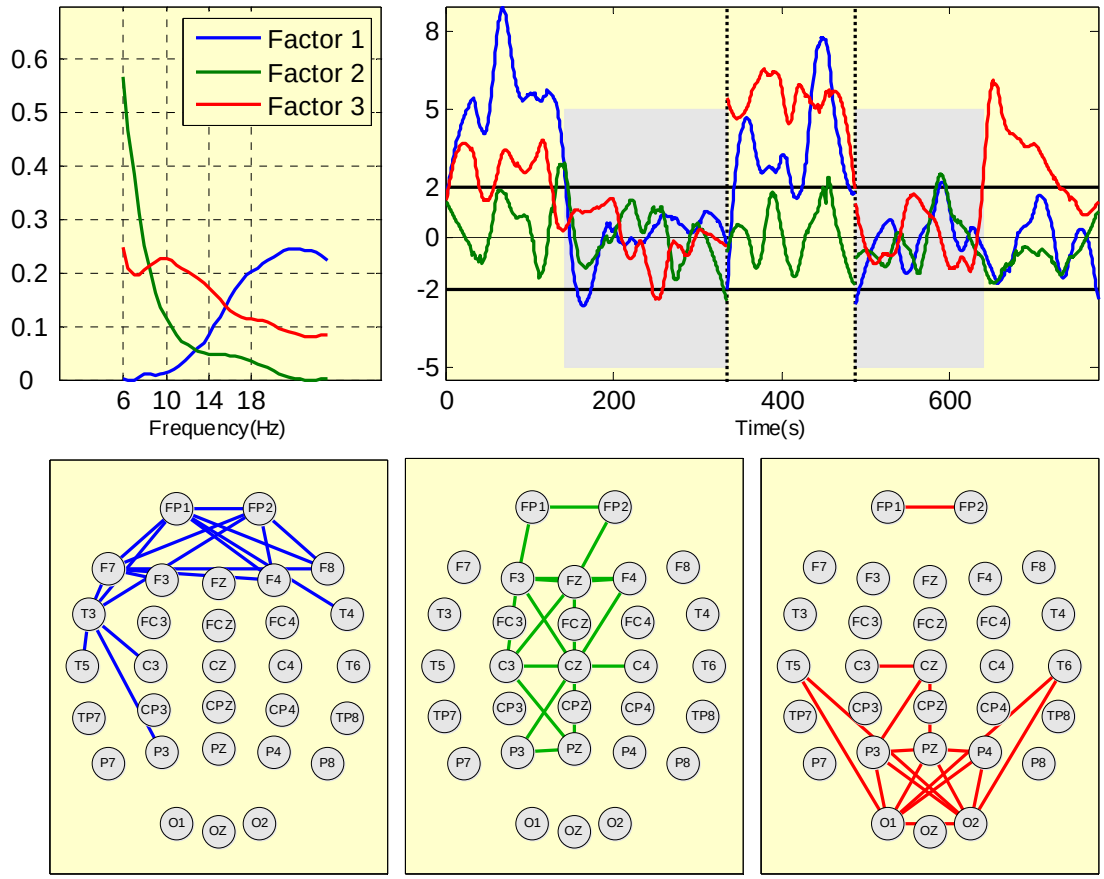

Figure 10. Loadings of the three PARAFAC atoms extracted from EEG recordings of Participant B using the full set of 19 electrodes. Top-Left panel: Spectral signatures. Top-right panel: Z-scores of the temporal signatures of the EEG atoms numbered in the right panel. Shaded areas indicate periods of low workload. For the Z-scores computation (mean and standard deviation) data of low workload periods were used. This was done for each trial separately. Vertical dotted lines separate two distinct experimental sessions. Moving average smoothing with the length of 60 points was used. Bottom panel: The coherence plot (connecting lines) of the electrode pairs exceeding the 90 percentile of the all coherence values distribution (Note, the label Factor in the plots means the same as Atom).

In Figure 10, Atom 3 with a peaked spectral concentration around 10 Hz and concentration at lower than 7 Hz can be observed. This evident peaked spectral concentration is in contrast to the case of using the spectral representation (Figure 5, Atom 1). The temporal signature of this atom nicely separates the periods of low and high workload. The value of 90 percentile was computed from the distribution of the spatial loading vector of electrode pairs and all pairs for which the loading values exceeded this percentile (value equal to 0.1032) are plotted in the bottom part of Figure 10. The plot suggests the importance of the parieto-ocipital and ocipito-ocipital electrode pairs for this workload discriminative atom (Atom 3). The spatial distribution of Atom 1 in the frontal and fronto-temporal sites suggests a movement related component in the EEG and somehow ruling out the fact that this atom represents an EEG beta band related component. Finally, Atom 2 represents the general EEG component with the decaying spectral characteristic and regular spatial distribution over the whole brain. Very similar spatial, temporal and spectral signatures to Participant B where observed in

Participants E, G, K, and I. For example, in Figure 11 the results for Participant I are plotted. In Figure 12 spatial and spectral signatures for the workload related atom (Atom 3 in Figure 10 or in Figure 11) are compared. Close match can be observed in the spatial distribution of the electrode pairs among all five participants (left plot). Although, some variation in the location of the spectral peak can be observed in the right plot of Figure 12, the overall pattern of this spectral signature seems to be consistent over all five participants.

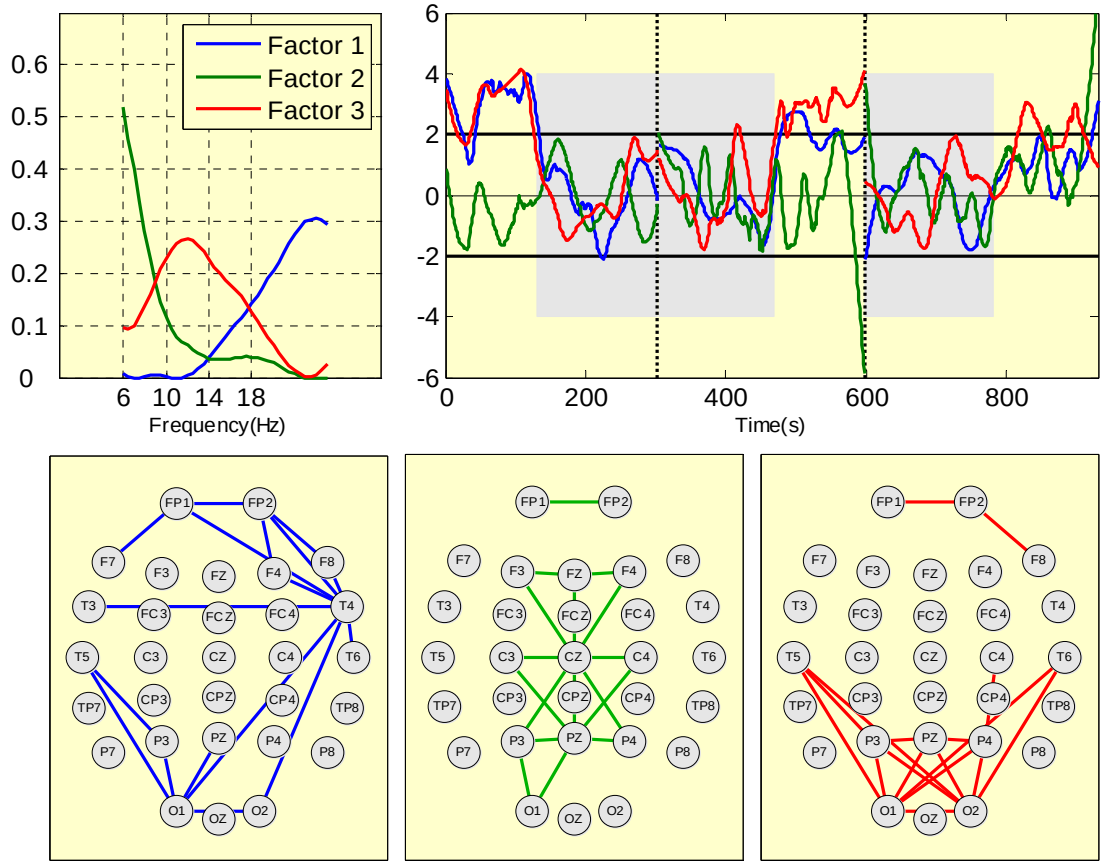

Figure 11. Loadings of the three PARAFAC atoms extracted from EEG recordings of Participant I using the full set of 19 electrodes. Top-Left panel: Spectral signatures. Plotting conventions are the same as in Figure 10.

5.2.2.2.7 Participant C

The atomic decomposition using the C_{xy} coherence data representation is depicted in Figure 13. We can observe three very distinct atoms which resemble the atoms in Figure 7 when spectral representation was used. However, more compact (peaked) spectral representation for Atom 1 and 3 can be observed now. We can clearly see that Atom 1 has the spectral peak at 13 Hz and almost zero loadings values at 8 Hz. Atom 3 is peaked at 10 Hz and a small spectral bump can be observed over the beta band (16 to 22 Hz). Comparing the temporal plots (not plotted here), the coherence representation also provides visually clearer separation of the low and high workload periods than can be observed in Figure 7 (this is specifically true for Atom 1). Coherence plots in Figure 13 indicates the importance the fronto-central and centro-parietal pairs with some importance of the local coherences around midline of all frontal, central, parietal, and also occipital sites. For Atom 3

the high coherence values were observed for the parieto-occiptal pairs. Lower loadings were observed between frontal channels and for the electrode pairs connecting to the T6 electrode site. We do not show results for the P_{xy} and T_{xy} measures, which appeared physiologically implausible.

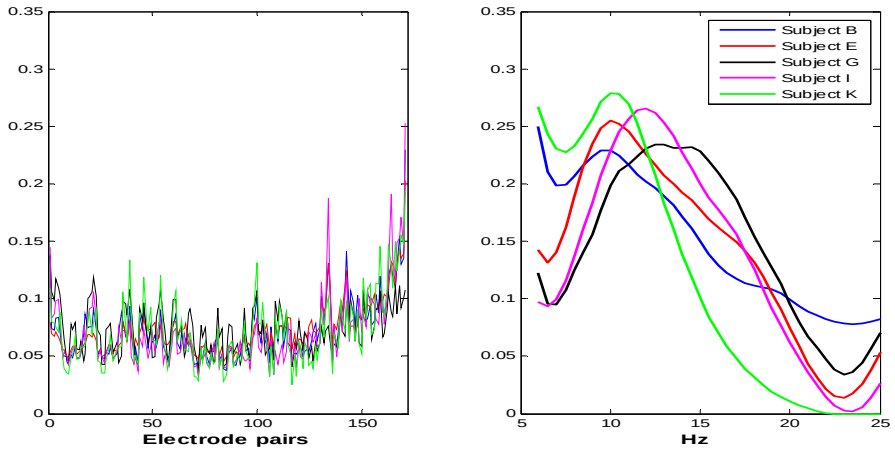

Figure 12. Participants B, E, G, I, and K. Left: Comparison of the spatial (electrode pairs) signatures (loading vectors) corresponding to the workload atom. Right: Comparison of the spectral signatures (loading vectors) corresponding to the workload atom. Examples of this workload atom are plotted in Figure 10, Atom 3, for Participant B and in Figure 11, Atom 3, for Participant I.

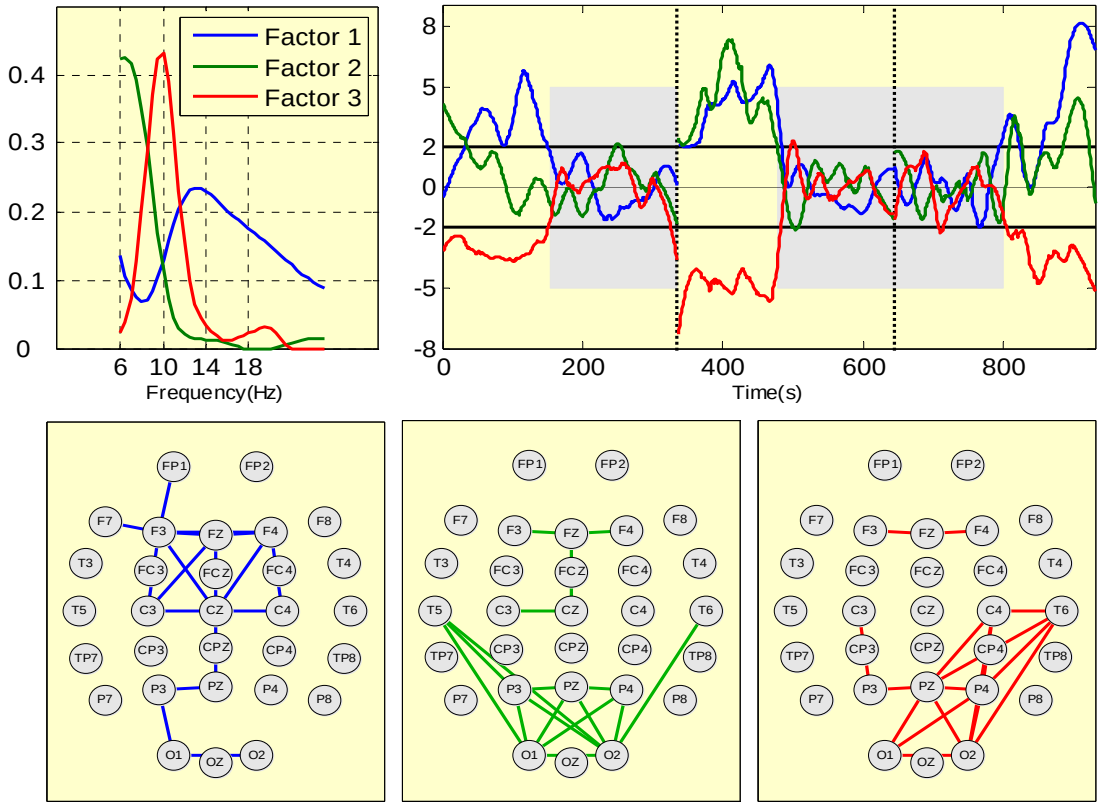

Figure 13. Loadings of the three PARAFAC atoms extracted from EEG recordings of Participant C using the full set of 19 electrodes. Plotting conventions are the same as in Figure 10.

5.2.3 USA-T Database

5.2.3.1 Methods

The USA-T database was derived from a prior ARO-funded SBIR Phase II contract awarded to Quantum Applied Science and Research.[2] Under a subcontract, PDT supported the studies performed under this contract, including experimental design, pre-processing data and developing algorithms for estimation and monitoring mental workload using PLS methods, reporting, and publications. The prime contractor has licensed our use of the data from the original ARO SBIR contract for further research.[33] The studies consisted of a series of experiments in which we established increasing control over task, performance, and physiological factors. The first two experiments primarily served to evaluate the major effects of workload on performance and physiological variables and to compare two candidate tasks for the third experiment.

A detailed description of experimental and analytical methods for the prior study, from which the current study data were obtained, has been submitted for publication and is available on line[6]. Briefly, data were collected from 16 participants recruited from the San Francisco Bay Area community. The participants included 12 males and 4 females with a mean age of 26.9 (SD = 7.4) years. Subjective moods were indexed by the Activation Deactivation Adjective Checklist [34] (AD-ACL) and the Visual Analogue Mood Scales[35] (VAMS) questionnaires. Observed behavior included ratings of activity and alertness from videotaped recordings of each participant's performance. The performance measures were response time and response accuracy. The physiological measures were derived from spontaneous EEGs and EOGs.

For the present analyses, we are concerned only with data from Experiment 2, in which participants performed a first person shooter simulation (Battlefield II) at three difficulty levels: one passive level (observe only) and two active levels, easy (1 enemy) and difficult (5 enemies). A secondary auditory tone-report task was used to obtain independent evidence of high workload states. The experimental design crossed the two auditory task levels (attend, ignore) with the two active difficulty levels. In the *attend tones* condition, participants were instructed to silently tally the numbers of kills, deaths, and tones, press a foot pedal to acknowledge the tones as quickly as possible, and report the tallies after each pedal press. The modified tone-report task served to provide a time-indexed measure of the workload imposed by the game difficulty manipulation. Because the tone-report task was not as time critical as simulated combat, we hypothesized that reaction times to the tones would be greater during high workload periods than during low workload periods. A spectral analysis of EEG activity was performed for each condition. Six participants performed the tasks. Of these the first two were for determination of measurements and procedures. The remaining four participants completed all conditions. We also asked each participant to complete the NASA TLX workload rating scale after he or she completed each game condition.

Here we have analyzed data from the four participants (A, B, C, D) who completed all conditions. Each participant performed two *sessions* (or repetitions of all conditions) on two separate days. For an outline of the protocol for sessions and days see Appendix 2

We recorded EEG from a standard 19-channel referential montage placed on the scalp according to the International 10-20 system. EEGs were sampled at 128 Hz with an analog low pass filter setting of 64 Hz. No additional filtering was applied to data. EEGs were then segmented into consecutive non-overlapping 2-s windows. As in the USAF-C analyses, we used the Thompson Multi-taper method to compute power spectral densities (PSD). From the PSDs we also computed three measures of coherence, the *magnitude squared coherence,* or $C_{xy,}$ the cross-*spectral power density,* or $P_{xy,}$ and *the transfer function estimate,* or $T_{xy,}$ as defined in Equations 2-5 above.

5.2.3.2 Results

5.2.3.2.1 Spectral representation

In the first step, a spectral representation of the EEG was used in the PARAFAC model. First, the PARAFAC model was run using the full set of 19 EEG electrodes. This was done by using the data from each day and each participant separately. However, the vector of electrode loadings with very high levels indicated a noise component on some electrode sites. Very high noise levels were in general observed at the temporal sites T7 and T8 and the frontal sites Fp1, Fp2, Fz, F4 or F5. This was already observed in the Quasar study. Therefore, the electrodes indicating high level of noise were selectively removed and the PARAFAC model was run again. This was done for each participant separately. In all the case this resulted into the extraction of the physiologically more plausible results in comparison to the models with the full EEG electrodes set. In addition the PARAFAC model has been run two times. After the convergence of the first run the points with high values of the residual variance and leverage, that is, points indicating noisy samples, were inspecting. The points exceeding 95 or 99 percentile of the residual variance and leverage distribution were removed and the PARAFAC model was run again. In general, this procedure removed points with very high values of temporal signatures. The core consistency[10] of these final models was in all cases greater than 85% indicating a good model fit.

5.2.3.2.1.1 Participant A

After running the PARAFAC model with the full set of electrodes, the electrodes located at sites Fz, F4, T7, T8, and Fp2 were removed from the further analysis. Figure 14 summarizes the results obtained by running the PARAFAC model on the first day data. Three distinct atoms can be observed. While the first atom seems to represent overall EEG power, the second and the third atoms discriminate workload increase and engagement/disengagement in the task. While the spectral signature vector of the second atom shows two peaks in the theta and alpha band, the spectral signature of the third atom has a single peak in lower alpha band. Note that these two spectral loading vectors have complimentary character. The bottom plot shows in details the temporal signature of the second atom where a nice separation of the individual workload levels can be observed. Note that for better visualization the values of the temporal loading vectors were smoothed with a robust quadratic fit smoothing method using the smoothing window of 10 points.

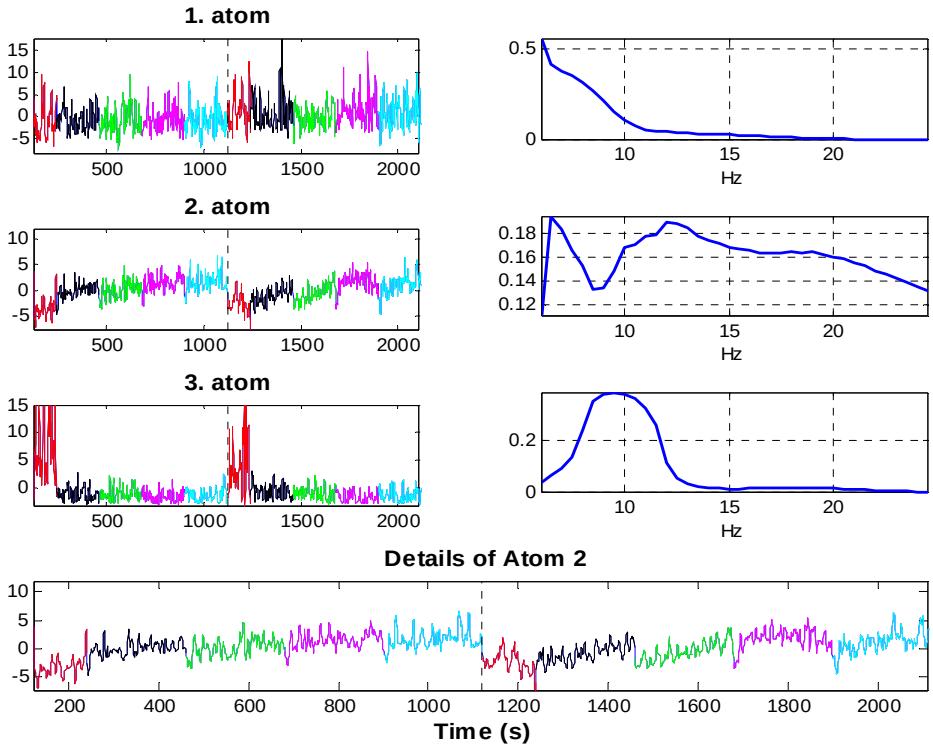

Figure 14. Loadings of the three PARAFAC atoms extracted from EEG recordings of Participant A, Day 1. Left panel: Temporal signatures of the EEG atoms. Colors indicate periods of different workload tasks (red - resting/relaxing; black - 1 enemy; green - 1 enemy + counting; purple - 5 enemies; cyan - 5 enemies + counting). Vertical dotted line separates two distinct experimental sessions. Bottom panel: The detailed plot of the temporal loadings of Atoms 2. Right panel: Spectral signatures corresponding to the atoms numbered in the left panel.

However, it is interesting to see temporal signatures without smoothing, especially during the transition periods between different workload tasks. This is depicted in Figure 15 for three different workload tasks. We can see very nice decrease during these transient periods when the protocol is re-set and participant is relaxed. The temporal signature values of these transition periods are similar to task 1 when the participants were instructed to be relaxed.

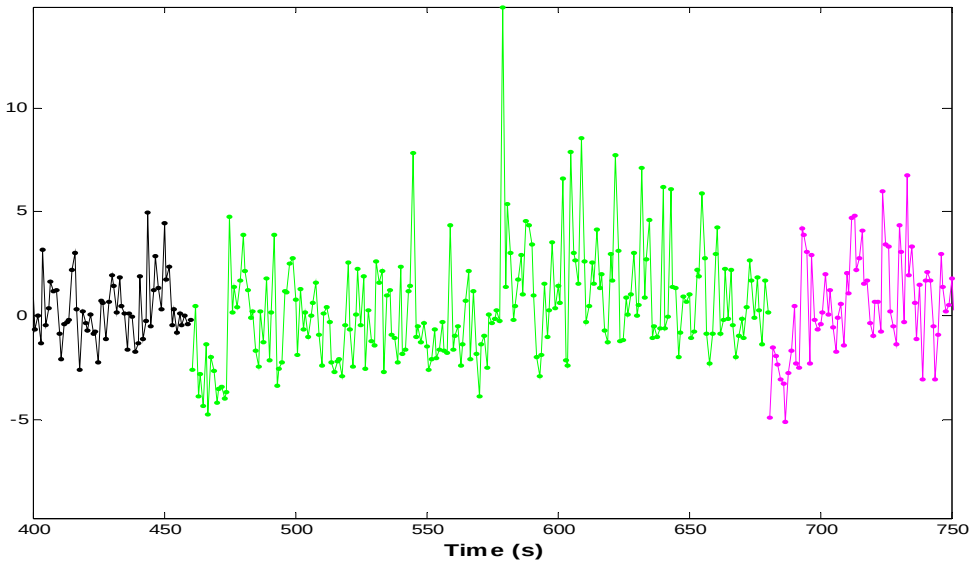

Figure 15. Transient periods between three different workload task (1 enemy + counting; 5 enemies; 5 enemies + counting). No smoothing of the loadings values was used.

Next, the same PARAFAC model setting was used for the second day data of the same participant. The results are depicted in Figure 16. Again we can see two distinct atoms reflecting workload levels (Atom 1) and engagement/disengagement (Atom 3). Although the Atom 1 does not show as clear peaks as in the case of Day 1 data, high levels of low frequency (theta) and an increase in the higher alpha is visible. Atom 3 reflecting engagement/disengagement seems to be stable over the both days. This stability can be also observed in the spatial signatures plotted in Figure 17. We can see that this 'engagement/disengagement atom' is associated with high loadings in midline parieto-central and occipital sites. The spatial loading vectors for the 'workload atom' are depicted in Figure 18. In this case the high spatial loading levels can be observed in the occipital region and over the P7 and P8 regions. The high values over the F7 and Fp1 observed during the first day were not observed in the second day results.

Next, the stability and predictability of these models were investigated by varying training data sets. First, the model was trained using the Day 1 data and the temporal signature corresponding to the workload atom was extracted using the second day data. This signature was then compared with the temporal signature extracted using the second day data only. Then, the procedure was repeated by switching the days; that is, the model was constructed using the second day data and the workload atom related temporal signature from the first day data was extracted. The results of this experiment are depicted in Figure 19 and Figure 20. We can see very close match between the predicted signatures atoms and the signatures extracted directly from the data. This is very promising result indicating ability of the method to extract stable data components which can be used for predicting workload levels from the data recorded at in time separated runs (days). The same stable temporal signatures reflecting workload levels were also observed in participant C.

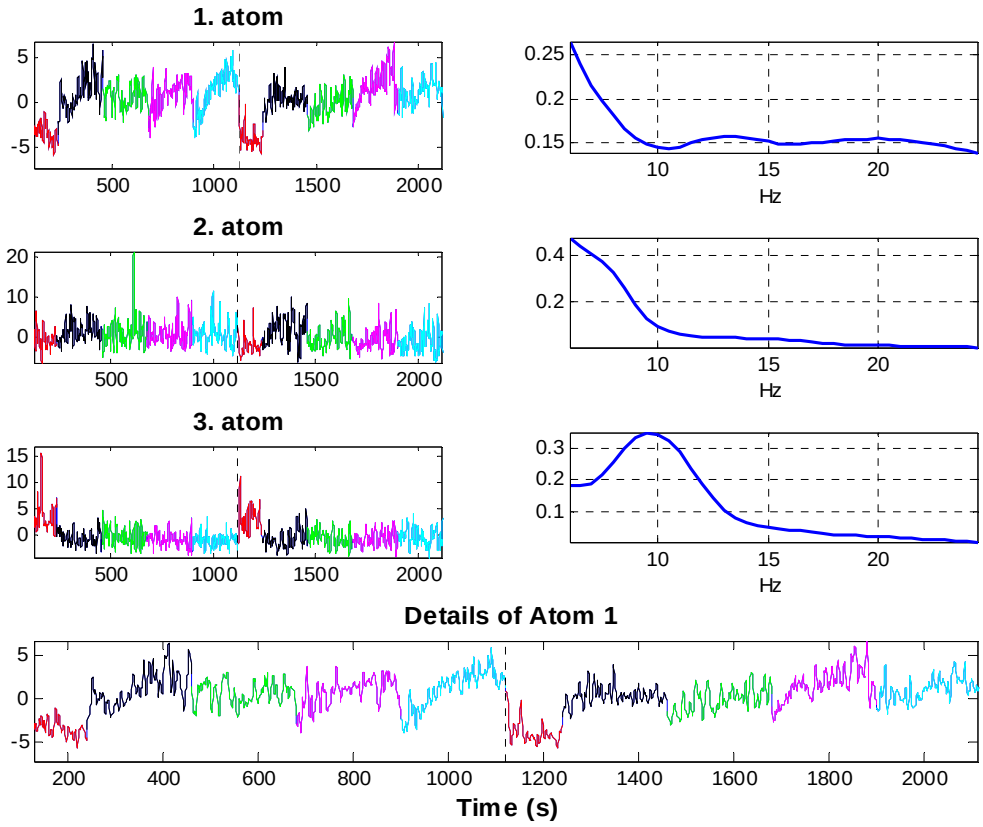

Figure 16. Loadings of the three PARAFAC atoms extracted from EEG recordings of Participant A, Day 2. Left panel: Temporal signatures of the EEG atoms. Plotting conventions are the same as in Figure 14. Bottom panel: The detailed plot of the temporal loadings of Atom 1. Right panel: Spectral signatures corresponding to the atoms numbered in the left panel.

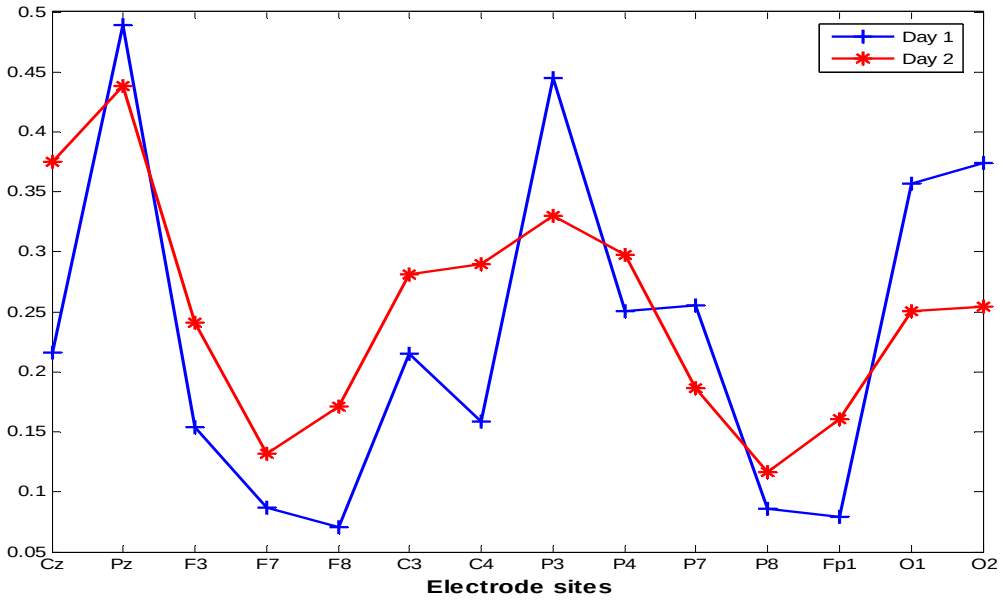

Figure 17. Participant A. Comparison of the Day 1 and Day 2 spatial signatures (loading vectors) corresponding to the engagement/disengagements atom.

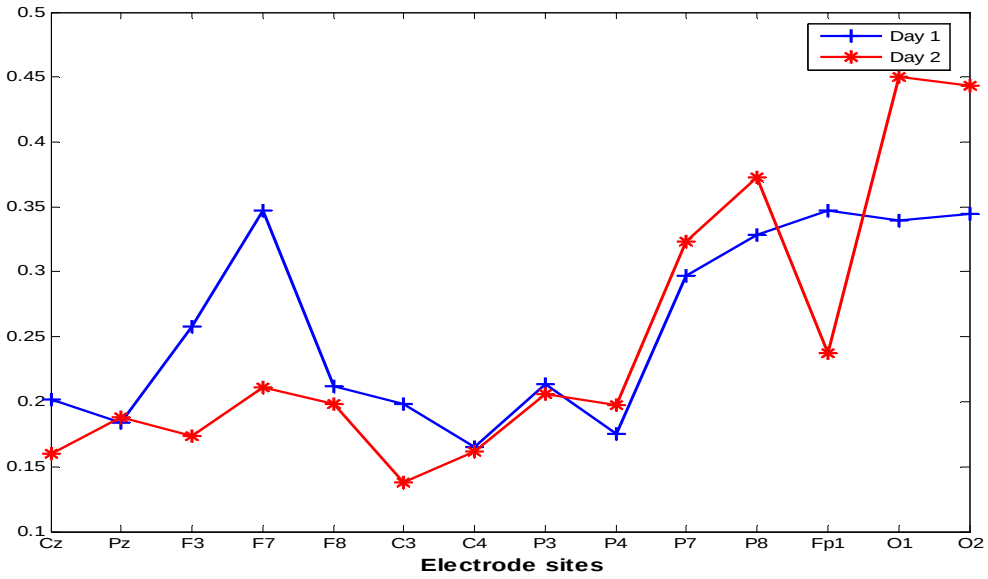

Figure 18. Participant A. Comparison of the Day 1 and Day 2 spatial signatures (loading vectors) corresponding to the workload atom.

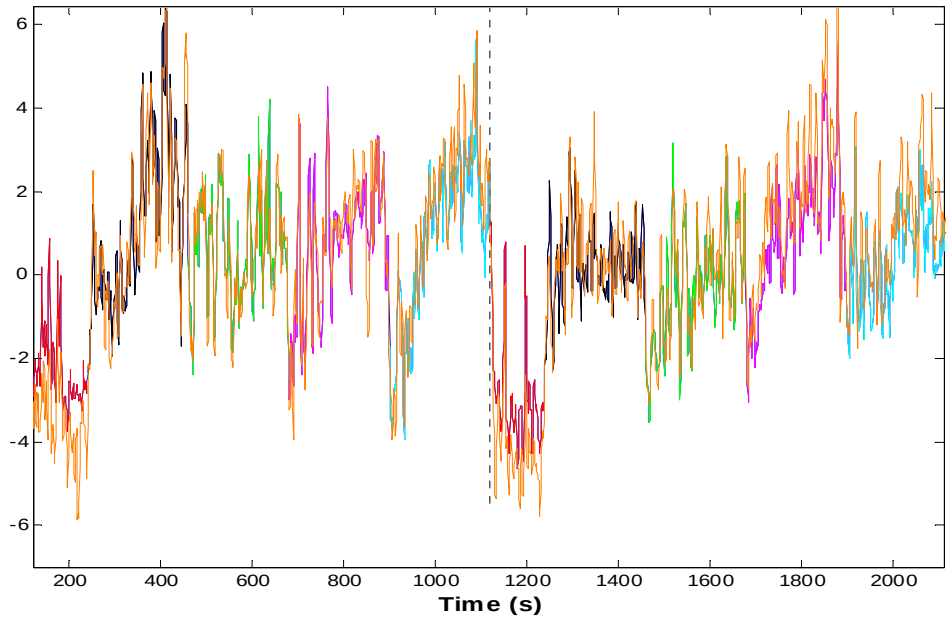

Figure **19**. Temporal signatures for Day 2. Comparison of the predicted temporal signature of the workload atom using the PARAFAC model trained on Day 1 data and the temporal signature (orange) extracted from the Day 2 PARAFAC model. Colors indicate periods of different workload tasks (red – resting/relaxing; black - 1 enemy; green - 1 enemy + counting; purple - 5 enemies; cyan - 5 enemies + counting).

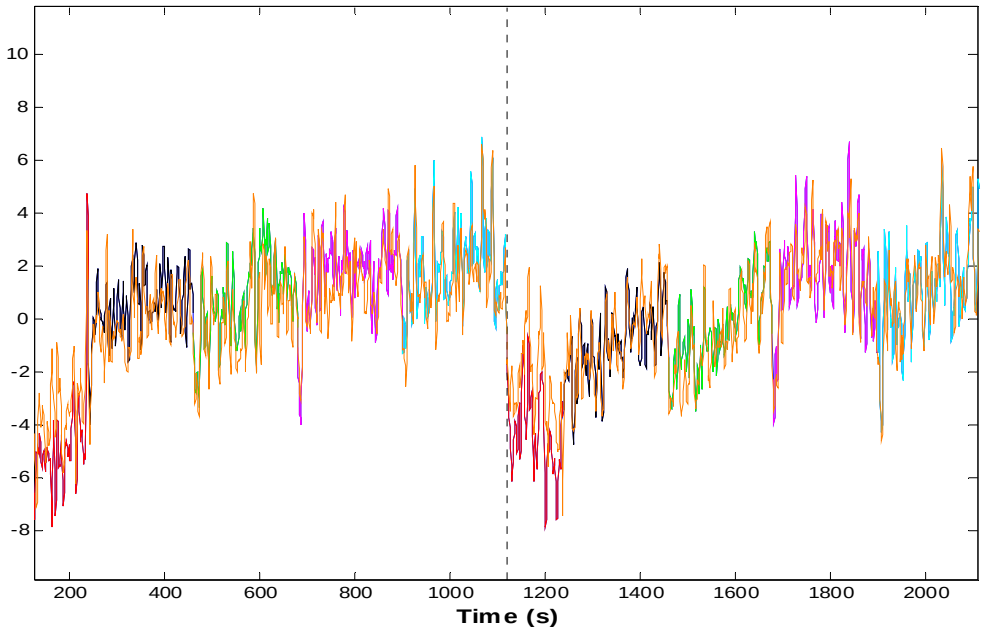

Figure **20**. Temporal signatures for Day 1. Comparison of the predicted temporal signatue of the workload atom using the PARAFAC model trained on Day 2 data and the temporal signature (orange) extracted from the Day 1 PARAFAC model. Colors indicate periods of different workload tasks (red - resting/relaxing; black - 1 enemy; green - 1 enemy + counting; purple - 5 enemies; cyan - 5 enemies + counting).

5.2.3.2.1.2 Participant B

Running the three components PARAFAC model in this participant resulted in a low (< 40%) core consistency value indicating a poor fit of the model. This was in spite of the fact that the EEG channels (Fz, F7, F8, T7, T8, and Fp2) showing a high level of noise was removed after running the PARAFAC model using the full set of 19 electrodes. Therefore, two components model was used.

The results of this model for the first day are depicted in Figure 21. Similar results were obtained for Day 2 and are not plotted here. Again, we can observed the temporal signatures reflecting the participant's engagement/disengagement in the task (Atom 1), but no clear atom reflecting the workload levels can be observed. The spatial signatures of Atom 1 were very similar to ones observed in participant A; that is, signatures with high values over midline parietal and occipital sites were observed.

5.2.3.2.1.3 Participant C

Due to high level of noise channels Fz, F3, F4, Fp1, Fp2, T7 and T8 were removed from the analysis. Three components PARAFAC model has shown three distinct atoms and the results also indicated good fit of the model to the data (core consistency > 85%). Results using the Day 1 and Day 2 data are depicted in Figure 22 and Figure 23, respectively. Again we can clearly see the temporal signatures discriminating participant's engagement and disengagement in the task (Atom 3, Day 1 and Atom 3, Day 2). This atom has spectral peak at about 8 Hz and its spatial distribution resemble the one already observed in Participants A and B; that is, a higher loadings can be observed over the mid-line centro-parietal and occipital regions. Again, similar to participant A, the workload related temporal signatures can be observed (Atom 2, Day 1, and Atom 3, Day 2).

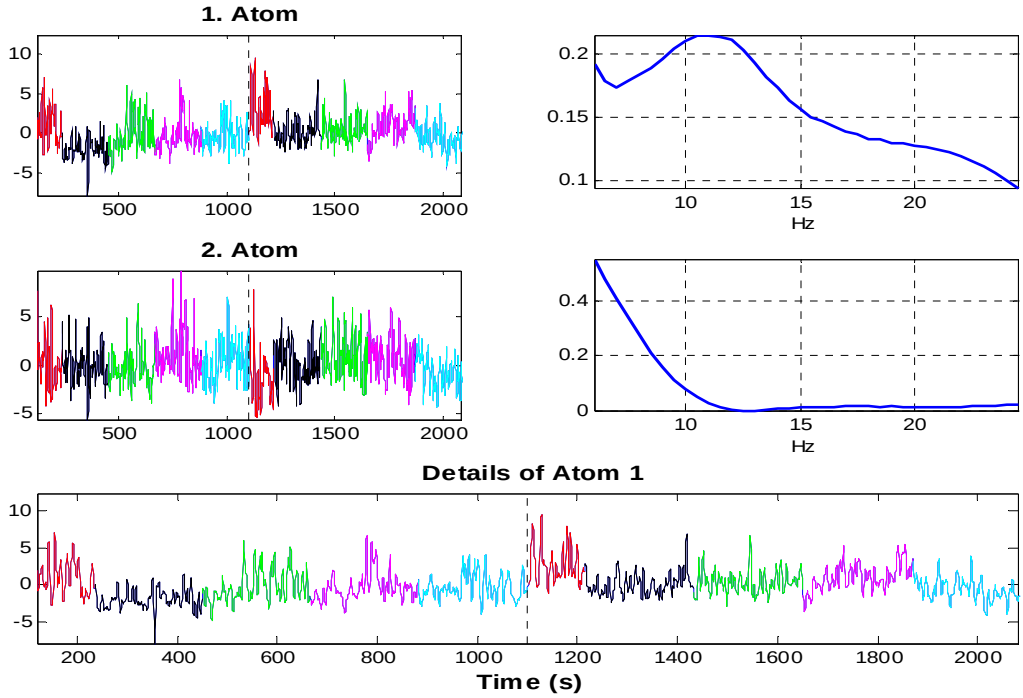

Figure 21. Loadings of the two PARAFAC atoms extracted from EEG recordings of Participant B, Day 1. Left panel: Temporal signatures of the EEG atoms. Plotting conventions are the same as in Figure 14. Bottom panel: The detailed plot of the temporal loadings of Atom 1. Right panel: Spectral signatures corresponding to the atoms numbered in the left panel.

The spatial distribution of this workload related atom reveled higher loading values over the occipital region, but in addition, and in contrast to participant A, higher values of the loading vectors were also observed over the midline central and parietal sites (Cz, Pz). Similar to participant A, testing for stability and predictability revealed highly consistent extraction of the temporal signatures when training and testing sets were varied; that is, building the model on one day and extracting the temporal signatures using the other day data. Finally, in contrast to participant A and B, the third temporal signature indicates possibility to discriminate periods when participant were instructed to count events versus the periods without counting. This atom (Atom 1 in Figure 22 and Figure 23) shows clear peak centered around 10 Hz and its spatial distribution shows concentration over the parietal sites (Pz, P3, P4). Note that the counting periods are somehow mixed with the periods of disengagement (red). This can be due to the fact that the engagement/disengagement atom is also characterized by high values of spatial loadings over the parietal sites (see Figure 17). However, in contrast to the 'counting/non-counting' atom, the engagement/disengagement atom has the spectral peak shifted to lower frequencies and centered at around 8 Hz. Interestingly, the combination of these two atoms suggests the ability of a hierarchical discrimination between engagement and disengagement in the first step, and in the second step the discrimination between counting and no counting periods when the participant in engaged in the task. Note that this is very interesting result not observed in the previous studies. However, until now this atomic decomposition was observed only in participant C.

5.2.3.2.1.4 Participant D

Channels F7, F8, T7, T8, Fp1 and Fp2 were removed after running the PARAFAC model with the full set of 19 EEG electrodes. Results for the three components PARAFAC model computed over the first day data are depicted in Figure 24. Again the first and the second atoms represent the engagement/disengagement and workload atoms already observed in the previous participants.

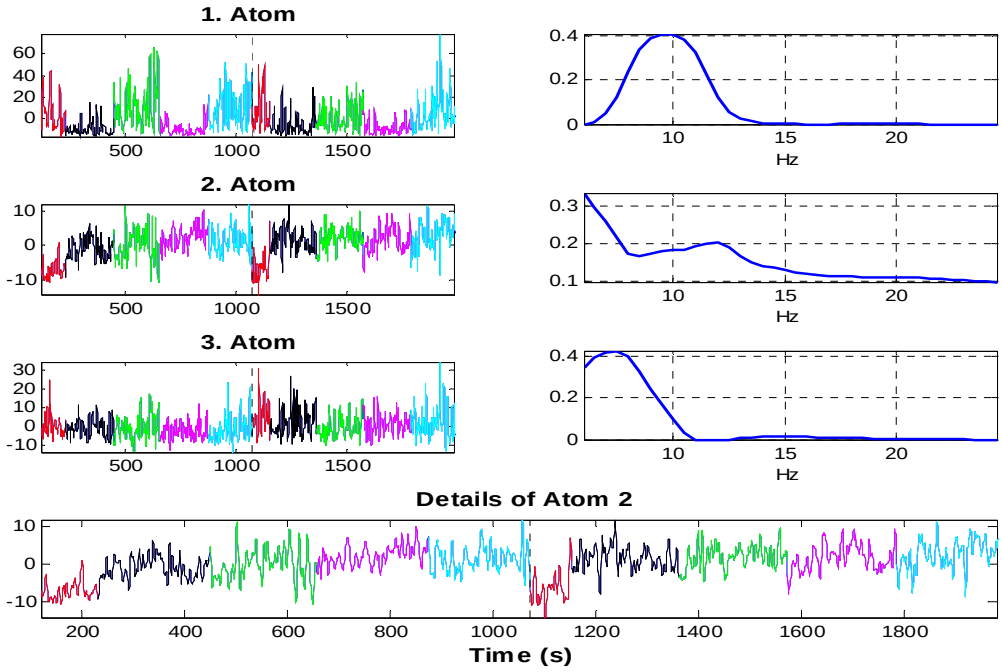

Figure 22. Loadings of the three PARAFAC atoms extracted from EEG recordings of Participant C, Day 1. Left panel: Temporal signatures of the EEG atoms. Plotting conventions are the same as in Figure 14. Bottom panel: The detailed plot of the temporal loadings of Atom 2. Right panel: Spectral signatures corresponding to the atoms numbered in the left panel.

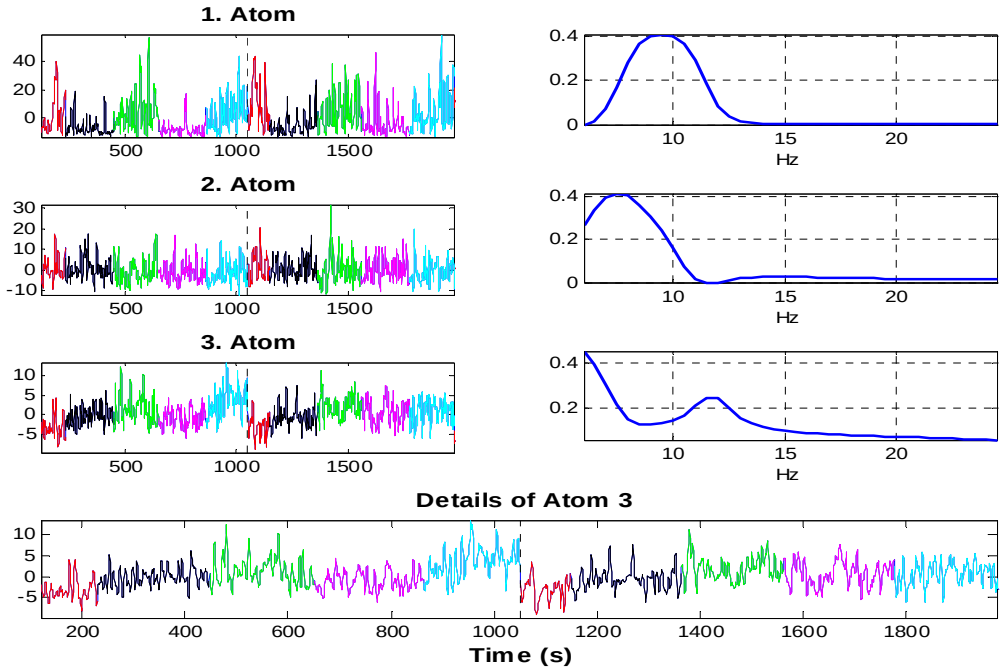

Figure 23. Loadings of the three PARAFAC atoms extracted from EEG recordings of Participant C, Day 2. Left panel: Temporal signatures of the EEG atoms. Plotting conventions are the same as in Figure 14. The detailed plot of the temporal loadings of Atom 3. Right panel: Spectral signatures corresponding to the atoms numbered in the left panel.

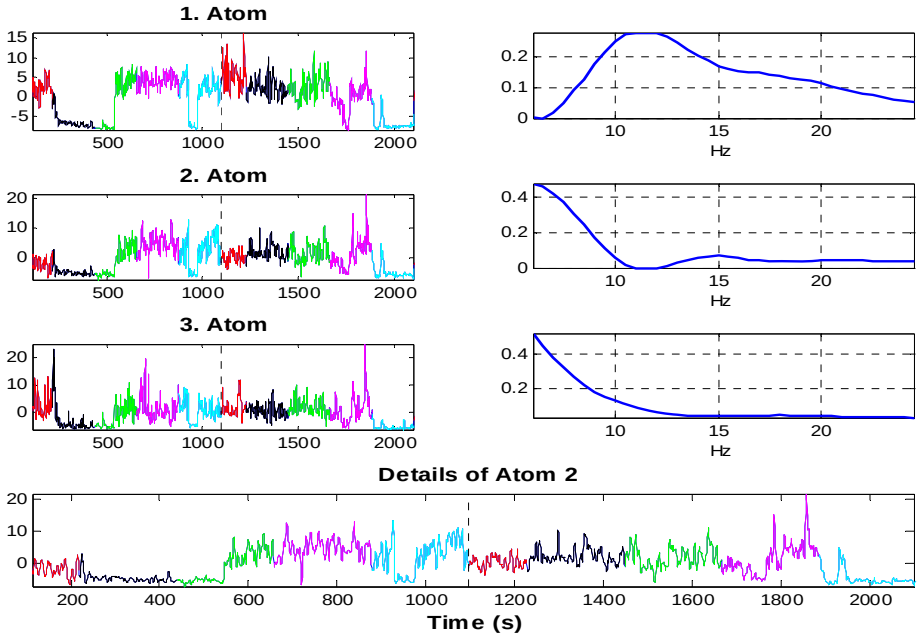

Figure 24. Loadings of the three PARAFAC atoms extracted from EEG recordings of Participant D, Day 1. Left panel: Temporal signatures of the EEG atoms. Colors indicate periods of different workload tasks (red – resting/relaxing; black- 1 enemy; green- 1 enemy + counting; purple - 5 enemies; cyan - 5 enemies + counting). Vertical dotted line separates two distinct experimental sessions. Bottom panel: The detailed plot of the temporal loadings of Atom 2. Right panel: Spectral signatures corresponding to the atoms numbered in the left panel.

Also the spatial distribution resembles the previously observed patterns of these two distinct atoms and is not plotted here. However, unexpectedly low values (drops) of the temporal signatures can be observed during several time periods. Detailed investigation of the PSD has revealed 4 to 5 times higher power over all EEG electrodes, predominately in the lower frequency bands, indicating severe noise component possibly due to the measuring device failure. Thus, the proposed atomic decomposition method also demonstrates ability to automatically detect noisy periods, and avoid the tedious task of the visual inspection of individual 2-sec periods one by one. Finally, results using the second day data are plotted in Figure 25. Again spectral and spatial (not plotted here) signatures indicate the presence of the engagement/disengagement (Atom 1) and the workload atom (Atom 3). However, these atoms seem to be somehow mixed. The spectral peak of the engagement/disengagement atom is more spread to higher frequencies and not compactly peaked as we could observe in the participants A, B and C. Also the temporal signatures does not indicate as high discrimination abilities between the engagement and disengagement periods and workload periods as we could observe especially in the participants A and C.

5.2.3.2.2 Coherence representation

Again, except the participant B a three- component PARAFAC model has shown a good fit to data. In the case of participant B two components model was preferred. For individual participants the same EEG electrodes were used as in the case of spectral representation. Coherence among all possible electrode pairs was computed and used in the model.

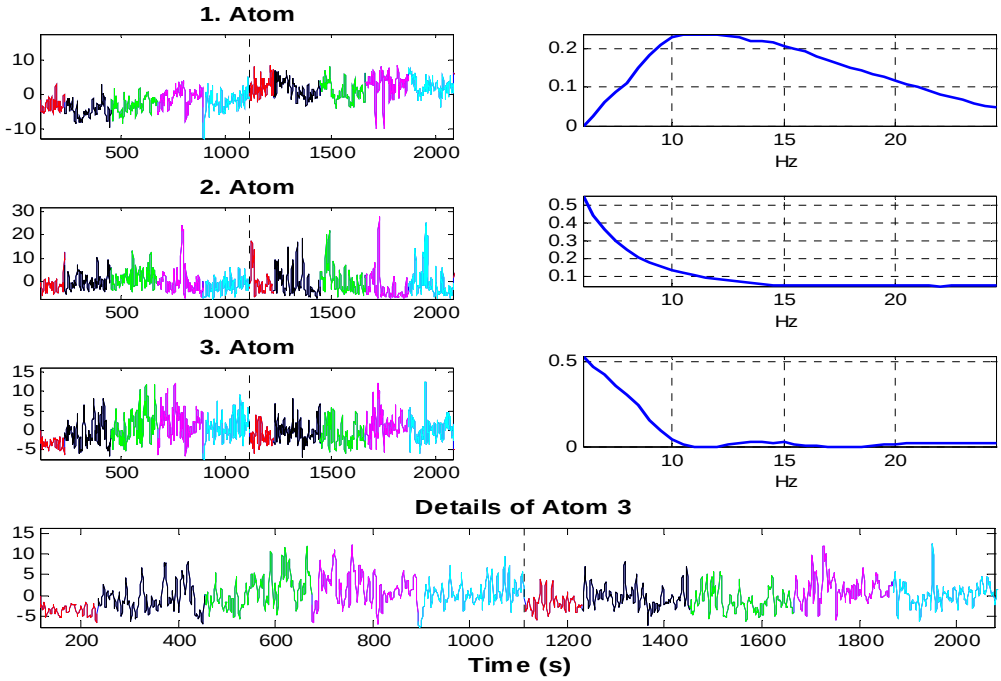

Figure 25. Loadings of the three PARAFAC atoms extracted from EEG recordings of Participant D, Day 2. Left panel: Temporal signatures of the EEG atoms. Colors indicate periods of different workload tasks (red – resting/relaxing; black- 1 enemy; green- 1 enemy + counting; purple - 5 enemies; cyan - 5 enemies + counting). Vertical dotted line separates two distinct experimental sessions. Bottom panel: The detailed plot of the temporal loadings of Atom 3. Right panel: Spectral signatures corresponding to the atoms numbered in the left panel.

5.2.3.2.2.1 Participant A

The PARAFAC model with the C_{xy} coherence representation resulted in the extraction of three distinct atoms (for Day 1, Figure 26). These atoms resemble the atoms observed when spectral representation was used (Figure 14). However, the coherence representation indicates a compactly peaked coherence at around 8 Hz (more narrow) for the engagement/disengagement atom (Atom 3) and a smooth frequency loadings representation for the workload atom (Atom 2). Similar results were observed for the second day data and are not plotted here. The value of 90 percentile was computed from the distribution of the spatial loading vector of electrode pairs and all pairs for which the loading values exceeded this percentile (value equal to 0.1307) were connected in the bottom plot of Figure 26. The spatial distribution of the workload atom (Atom 2) indicates importance of the parieto-ocipital, occipito-occipital, but also some influence of the parieto-central and front-frontal pairs. The same procedure was repeated for Atom 3 representing the engagement/disengagement. Ninety percentile was equal to 0.1611 and extracted coherence pairs indicating mainly the importance of the centro-frontal, centro-central, and centro-parietal pairs. The influence of the fronto-frontal and fronto-central pairs can be also observed but coherence values for these electrode pairs were smaller. Next, in Figure 27 the distribution of the spatial signatures representing importance of the individual coherence electrode pairs is compared for Day 1 and Day 2. Very good match between these two days can be observed for both the workload and engagement/disengagement atoms indicating stability of these components over two distinct days.

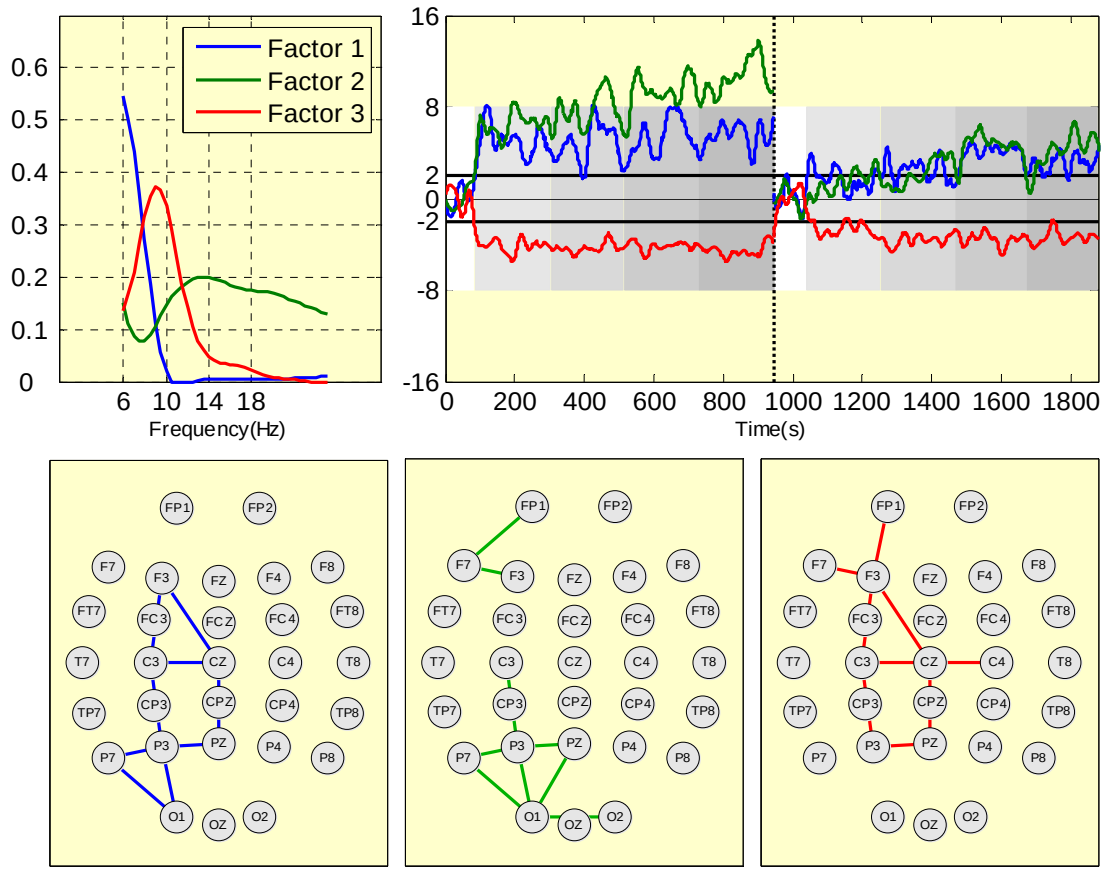

Figure 26. Loadings of the three PARAFAC atoms extracted from EEG recordings of Participant A, Day 1. Top-Left panel: Spectral signatures. Top-right panel: Z-scores of the temporal signatures of the EEG atoms numbered in the right panel. Shaded areas indicate periods of different workload (from left to right: (resting/relaxing; 1 enemy; 1 enemy + counting; 5 enemies; 5 enemies + counting). For the Z-scores computation (mean and standard deviation) data of low workload periods were used. This was done for each trial separately. Vertical dotted line separates two distinct experimental sessions. Moving average smoothing with the length of 60 points was used. Bottom panel: The coherence plot (connecting lines) of the electrode pairs exceeding the 90 percentile of the all coherence values distribution.

In contrast to $C_{xy,}$ the P_{xy} and T_{xy} coherence measures did not reveal clear discriminative power of the temporal signatures corresponding to the engagement/disengagement and workload atoms. However, a distinct atom separating the periods of engagement and disengagement was observed in the case of T_{xy} during the both days. The vectors of temporal, spatial and frequency signatures of this atom are plotted in Figure 28. High values of loadings concentrated at frequencies above 19 Hz can be observed. This suggest the importance of the beta frequencies but also the possibly of a noise component due to the movement. Note that this atom nicely separates engagement periods versus disengagements periods also when participants are shortly relaxed during the periods when the workload task are reset. To better understand this atom, the spatial distribution of the electrode pairs was investigated. It can be observed that the dominate coherence pairs are almost all connected to P8, therefore indicating possible movement related component in EEG which helps to separate the periods on task engagement versus disengagement. This is important finding because one can possibly filter out this component if this movement related atom is not of interest.

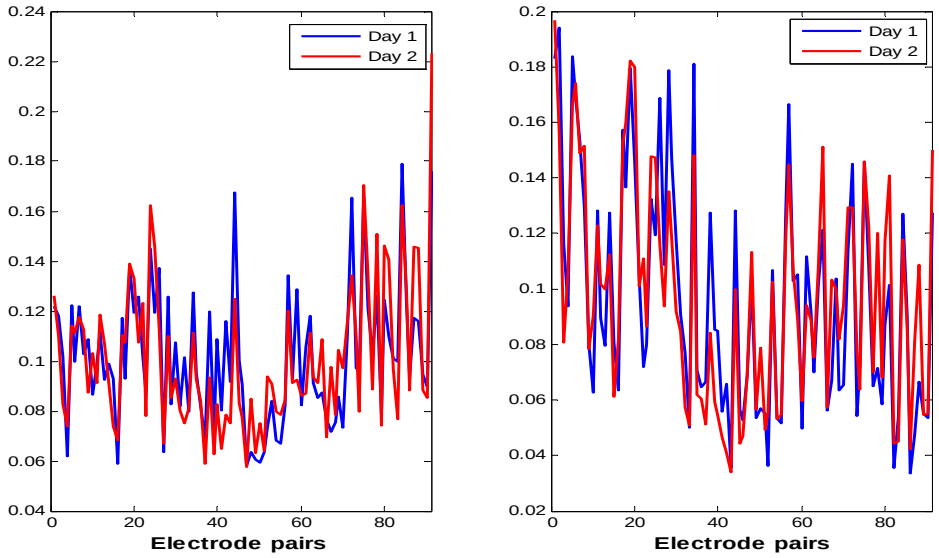

Figure 27. Participant A. comparison of the Day 1 and Day 2 spatial (electrode pairs) signatures (loading vectors) corresponding to the workload (left) and engagement/disengagements atoms (right).

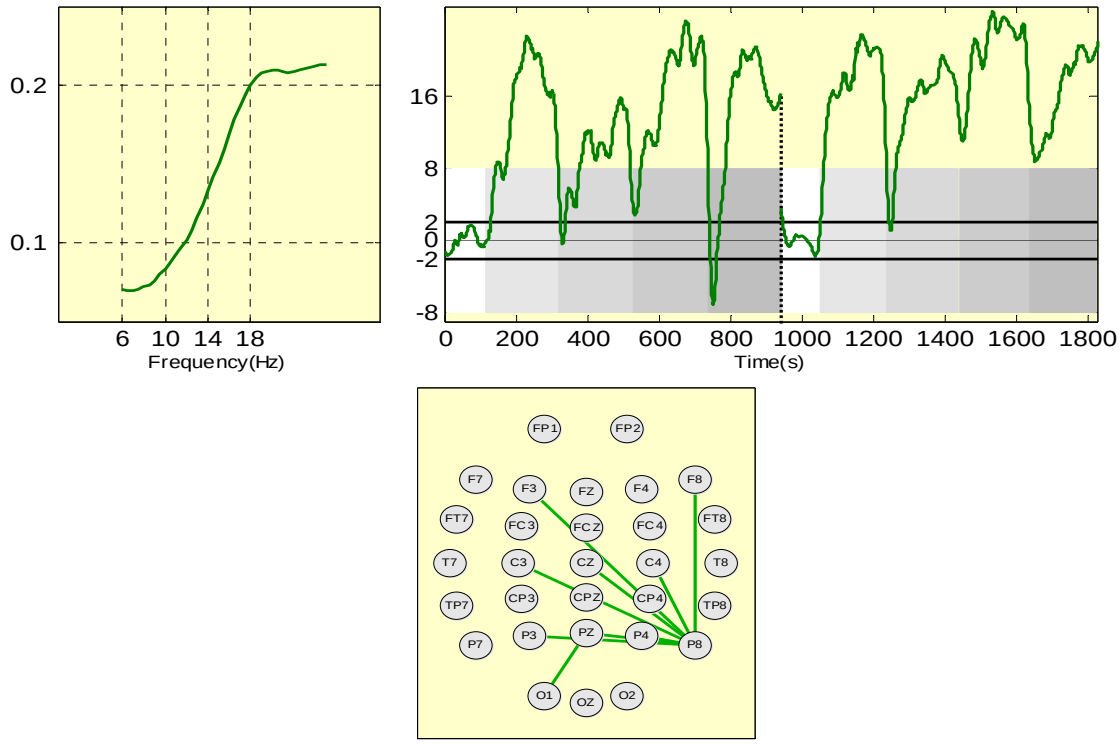

Figure 28. Loadings of the 'movement related' PARAFAC atom (Atom 2) extracted from EEG recordings of Participant A, Day 2. Top-Left panel: Spectral signatures. Top-right panel: Z-scores of the temporal signatures of the EEG atoms numbered in the right panel. Plotting conventions are the same as in Figure 26. Bottom panel: The coherence plot (connecting lines) of the electrode pairs exceeding the 90 percentile of the all coherence values distribution.

5.2.3.2.2.2 Participant B

Similar to the spectral representation, the coherence representation did not reveal the workload related atom in this participant. The engagement/disengagement atom has shown more compact spectral profile (narrow) peak around 11 Hz in comparison to the spectral signature plotted in Figure 21. Interestingly, T_{xy} representation has revealed the movement related atom similar to the one already observed in participant A. However, now the coherence pairs showing the highest loadings values were associated with P7 and not the P8 electrode.

5.2.3.2.2.3 Participant C

The PARAFAC atomic decomposition revealed three distinct atoms related to workload, task engagement/disengagement and the atom discriminating the counting and non-counting periods. Although this was already observed while using the spectral representation, the frequency distribution of the C_{xy} coherence is more peaked and interestingly the vector of temporal loadings indicate no mixing among the periods of counting and the relaxed to task disengaged periods. This is demonstrated in Figure 29.

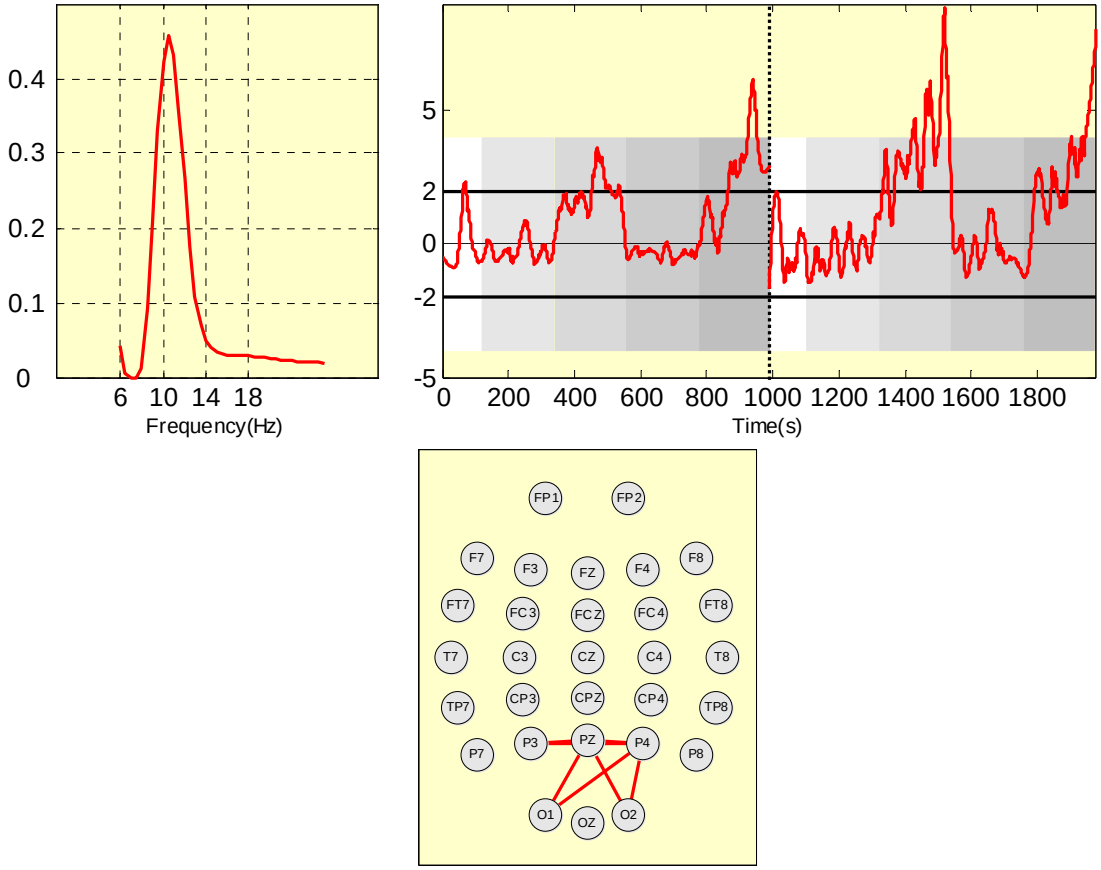

Figure 29. Loadings of the 'counting versus non-counting related' PARAFAC atom (Atom 3) extracted from EEG recordings of Participant C, Day 2. Top-Left panel: Spectral signatures. Top-right panel: Z-scores of the temporal signatures of the EEG atoms numbered in the right panel. Plotting conventions are the same as in Figure 26. Bottom panel: The coherence plot (connecting lines) of the electrode pairs exceeding the 90 percentile of the all coherence values distribution.

This interesting feature of the coherence representation is giving raised to the possibility to clearly discriminate the periods of task engagement, and subsequently to discriminate periods of counting versus the periods of non-counting. The spatial distribution of high loadings (90 percentile) shows the importance of the midline oriented parietal and occipital coherence pairs at the frequency peaked around 10.5 Hz. Finally, no movement related atom discriminating the periods of task engagement from relaxing periods was observed in this participant. Finally, no movement related atom discriminating the periods of task engagement from relaxing periods was observed in this participant.

5.2.3.2.2.4 Participant D

The previously reported spectral representation results indicated the periods of possible electrodes or measurement device failure in this participant during the first day experiment. The same pattern was observed for the C_{xy} coherence measure. In contrast, the P_{xy} and T_{xy} coherence measures do not show these extreme temporal loadings drops possibly due to the fact that the values of these measures are normalized using the power spectrum density of both or a single channel. However, none of these measures have shown atoms clearly discriminating the different workload levels or engagement vs. disengagement periods. This is not surprising because the noisy element in the data cannot be simply filtered out just by using the different coherence measures. Atomic decomposition similar to the one already depicted in Figure 25was observed when using the Day 2 data.

Participants: a) were given an orientation to the study, b) read and signed an informed consent document, c) completed a brief demographic questionnaire (age, handedness, hours of sleep, etc.), d) practiced the arithmetic task for 10 minutes, and e) were prepared for EEG and EOG data collection. They then completed the pretest self-report measures (i.e., the AD-ACL and VAMS) and performed the mental arithmetic task until either three hours had elapsed or they were unwilling to continue. After the task, they completed post-test self-report measures and were debriefed.

The EEGs were: a) submitted to an algorithm for the detection and elimination of eye-movement artifact, b) visually examined and blocks of data containing artifact were manually rejected, c) epoched around the stimulus (i.e., from –5 s pre-stimulus to +8 s post -stimulus), d) low pass filtered (50 Hz; zero phase shift; 12 dB/octave roll off), and e) submitted to an automated artifact rejection procedure (i.e., absolute voltages > 100 µV). The overall single-epoch rejection rate was 47%. The 'cleaned and filtered' epochs were decimated to a sampling rate of 128 Hz. EEG power spectra were estimated with Welch's periodogram method at 833 frequencies from 0-64 Hz.

5.2.4 NASA-C Database

5.2.4.1 Methods

5.2.4.1.1 Task and Data Collection Procedures

Participants sat in front of a computer with their right hands resting on a 4-button keypad and performed arithmetic summation problems, consisting of four randomly generated single digits, three operators, and a target sum (e.g., 4+7–5+2=8), which were displayed on a computer monitor continuously until the subject responded. The participants: a) solved the problems, b) decided whether their 'calculated sums' were less than, equal to, or greater than the target sums provided, c) indicated their decisions by pressing the appropriate key on the keypad. The keypad buttons were labeled "<," "=," and ">," respectively. Subjects were told to answer as quickly as possible without sacrificing accuracy. After a response, there was a 1 s inter-trial interval, during which the monitor was blank. Participants performed the task until either they quit from exhaustion or 3 h had elapsed. All participants performed the task for at least 90 min and eleven participants completed the maximum 3 h period.

During the task, the EEG was recorded continuously using 32 Ag/AgCl electrodes embedded in a Quik-Cap™.[36] The reference electrodes were averaged mastoids and the ground electrode was located at AFz. Vertical and horizontal EOG were recorded using bipolar pairs of 10 mm Ag/AgCl electrodes (i.e., one pair above and below the left eye; another pair to the right and to the left of the orbital fossi). Impedances were maintained at less than 5 kΩ for EEG electrodes and less than 10 kΩ for EOG electrodes. The EEG was amplified and digitized with a calibrated 64-channel Synamps™ system**Error! Bookmark not defined.**, with a gain of 1,000, sampling rate of 500 Hz and a pass band of 0.1 to 100 Hz, then digitized and stored on magnetic and optical media.

5.2.4.1.2 Spectral representation of EEG

In the first step, a spectral (PSD) representation of the EEG was used in the PARAFAC model. First, the PARAFAC model was run using the full set of 30 EEG electrodes. This was done by using the data from each participant separately. However, as in the other databases the vector of electrode loadings with very high levels indicated a noise component on some electrode sites. Very high noise levels were in general observed at the temporal sites T7 and T8 and the frontal sites Fp1, Fp2, Fz, F4 or F5. We used the same method of electrode removal as for the APECS-W algorithm development described in the preceding sections. The electrodes indicating high level of noise were selectively removed from each participant's data and the PARAFAC model was run again. This was done for each participant separately. In all cases this resulted into the extraction of the physiologically more plausible results in comparison to the models with the full EEG electrodes set. In addition we ran the PARAFAC model twice for each participant. After the convergence of the first run the points which exceeded the 90th percentile (lower than the 95 or 99 percentiles used for APECS-W) of the residual variance and leverage distributions (i.e., points indicating noisy samples) were removed and the PARAFAC model was run again. In general, this procedure removed points with very high values of temporal loadings (signatures). The core consistency[10] of these final models was in all cases greater than 80% indicating a good model fits.

We experimented with two-atom, three-atom, and four-atom models. Across subjects, the three atom models were often sufficient to explain all of the experiment-wise variance. For most subjects, however, four-atom models provided fits that were more plausible physiologically. In a few subjects, four-atom models resulted in factors that appeared to split variance spatially but preserve variance temporally and spectrally. For this reason we limited our further investigations to three- or four-atom models choosing the most appropriate model for each subject. Unlike the APCES-W algorithms and the coherence analyses presented below, for all atomic models in these spectral analyses, we did not constrain the solutions for loadings to be nonnegative or unimodal, i.e., no constraints. These PSD analyses were done first, and were extensive, and only later we appreciated that constraints would lead to more easily interpretable models, especially for PSD and coherence measures. However, we chose to leave the PSD analyses in the unconstrained state to allow time for the coherence models, which were more interesting and novel.

We present results from a two-atom model fit to one participant's data to illustrate the effects of a noisy electrode (F1). For this demonstration, a two-atom model was fit to the data. The first atom (blue line) had an extremely large loading on a single, noisy electrode (F7). This atom had a broad spectrum, and loadings on other electrodes were relatively small and unstructured. In contrast, a second atom had a peak near 9 Hz in the power spectrum and loadings that were selectively high at central electrode sites, especially Pz and CPz. This suggests a close association of this atom with the alpha rhythm of the EEG. Interestingly, the loadings of the second atom in the time dimension clearly reflect the development of fatigue between the first 15 minutes of task performance (alert period) and the final 15 minutes (fatigued period). This finding is consistent with effects of increased power in the alpha band during the development of mental fatigue we observed previously with this

data set.[Error! Bookmark not defined.] On the other hand the time loadings of Atom 1, with the broad spectrum and noisy electrode do not reflect the development of fatigue. This suggests a potential method based on atomic decomposition for removal of contaminants from data that are uncorrelated with the experimental treatments or effects.

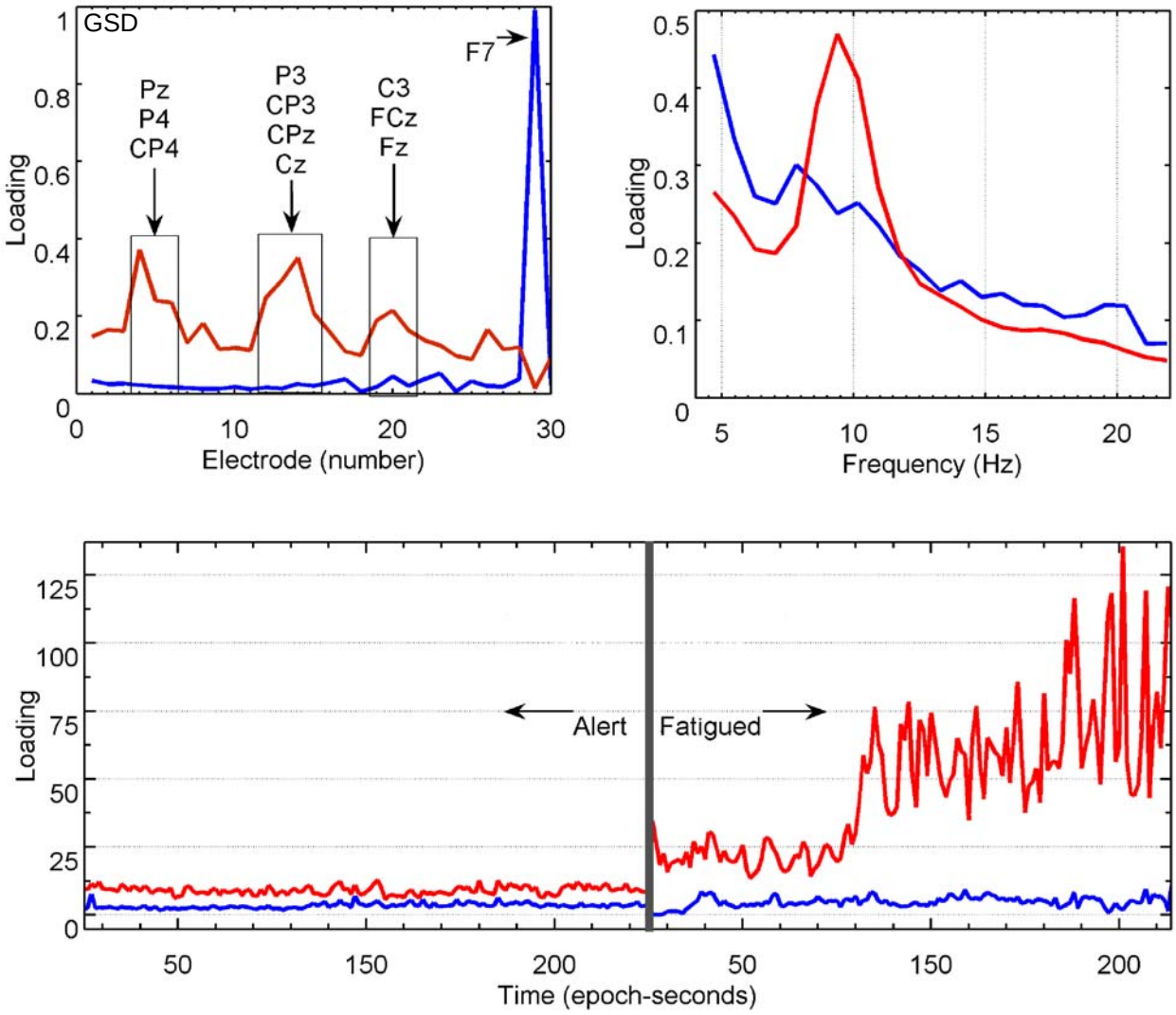

Figure 30. A two-atom model fit to EEG from one participant GSD illustrates the effects of a noisy electrode (F1). Top left panel: the Atom 1 (blue line) had an extremely large loading on a single, noisy electrode (F7), where as the Atom 2 (red line) had selectively high loadings at central electrode sites, especially Pz and CPz. Top right panel: Atom 1 (blue line) had a broad spectrum, whereas Atom 2 (red line) had a single peak near 9 Hz in the power spectrum. Lower panel: the loadings of Atom 2 (red line) in the time dimension clearly reflect the development of fatigue between the first 15 minutes of task performance (alert period) and the final 15 minutes (fatigued period) unlike Atom 1 (blue line). Time is measured in epochs * seconds and is not continuous due to gaps where EEG artifacts where rejected. A smoothing filter with a span of 0.10 was used to illustrate trends.

5.2.4.1.3 General observations

We performed an analysis of the PSDs from EEG recordings of 12 participants in the NASA-C study. The time on task varied considerably among participants, ranging from less than one hour to three

hours. Prior results had shown clearly that fatigue developed during the first 15 to 45 minutes in most participants, so we expected to observe a contrast between alert and fatigued periods when participants performed the task for at least one hour. Participants who did not complete at least one hour of task performance were excluded from the analyses. The analyses are extensive and will require additional examination and statistics for general publication. Nevertheless the results are striking and clearly illustrate the power of the atomic decomposition method for EEG-based estimation of mental fatigue. Eleven of the 12 participants showed evidence of EEG atoms in the alpha and theta bands that changed significantly over time on task. Each subject's results are summarized in a three-part figure, similar to Figure 30. Because the figures are large and numerous, we have included them in an appendix for ease of reference (Appendix 3).

5.2.4.1.4 Three classes of participants

The figures in Appendix 3 contain vast amounts of information that will require additional analyses. However to the point of this study, we are able to confirm the effectiveness of atomic decomposition for isolating atoms that are sensitive to the development of mental fatigue. As the figures in Appendix 3 show, we gauged the significance of a change in the loadings of an atom over time on task by measuring each series of loadings as a set of standard scores (z-scores) which were normalized to the mean and variance of the first fifteen-minute block, when all subjects were alert. We are also able to distinguish individual differences that roughly sort the participants into three classes. The first class contains the vast majority of participants and is characterized by having atoms that reflect EEG power in the theta and alpha bands, where the loadings in both bands change significantly over the course of the task. This class includes eight of the 12 participants: ARB, GSD, JCH, KTT, MMB, MMC, RWC, and RGR. The second class consisted of participants who had only one atom that changed significantly over time on task. This class included JCS, who had only a theta-related atom sensitive to fatigue, and SKH and TBN, who had only an alpha-related atom sensitive to fatigue. The third class included a single subject, WXS, whose EEG atoms did not clearly reflect a trend over time on task. In some cases changes in loadings of atoms over time were increases (mostly) and in other cases they were decreases. The meaning of the direction of change in an atom's loadings is not readily interpretable, as the loadings in other dimensions can be negative or positive, and the sense of the loadings can be inverted without changing the solution of the model from the data. Separate analyses will be required to interpret the meaning of directions of change in the loadings.

5.2.4.1.5 Coherence representation of EEG

As for the other two databases, we used three types of the coherence estimates: 1) the Cross Power Spectral Density (CPSD) estimate via Welch's method (here denoted C_{xy}), 2) the Magnitude Squared Coherence Estimate (denoted P_{xy}), 3) the estimate of the transfer function of the system using the Welch's averaged periodogram method (denoted T_{xy}).

As for the spectral representations, we experimented with two-component, three-component, and four-component models. Again, across subjects, the four component models were sufficient to explain all of the experiment-wise variance and for coherence, we limited our further investigations to four-component models only. For individual participants the same EEG electrodes were used as in the case of spectral representation. Coherence among all possible electrode pairs was computed and used in the model, excluding self-pairings of electrodes.

5.2.4.1.6 General observations

As for the PSDs, we performed an analysis of the magnitude-squared coherences, or C_{xy}, of EEG recordings from 12 participants in the NASA-C study. Prior results with coherence measures had not been examined for these data, so we followed the analysis approach used for the PSDs. Again,

participants who did not complete at least one hour of task performance were excluded from the analyses. Like the PSD analyses, the coherence analyses are also extensive and will require additional examination and statistics for general publication. Each subject's results are summarized in a three-part figure, similar to Figure 26, but with some important differences. Because the number of electrodes was considerably higher than for the APECS-W algorithm developments, we changed the topographical representation. We use instead a mapping algorithm that projects the spherical coordinates of the EEG electrodes on a plane, while preserving the sense of distance and curvature of the head. This is known in map projection geometry as the *Werner* projection, a nonconformal equal-area projection.[37] Although this projection is seldom used in modern cartography, we found it useful for mapping EEG coherences because the projection helps to minimize overlap of lines connecting pairs of electrodes.

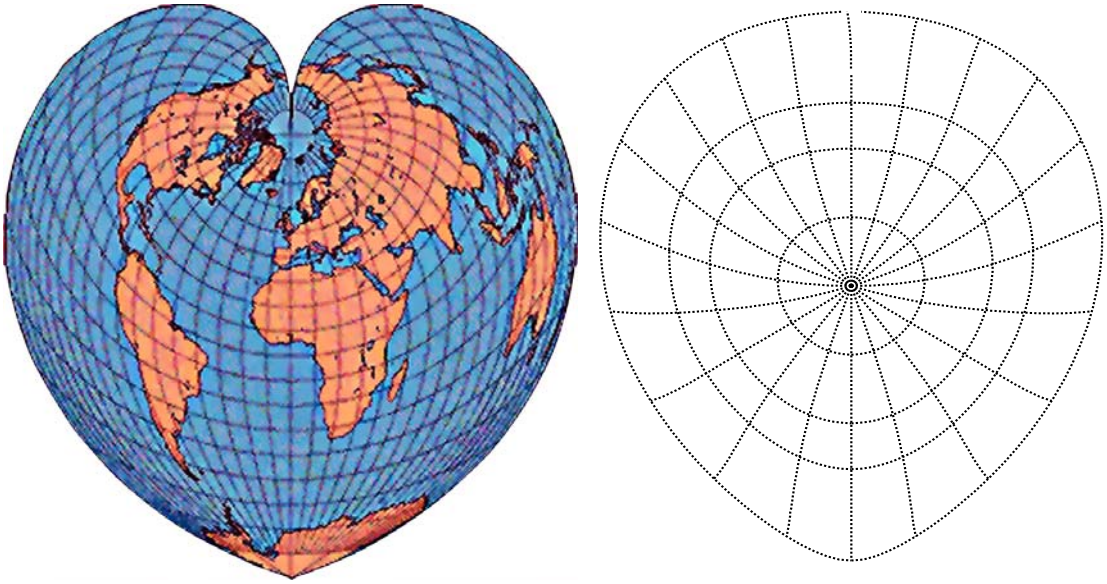

Figure 31. Spherical-planar projection used to map electrode locations and links representing coherences. *Left panel*: in the *Werner Projection*; sectors delimited by standard meridians and parallels have equal area and no overlap. *Right panel*: our projection for mapping EEG coherences, where the North Pole (center) represents the vertex, Cz, frontal direction is up, occipital direction is down, and the right and left are mapped as East and West. The origin of our projection is 70°N, 180°W. The standard meridians lie at increments of 18° and standard parallels lie at increments 30°, 45°, and 67.5°, which align approximately with lines of the International 10-20 system of EEG electrode placement.

As for the PSD analyses, the figures for the coherence analyses are large and numerous, so we have also included them in an appendix for ease of reference (Appendix 4). The results are complex, but also quite striking. They reveal a complexity of interconnections and marked individual differences in the EEG correlates of mental fatigue. Nevertheless there are some unmistakable commonalities among the coherence signatures of certain atoms among the participants. Whereas 11 of the 12 participants showed evidence of PSD atoms sensitive to mental fatigue, all of the participants showed evidence of coherence atoms sensitive to mental fatigue.

Obviously this is a rich and interesting set of results, which call for deeper analysis than afforded by this limited research program. Here, we begin this analysis by summarizing the results according to these broad parameters (Table 2). The patterns are involved, but we can summarize them in terms of three broad parameters: coherence spectrum (theta effects, alpha effects, and effects in non-specific bands such as very low-frequency, high-frequency, or broadband effects), spatial focus (frontal central, parietal), and range of coherence (short, medium, long). It is clear that all regions of the EEG

scalp distribution are affected by fatigue to some degree, in some cases with a narrow focus, and in others with long-range and diverse connections.

The summary shows that 11 of 12 participants had evidence of an atom with a focus in the theta band. Of these 11, eight had medium to long-range coherence interactions with central and parietal regions. In seven of the 12 participants, there was evidence of an atom with a focus in the alpha band. Of these seven, five had medium to long-range interactions with central or frontal regions. Four participants also showed evidence of nonspecific or broadband effects, all of these with medium to long-range interactions and mostly in frontocentral regions. The one participant who did not have a clear effect of fatigue on atoms derived from PSDs had two nonspecific atoms which were clearly sensitive to mental fatigue, one for low-frequency EEG coherences, and another for high-frequency coherences.

Table 2. Summary of EEG coherence atoms among the 12 participants of the NASA-C study.

Participant	**Theta Effect**		**Alpha Effect**		**Other/broadband Effect**	
	Spatial Focus	Range	Spatial Focus	Range	Spatial Focus	Range
ARB	Frontal	Med-long	Parietal	Med-long		
GSD	Central	Med-long	Parietal	Med-long		
JCH	Frontal	Med-long				
JCS	Parietal	Medium	Frontocentral	Med-long		
	Frontoparietal	Long				
KTT	Frontocentral	Med-long			Frontal	Med-long
MMB	Frontal	Short-med	Frontal	Med-long	Central	Med-long
MMC	Centroparietal	Medium			Parietal	Med-long
RGR	Frontocentral	Medium-long	Centroparietal	Short-med		
RWC	Central	Short-med	Frontal	Short-med		
			Parietal	Short-med		
SKH	Frontocentral	Med-long				
TBN			Frontoparietal	Long		
WXS	Frontocentral	Long			Frontocentral (lo-F)	Med-long
					Frontocentral (hi-F)	Med-long

5.2.4.2 Discussion

As for the APEC-W algorithms applied to mental workload estimation in the USAF-C and UST-T databases, the APECS-F algorithms provided atomic decompositions that isolated frequency bands, electrode locations, and coherent interactions that were significantly associated with the development of mental fatigue. Of the two approaches, PSD and coherence, the latter seemed to provide a more thorough and precise description of fatigue effects across all participants. In particular, it is evident that mental fatigue generally involves changes in coherences in the theta band, which are distributed in the frontocentral and central regions and involve medium- to long-range interactions. Surprisingly,

short-range coherences, although present in atoms of most participants, were not often associated with mental fatigue, as gauged by time on the mental arithmetic task. This result reinforces the notion that the coherences linked to fatigue-sensitive atoms are not artifacts of the method because it is well known that the highest coherences generally occur between closely spaced electrodes and tend to fall of as the inter-electrode distance increases.

6 General discussion and conclusions

This project has proven to be an extremely fruitful and penetrating view of an entirely new approach to multidimensional analysis of experiments in which EEG is used to detect changes in mental states. The results speak conclusively to the fact the atomic decomposition provides a novel view and powerful insight concerning the interactions of brain regions and oscillatory EEG sources as they change with mental states. Although the results are impressive, we feel that this project has barely scratched the surface of the potential for application of atomic decomposition to EEG.

7 Future research directions

Of most importance to the US Army and its need to accurately assess operator functional states, the methods we have developed here should be extended in two important directions. First, as with our prior work using PLS and linear or nonlinear classifiers, we must use atomic decomposition to extract features of EEG that serve as inputs to classifiers of mental states. Our experience with such classification work and testing will allow us to rapidly develop these methods and apply them to the existing data sets with minimal effort. Secondly, as atomic decomposition is relatively new in the analysis of EEG, we must design specific experiments that will allow us to test hypotheses concerning the validity and utility of the method in controlled studies. For this to succeed we will seek partnerships with experimental groups and add our methodology to ongoing and planned experiments, to be as efficient as possible in the early development of the methodology. Should atomic decomposition methods prove generally valid and useful in EEG applications, we will aim to publish the fundamental advances in academic journals and distribute the underlying software technology through commercial avenues.

8 Appendix 1

Application of Multi-way EEG Decomposition for Cognitive Workload Monitoring

[1, 2]Roman Rosipal [2]Leonard J. Trejo [2]Paul L. Nunez

[1]Department of Medical Cybernetics and Artificial Intelligence, Center for Brain Research,
Medical University Vienna, Vienna A-1010, Austria
E-mail: roman.rosipal@meduniwien.ac.at
[2] Pacific Development and Technology, LLC Palo Alto, CA 94303, USA
E-mail: ltrejo@pacdel.com

Abstract: This paper describes the use of multi-way decomposition methods to efficiently summarize electroencephalographic (EEG) data. A space-frequency-time atomic decomposition was applied to EEG data recorded while subjects performed tasks associated with varying levels of cognitive performance. The new atomic decomposition of cognitive workload data revealed alpha and theta EEG oscillations which agree with observations reported in the brain research literature. The temporal signature of the atoms discriminates between different levels of cognitive activity. The results and analysis confirm the utility of the multi-way decomposition method to construct new models and algorithms for monitoring cognitive status, which can supplement or overcome existing approaches based on conventional two-dimensional space-time or frequency-time data decomposition.

Keywords: multi-way decomposition, PARAFAC, cognitive workload

1 Introduction

Accurate and timely estimation and classification of operator functional state has important practical consequences in many safety-critical operational situations. Impairment of cognitive performance in subjects during a safety-critical task poses a high risk for procedural errors, often leading to severe consequences with high economic or life losses. Cognitive impairment has been documented in different operational situations, and attributed to several factors, including time on duty, sleep loss, extended time on single tasks, unusually high mental workload, psychosocial stress, exposure to neurotoxins and vestibular dysfunction.

Despite the extensive prior efforts to develop physiological methods for monitoring arousal and cognition, methods for monitoring mental workload are still unreliable. EEGs are considered to be the gold standard for objective detection of mental status and cognitive function and currently may be recorded and analyzed in almost any occupational setting. However, EEGs are usually recorded as a high-dimensional in time-space distributed data and many conventional 2-D decomposition techniques (for example, principal component analysis (PCA) or independent component analysis, Hyvärinen et al., 2001) may not be ideally suited to reveal the existing latent data structure, because unfolding 2-D decompositions can be done in several ways, and interactions of dimensions are not modeled

This research was sponsored by the Austrian Science Fund FWF, stand-alone project P19857 entitled "Multi-sensor sleep modeling based on contextual data fusion" and by a grant to Pacific Development and Technology, LLC from the U.S. Army Research Office, entitled, "Advanced Physiological Estimation of Cognitive Status." This report does not necessarily reflect the position or the policy of the U.S. Government and no official endorsement should be inferred.

well in 2-D decompositions. Recently, promising results were achieved by applying multi-way decomposition models such as PARAFAC or TUCKER3 to EEG data (Estienne et al., 2001; Miwakeichi et al., 2004). Using these multi-way decomposition models we analyzed EEG data recorded from participants in a study of mental workload. To our knowledge this is the first time that multi-way decomposition models have been applied to the problem of mental workload analysis and monitoring.

2 Methods

2.1 Data acquisition and preprocessing

Two subjects were trained to stable performance on a simulated Unmanned Air Vehicle (UAV) task. The task consists of monitoring of the progress of four UAVs as they flew a preplanned mission. Each subject participated in three in time-separated sessions. Five channels of EEG (electrodes located at Fz, F7, Pz, T5 and O2 with a linked mastoid reference), ECG, vertical and horizontal EOG were recorded. In this study only the EEG data were used. The EEG data were sampled at 200 Hz and low-pass filtered with cutoff of 30 Hz. Next, the data were segmented into 2-s long windows with an overlap of 500 ms. For each segment the power spectral density (PSD) was computed using the Thomson multitaper method (Thomson, 1982). Frequencies in the range of 2.5 to 20 Hz were considered in this study. Initial analyses revealed a high level of power at frequencies below 4 Hz. Power at these frequencies often arose from motion artifacts and confounded the PARAFAC analyses of EEG. For this reason only frequencies from 5 to 20 Hz were considered for further analyses. This procedure was repeated for each EEG channel separately and a three-dimensional matrix $\mathbf{X}_{(I \times J \times K)}$ with I time segments, J electrodes and PSD estimates at K frequencies was constructed.

2.2 The PARAFAC model

A three-way PARAFAC model was applied to data. PARAFAC can be seen as a generalization of PCA for dealing with multi-dimensional data (Bro, 1997). Three loading matrices, **A**, **B**, and **C** with elements a_{if}, b_{jf}, and c_{kf} defines the model that can be mathematically described as

$$x_{ijk} = \sum_{f=1}^{F} a_{if} b_{jf} c_{kf} + \varepsilon_{ijk}$$

where ε_{ijk} are the residual elements or errors and F stands for number of components or *atoms* that are considered. The loadings elements are then found by minimizing the sum of squares of the residuals ε_{ijk} (Bro, 1997), that is

$$\min_{a_{if} b_{jf} c_{kf}} \| x_{ijk} - \sum_{f=1}^{F} a_{if} b_{jf} c_{kf} \|^2$$

For the analyses reported here we used proprietary m-codes developed by Pacific Development and Technology, LLC, and subroutines from the *N*-way toolbox for Matlab® (Andersson and Bro, 2000).

3 Results

A three-atom PARAFAC model was observed to provide acceptable and physiologically interpretable results for EEG recordings of both subjects, for which *core consistency diagnostic* values, which index the stability of the decompositions, reached 87% and 97%, respectively (Bro and Kiers, 2003; Andersson and Bro, 2000).

Three distinct spectral signature atoms (components) were observed in the first subject (Figure 1, right). Atom 1

any specific rhythm or band, and most likely reflects background EEG. Atom 2 shows a concentration of high loadings for frequencies in the theta band. Loadings for Atom 3 were maximal in the band 5-9.5 Hz. The spatial loadings of Atom 1 were the same as for Subject 1 (Fz, Pz, Oz), whereas those of Atom 2 were maximal at Fz, indicating an association with theta rhythm. The spatial loadings of Atom 3 were maximal at Fz and Pz, also indicating association with theta and low alpha rhythms. The temporal loadings of Atoms 1 and 2 did not show a marked relationship to workload conditions; however, the temporal loadings of Atom 3 tracked closely with the various mental workload conditions and rest periods.

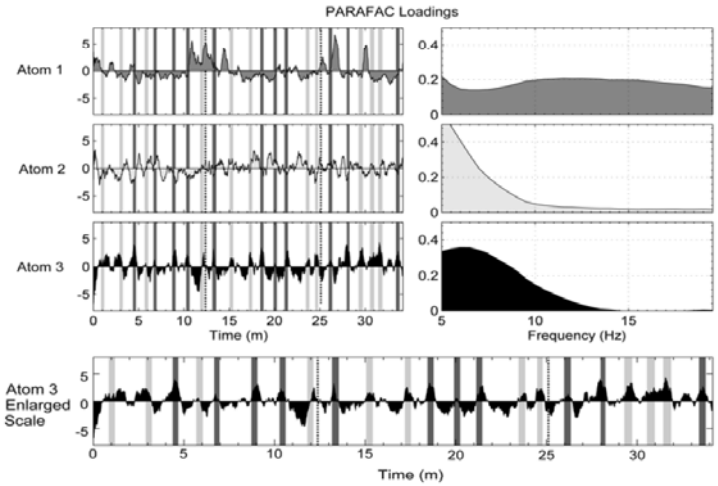

Figure 2 Subject 2. Left panel: Temporal signatures of the EEG decomposition. Light gray areas mark lower mental workload states while the higher workload states are marked by the dark gray areas. Vertical dotted lines separate three in time distinct experimental sessions. Bottom panel: The third temporal atom alone. Right panel: Spectral signatures corresponding to temporal atoms plotted in the left panel.

4 Conclusions

The results of this study show that mental workload may be tracked by EEG components isolated using parallel factor analysis or PARAFAC. Components or atoms of the PARAFAC decomposition had high loadings in the frequency spectrum and across electrodes, which reflected alpha, theta, and broad-band EEG processes. Unlike other approaches to isolate EEG factors related to mental workload, our application of PARAFAC begins with a truly three-dimensional model of EEG variance observed during performance of a cognitive task. This model is fit to the EEG simultaneously in frequency, space, and time. The time dimension in the present study reflects imposed task demands that produced calibrated states of low-or high mental workload.

For an unsupervised method of decomposition, these PARAFAC results are remarkable. Using a small number of electrodes, the loadings of several PARAFAC atoms in time, co-varied with task demands and mental workload. Admittedly, these results are based on a small sample of two subjects. However, the task performances were long, providing about 30 minutes of EEG recordings for analysis. In our extensive experience with similar experiments, the discovery of EEG atoms that track workload and have meaningful spectral and spatial propertied from recordings of these durations is not likely to arise from chance.

We are extending our research in two directions. First we are increasing the number of tasks and subjects in which we are applying the PARAFAC method. Two additional studies are in process, including a cognitive fatigue study and a warfare simulation task. Second, we are now testing a fourth dimension in the PARAFAC model: coherence of EEG sources. Short-and long range coherence of alpha and theta sources are expected to increase with cognitive effort, based on theoretical studies of EEG dynamics and considerable experimental data (Nunez and Srinivasan, 2005). We expect models that can encompass the direction, bandwidth, and extent of EEG coherence will help to further define neural sources that interact in cognition.

References

[1] Andersson C.A., Bro R. (2000) The *N*-way Toolbox for MATLAB, *Chemometrics and Intelligent Laboratory Systems*, 52, 1-4.

[2] Bro R. (1997) PARAFAC. Tutorial and applications, *Chemometrics and Intelligent Laboratory Systems*, 38, 149-171.

[3] Bro R., Kiers H.A.L. (2003) A new efficient method for determining the number of components in PARAFAC models, *Journal of Chemometrics*, 17, 274-286.

[4] Estienne F., Matthijs N., Massart D.L., Ricoux P., Leibovici D. (2001) Multi-way modelling of high-dimensional electroencephalographic data, *Chemometrics and Intelligent Laboratory Systems*, 58, 59-72.

[5] Hart S.G., Steveland L.E. (1998) Development of NASA-TLX (Task Load Index) : Results of empirical and theoretical research, in: *Human Mental Workload*, Hancock P.A. & Meshkati N. (Eds.), North Holland Press.

[6] Hyvärinen A., Karhunen J., Oja E. (2001) *Independent Component Analysis.* Wiley, New York.

[7] Klimesch W. (1999) EEG alpha and theta oscillations reflect cognitive and memory performance: a review and analysis, *Brain Research Reviews*, 29, 169-195.

[8] Miwakeichi F., Martínez-Montes E., Valdés-Sosa P.A., Nishiyama N., Mizuhara H., Yamaguchi Y. (2004) Decomposing EEG data into space-time-frequency components using Parallel Factor Analysis, *NeuroImage*, 22, 1035-1045.

[9] Nunez P.L, Srinivasan R. (2005) *Electric Fields of the Brain.* Oxford University Press, New York.

[10] Thomson D.J. (1982) Spectrum estimation and harmonic analysis. in: *Proceedings of the IEEE*, 70, 1055-1096.

[11] Smilde A., Bro R., Geladi P. (2004) *Multi-way Analysis: Applications in the Chemical Sciences.* Wiley.

9 Appendix 2

PROTOCOL SHEET

Gamer Study No. 2

	TASK	TONES*	COUNT
	3.5 minutes with 1 enemy	NO	NO
☐	3.5 minutes with 0 enemies	NO	NO
☐	7 minutes with 1 enemy	NO	NO
☐	7 minutes with 1 enemy	YES	YES
☐	7 minutes with 5 enemies	NO	NO
☐	7 minutes with 5 enemies	YES	YES
Alcohol or placebo administration occurs here.			
☐	3.5 minutes with 0 enemies	NO	NO
☐	7 minutes with 1 enemy	NO	NO
☐	7 minutes with 1 enemy	YES	YES
☐	7 minutes with 5 enemies	NO	NO
☐	7 minutes with 5 enemies	YES	YES
☐	3.5 minutes with 0 enemies	NO	NO
☐	3.5 minutes with 0 enemies	YES	YES

*"No" means that the participant does not need to listen to tones and does not report kills or death

10 Appendix 3

Figures for PSD Analyses of 12 Participants' EEG from the NASA-C Database

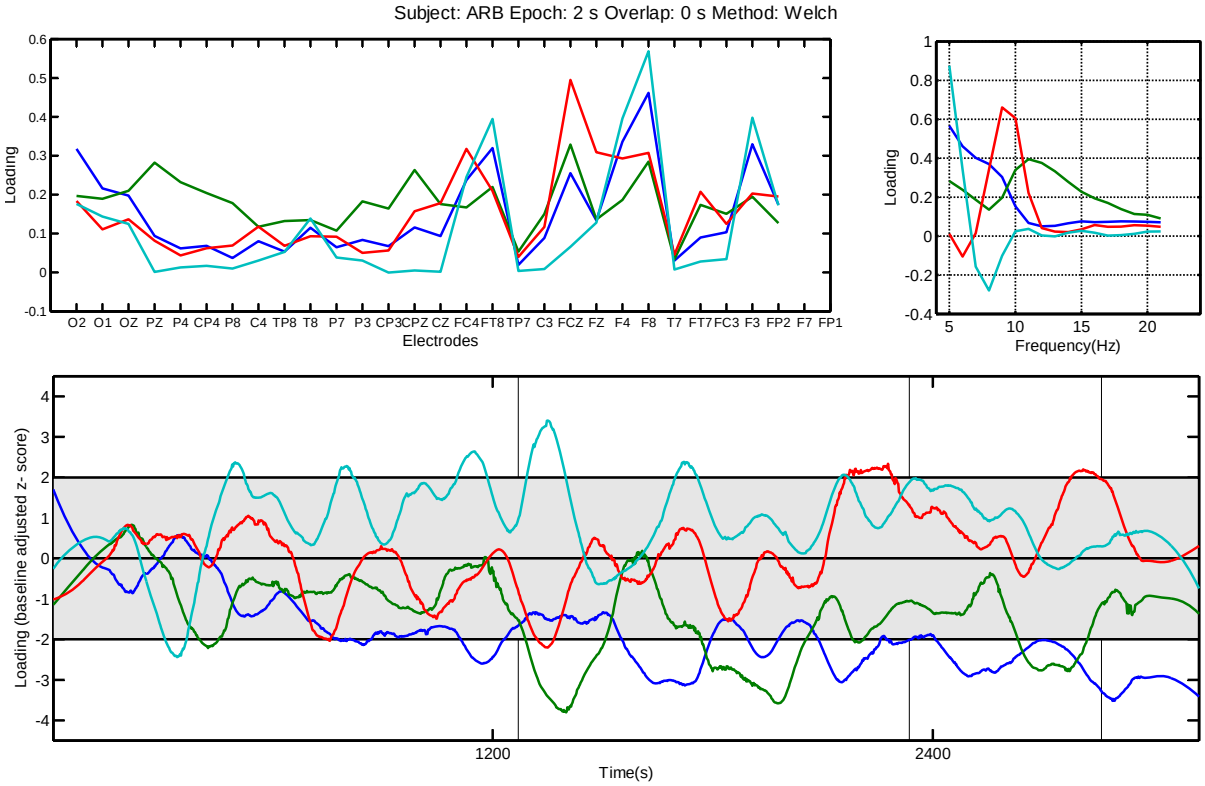

Figure 32. Atomic decomposition of EEG from participant ARB of the NASA-C study. Participants solved mental arithmetic problems on a computer for up to three hours without rest. EEG recordings from 30 channels were processed using PARAFAC decomposition to yield a model consisting of four atoms, each have dimensions of space (electrodes), frequency (power spectral density) and time (time on task). *All panels*: Atoms 1-4 are represented by colored lines in the order blue, red, green, cyan. *Upper left panel:* distributions of loadings for EEG atoms across a 32-channel montage. Certain electrodes may have been excluded from analyses if they were judged to contain high levels of noise, as illustrated in Figure 30. In this participant, electrodes F7 and FP1 were excluded. *Upper right panel*: distribution of loadings for EEG atoms across frequency bins analyzed in the PSD estimate. *Lower panel*: distributions of loadings for EEG atoms across time on task. The fine vertical lines separate 15-minute blocks of time. The first two blocks are consecutive and were at the beginning of the session. The last two blocks were also consecutive and were at the end of the session. This participant performed the task for one hour, or four 15-minute blocks. The time axis measures time as multiples of 2-s long EEG epochs which were not all contiguous, due to rejection of EEG segments containing movement or other artifacts. The last pair of blocks has fewer epochs because the incidence of EEG artifacts increased over time in this participant.

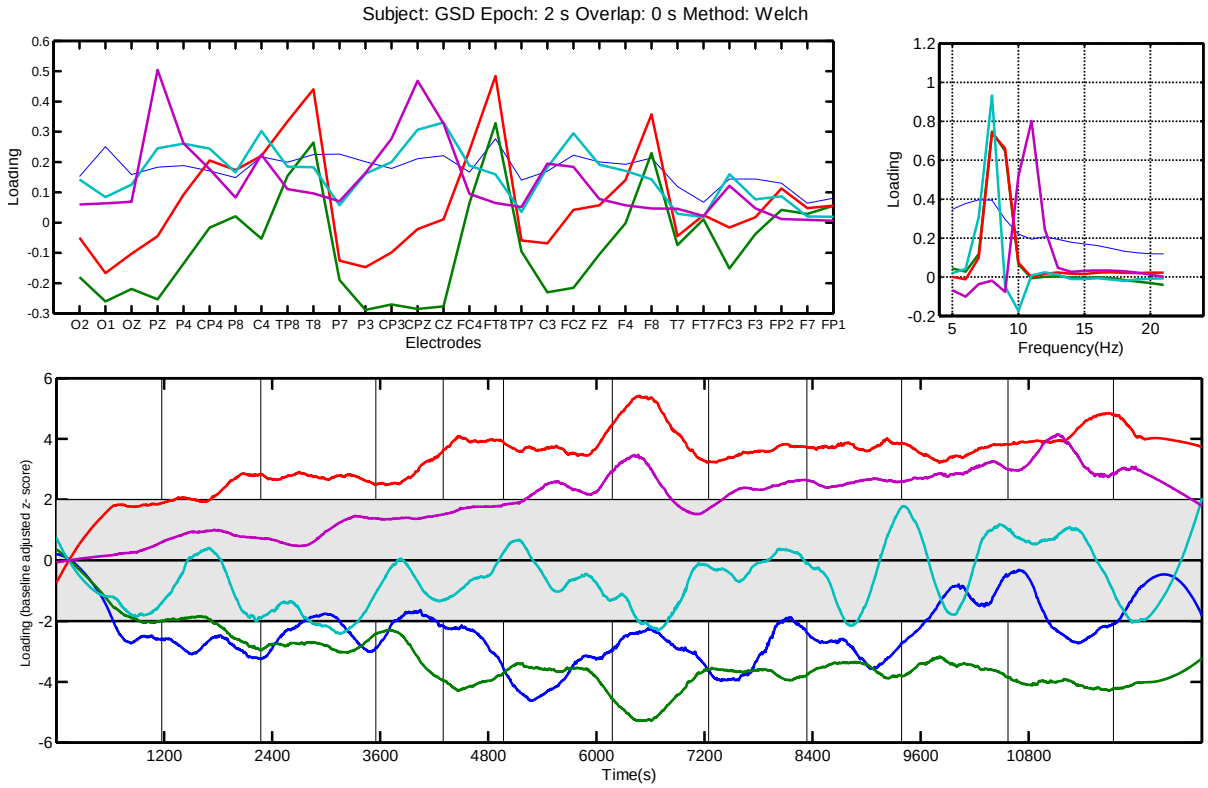

Figure 33. Atomic decomposition of EEG from participant GSD of the NASA-C study. EEG recordings from 30 channels were processed using PARAFAC decomposition to yield a model consisting of four atoms, each have dimensions of space (electrodes), frequency (power spectral density) and time (time on task). *Graphical conventions are the same as in Figure 32.* This participant performed the task for three hours, or 12 15-minute blocks. The time axis measures seconds as multiples of 2-second long EEG epochs which were not all contiguous, due to rejection of EEG segments containing movement or other artifacts. Some blocks have fewer epochs than others because the incidence of EEG artifacts increased during those blocks.

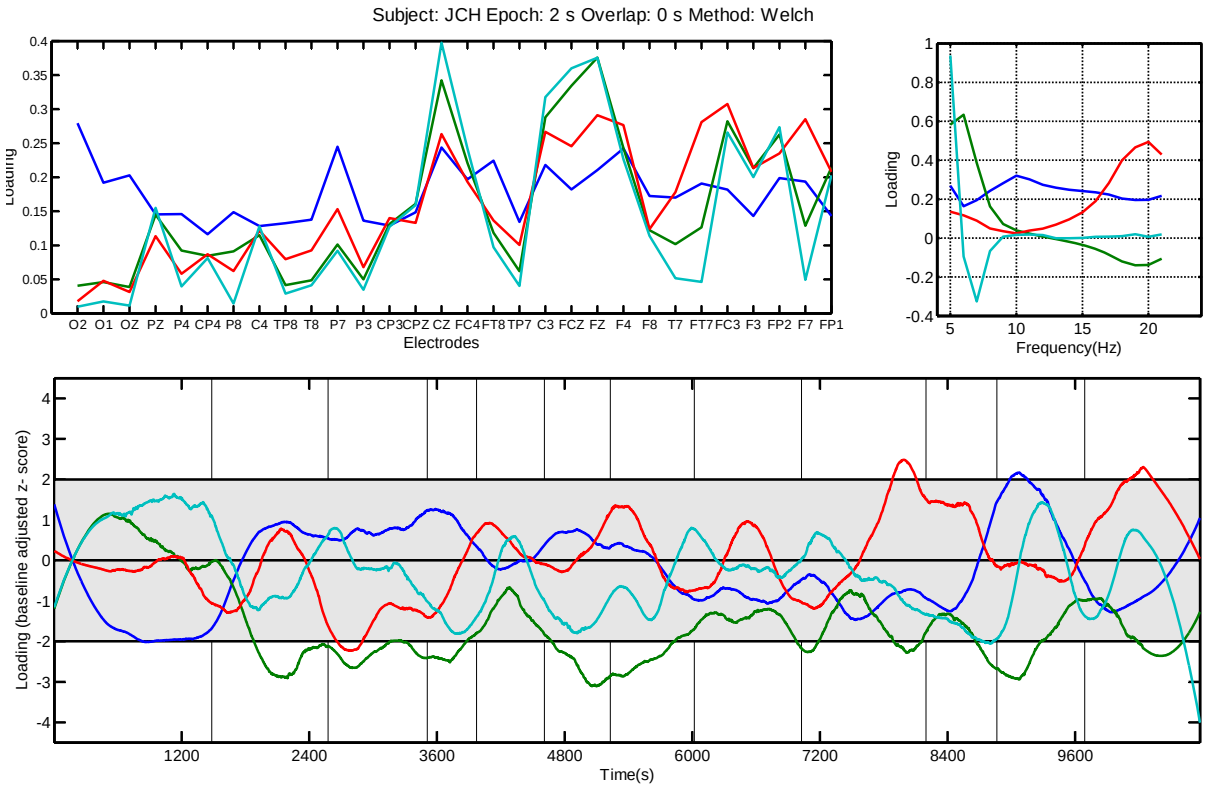

Figure 34. Atomic decomposition of EEG from participant JCH of the NASA-C study. EEG recordings from 30 channels were processed using PARAFAC decomposition to yield a model consisting of four atoms, each have dimensions of space (electrodes), frequency (power spectral density) and time (time on task). *Graphical conventions are the same as in Figure 32.* This participant performed the task for three hours, or 12 15-minute blocks. The time axis measures seconds as multiples of 2-second long EEG epochs which were not all contiguous, due to rejection of EEG segments containing movement or other artifacts. Some blocks have fewer epochs than others because the incidence of EEG artifacts increased during those blocks.

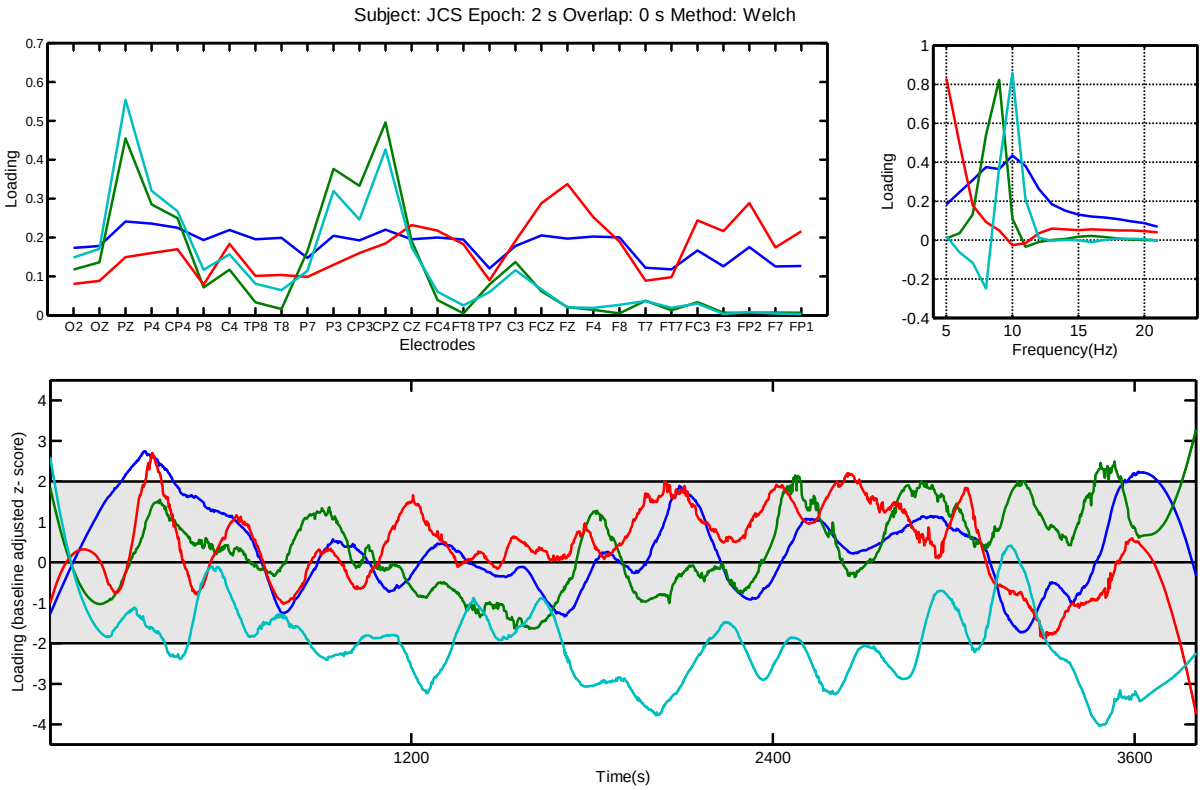

Figure 35.Atomic decomposition of EEG from participant JCS of the NASA-C study. EEG recordings from 30 channels were processed using PARAFAC decomposition to yield a model consisting of four atoms, each have dimensions of space (electrodes), frequency (power spectral density) and time (time on task). *Graphical conventions are the same as in Figure 32.* This participant performed the task for 1.75 hours, or seven 15-minute blocks. The time axis measures seconds as multiples of 2-second long EEG epochs which were not all contiguous, due to rejection of EEG segments containing movement or other artifacts. Some blocks have fewer epochs than others because the incidence of EEG artifacts increased during those blocks.

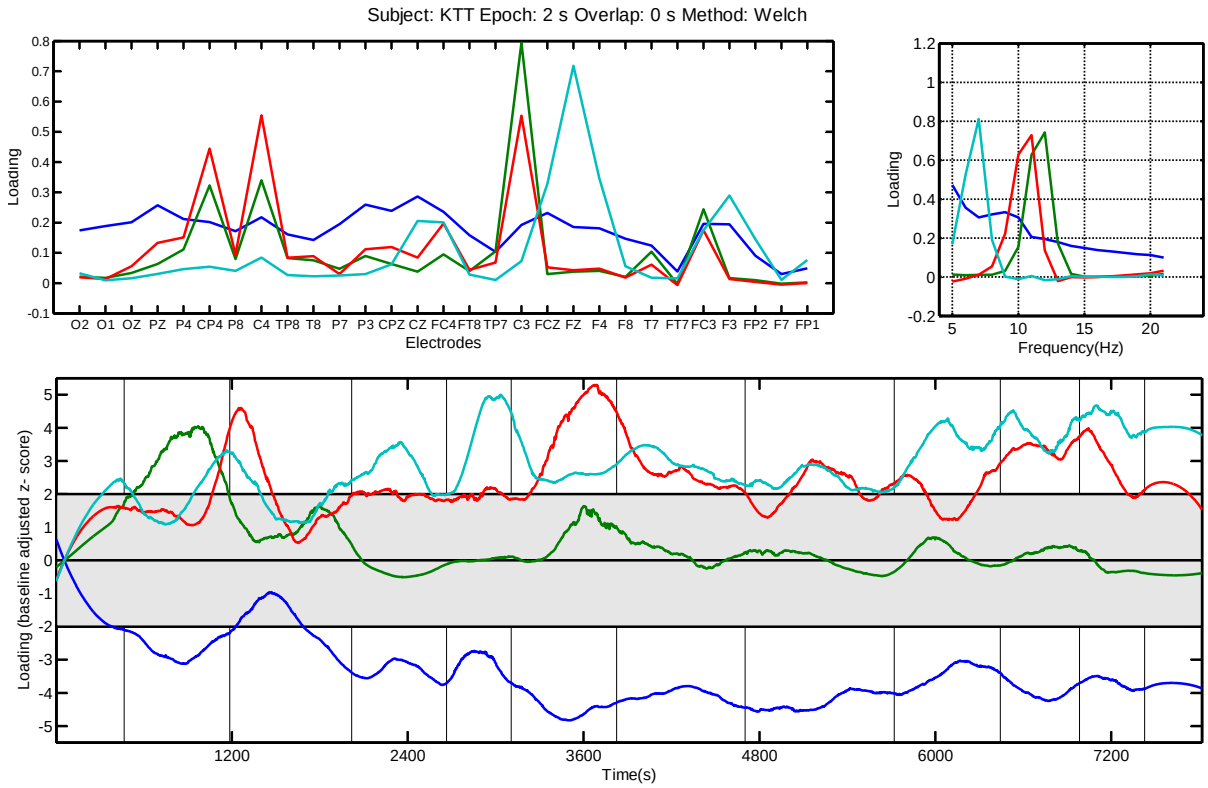

Figure 36.Atomic decomposition of EEG from participant KTT of the NASA-C study. EEG recordings from 30 channels were processed using PARAFAC decomposition to yield a model consisting of four atoms, each have dimensions of space (electrodes), frequency (power spectral density) and time (time on task). *Graphical conventions are the same as in Figure 32.* This participant performed the task for three hours, or 12 15-minute blocks. The time axis measures seconds as multiples of 2-second long EEG epochs which were not all contiguous, due to rejection of EEG segments containing movement or other artifacts. Some blocks have fewer epochs than others because the incidence of EEG artifacts increased during those blocks.

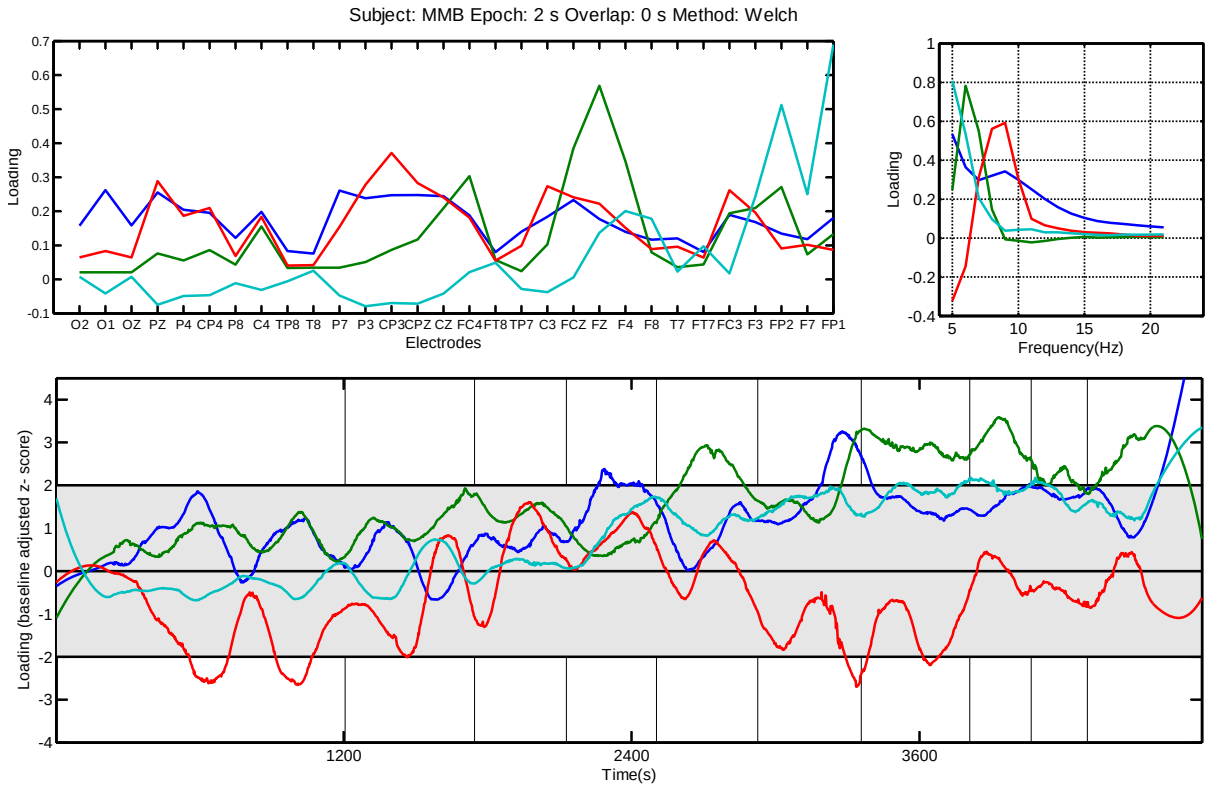

Figure 37. Atomic decomposition of EEG from participant MMB of the NASA-C study. EEG recordings from 30 channels were processed using PARAFAC decomposition to yield a model consisting of four atoms, each have dimensions of space (electrodes), frequency (power spectral density) and time (time on task). *Graphical conventions are the same as in Figure 32.* This participant performed the task for 2.5 hours, or 10 15-minute blocks. The time axis measures seconds as multiples of 2-second long EEG epochs which were not all contiguous, due to rejection of EEG segments containing movement or other artifacts. Some blocks have fewer epochs than others because the incidence of EEG artifacts increased during those blocks.

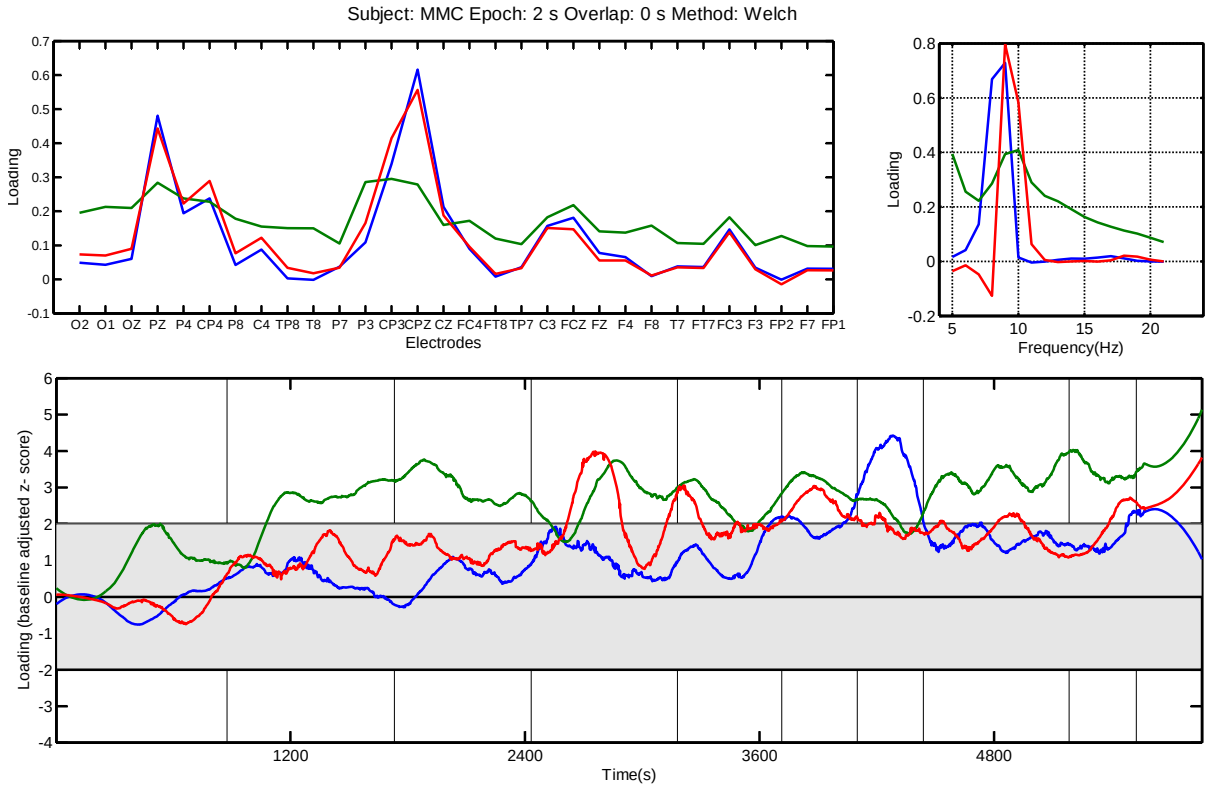

Figure 38.Atomic decomposition of EEG from participant MMC of the NASA-C study. EEG recordings from 30 channels were processed using PARAFAC decomposition to yield a model consisting of three atoms, each have dimensions of space (electrodes), frequency (power spectral density) and time (time on task). *Graphical conventions are the same as in Figure 32.* This participant performed the task for 2.5 hours, or 10 15-minute blocks. The time axis measures seconds as multiples of 2-second long EEG epochs which were not all contiguous, due to rejection of EEG segments containing movement or other artifacts. Some blocks have fewer epochs than others because the incidence of EEG artifacts increased during those blocks.

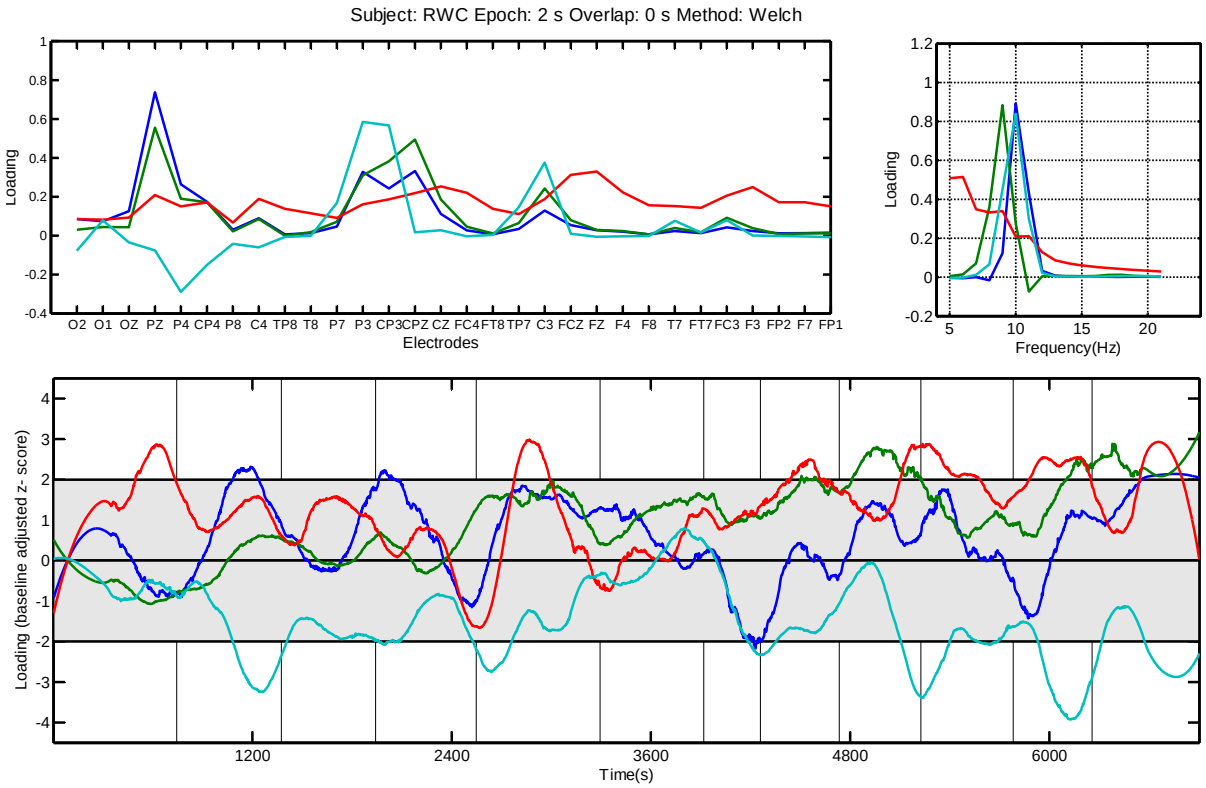

Figure 39. Atomic decomposition of EEG from participant RWC of the NASA-C study. EEG recordings from 30 channels were processed using PARAFAC decomposition to yield a model consisting of four atoms, each have dimensions of space (electrodes), frequency (power spectral density) and time (time on task). *Graphical conventions are the same as in Figure 32.* This participant performed the task for three hours, or 12 15-minute blocks. The time axis measures seconds as multiples of 2-second long EEG epochs which were not all contiguous, due to rejection of EEG segments containing movement or other artifacts. Some blocks have fewer epochs than others because the incidence of EEG artifacts increased during those blocks.

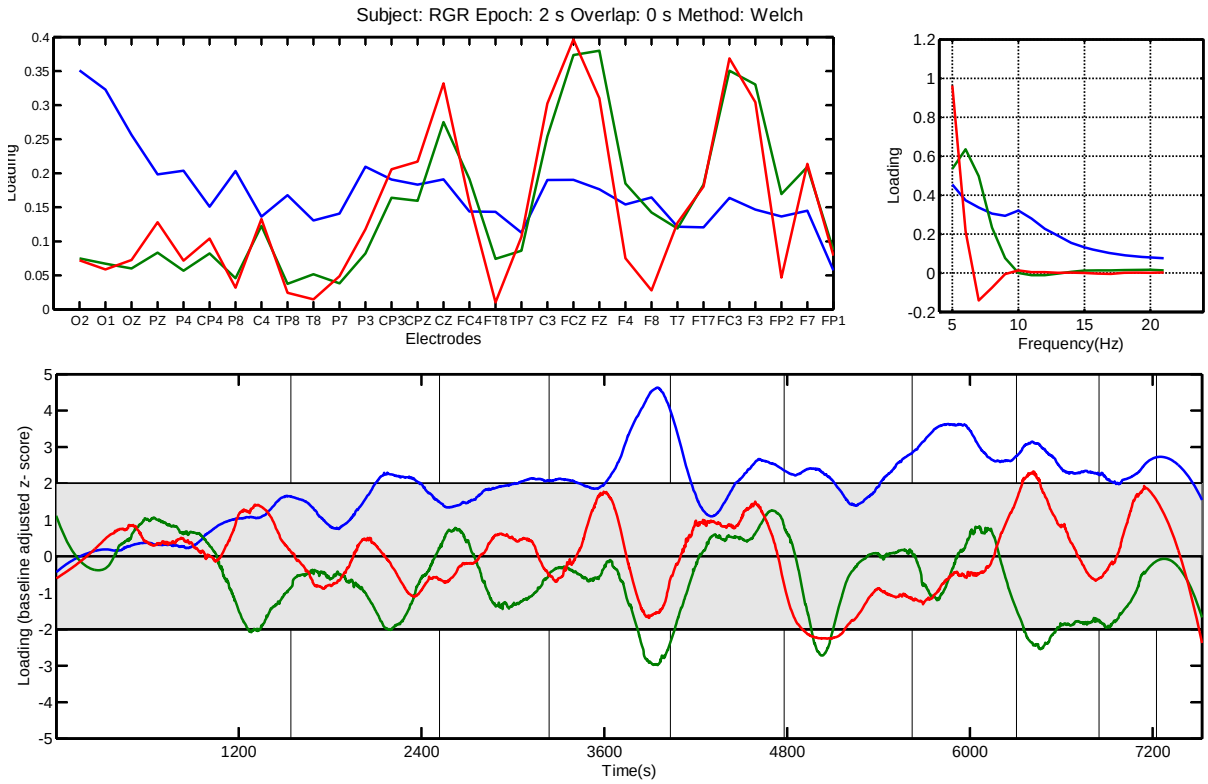

Figure 40. Atomic decomposition of EEG from participant RGR of the NASA-C study. EEG recordings from 30 channels were processed using PARAFAC decomposition to yield a model consisting of four atoms, each have dimensions of space (electrodes), frequency (power spectral density) and time (time on task). *Graphical conventions are the same as in Figure 32.* This participant performed the task for 2.5 hours, or 10 15-minute blocks. The time axis measures seconds as multiples of 2-second long EEG epochs which were not all contiguous, due to rejection of EEG segments containing movement or other artifacts. Some blocks have fewer epochs than others because the incidence of EEG artifacts increased during those blocks.

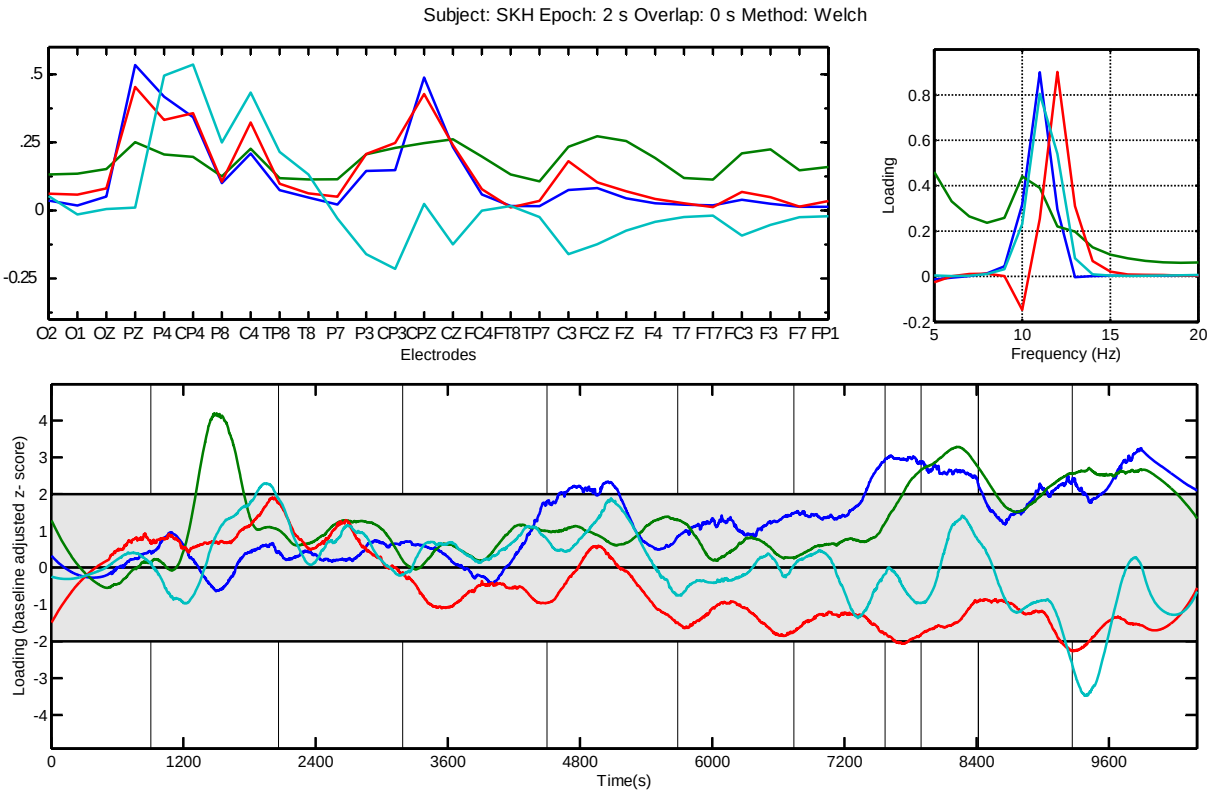

Figure 41.Atomic decomposition of EEG from participant SKH of the NASA-C study. EEG recordings from 30 channels were processed using PARAFAC decomposition to yield a model consisting of four atoms, each have dimensions of space (electrodes), frequency (power spectral density) and time (time on task). *Graphical conventions are the same as in Figure 32.* This participant performed the task for 2.75 hours, or 11 15-minute blocks. The time axis measures seconds as multiples of 2-second long EEG epochs which were not all contiguous, due to rejection of EEG segments containing movement or other artifacts. Some blocks have fewer epochs than others because the incidence of EEG artifacts increased during those blocks.

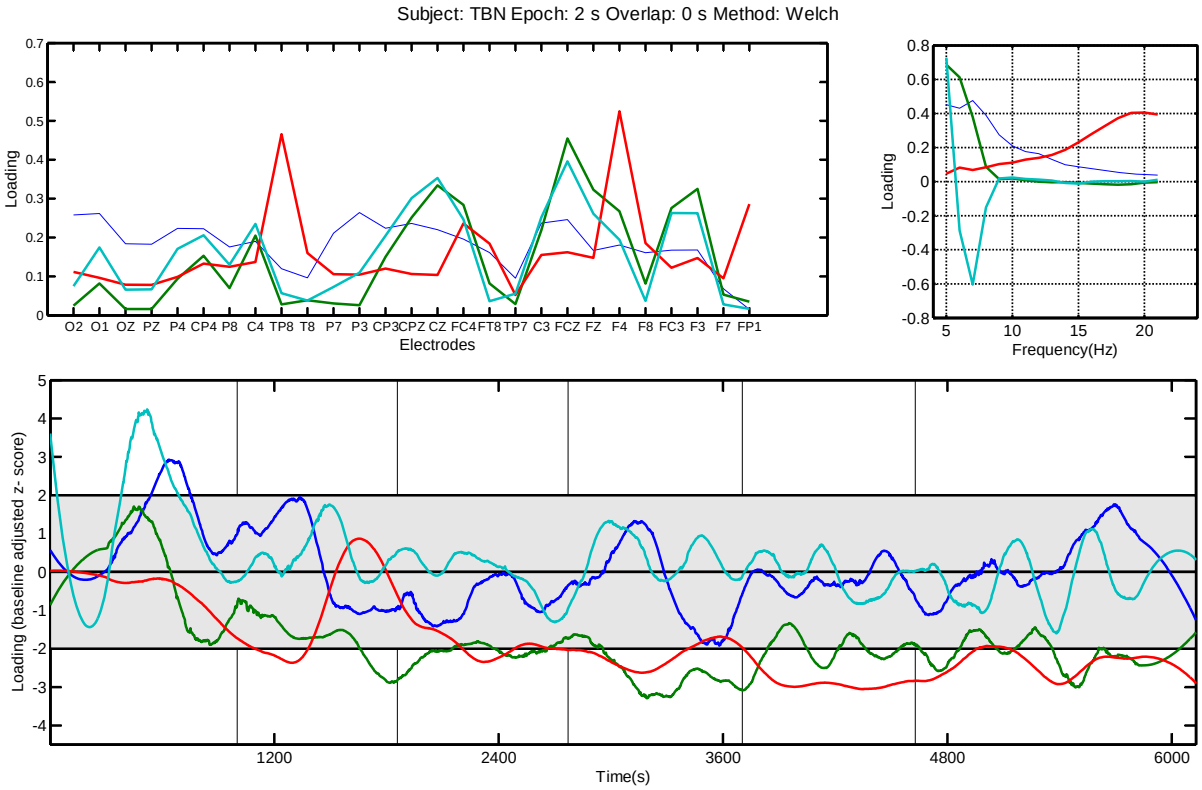

Figure 42.Atomic decomposition of EEG from participant TBN of the NASA-C study. EEG recordings from 30 channels were processed using PARAFAC decomposition to yield a model consisting of four atoms, each have dimensions of space (electrodes), frequency (power spectral density) and time (time on task). *Graphical conventions are the same as in Figure 32.* This participant performed the task for 1.5 hours, or 6 15-minute blocks. The time axis measures seconds as multiples of 2-second long EEG epochs which were not all contiguous, due to rejection of EEG segments containing movement or other artifacts. Some blocks have fewer epochs than others because the incidence of EEG artifacts increased during those blocks.

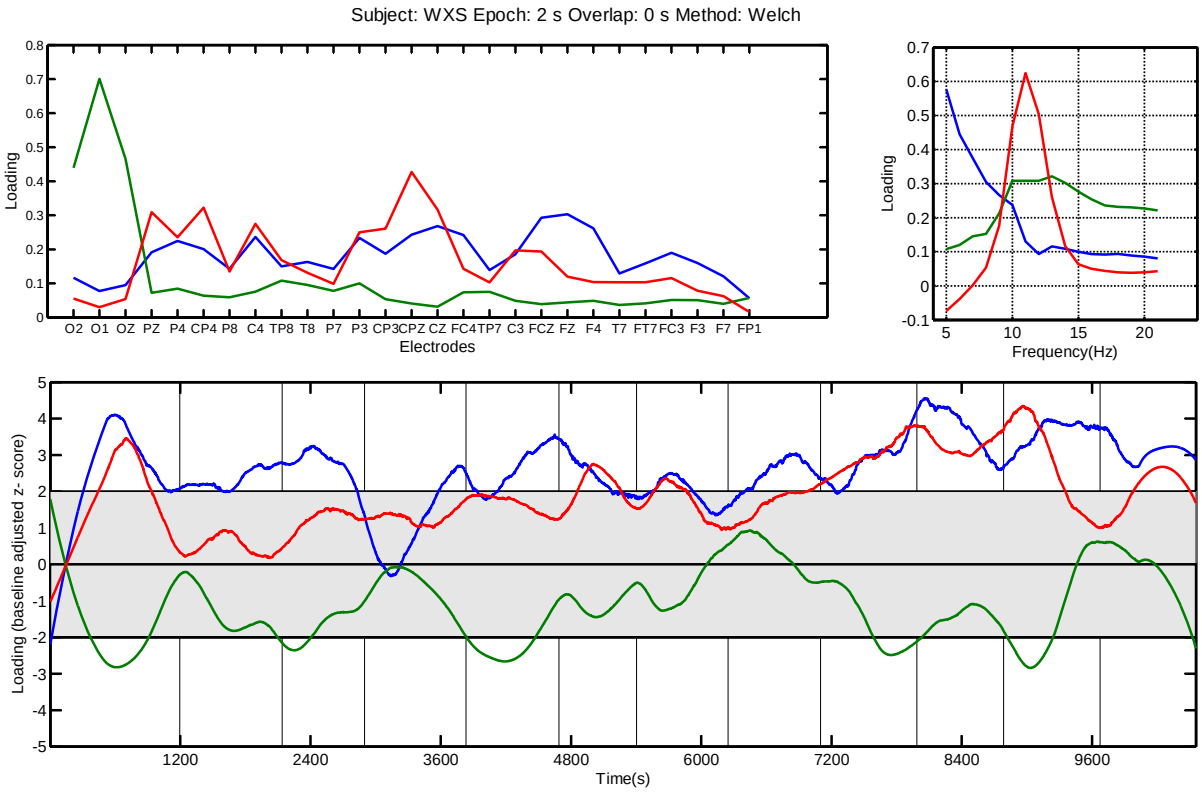

Figure 43. Atomic decomposition of WXS from participant KTT of the NASA-C study. EEG recordings from 30 channels were processed using PARAFAC decomposition to yield a model consisting of four atoms, each have dimensions of space (electrodes), frequency (power spectral density) and time (time on task). *Graphical conventions are the same as in Figure 32.* This participant performed the task for three hours, or 12 15-minute blocks.. The time axis measures seconds as multiples of 2-second long EEG epochs which were not all contiguous, due to rejection of EEG segments containing movement or other artifacts. Some blocks have fewer epochs than others because the incidence of EEG artifacts increased during those blocks.

11 Appendix 4

Figures for Coherence Analyses of 12 Participants' EEG from the NASA-C Database

Figure 44 (next page). Atomic decomposition of EEG coherence from participant ARB of the NASA-C study. EEG coherences from 30 channels were processed using PARAFAC decomposition to yield a model consisting of four atoms, each have dimensions of space (electrodes), coherence (magnitude squared coherence) and time (time on task). *Upper left panel:* distributions of loadings for Atoms 1-4 (black, blue, green, & red lines) across EEG frequency bins (due to a labeling error in the legend, atoms are numbered 0-3 in this panel, but we shall refer to them everywhere as Atoms 1-4 in the same order). Unlike the figures for the APEX-W and APECS-F/PSD analyses, here the loadings of each atom across frequencies were normalized to the range of 0.0 to 1.0 for all atoms. We did this to emphasize the shape of the coherence loading spectra, as the raw loadings varied considerably in scale across atoms. *Upper right panel:* distributions of loadings for Atoms 1-4 across time on task. Unlike the PSD analyses, where all blocks were analyzed for each participant, here only the first (alert) 30 minutes and last (fatigued) 30 minutes of time on task were analyzed for each participant. The first and last 30 minutes are separated by the dashed vertical line. Total times on task for each subject and the description of the time axis appear in corresponding figures of Appendix 3. *Lower Four Panels:* Modified *Werner* projections of electrode pairs of Atoms 1-4, in which only pairs with coherence loadings exceeding the 90^{th} percentile of all coherence loadings for that atom are plotted. Conventions for the projection are explained in Figure 31. Electrode pairs are divided into three groups, based on linear inter-electrode distances on straight lines through the sphere (not along the surface). The criteria for these distances were derived from a spherical head model with a radius of 9 cm. Short-range pairs are connected by wide magenta lines, and are limited to pairs whose inter-electrode distance is less than 6.0 cm. Respectively, medium-range (6.0 to 12.0 cm) pairs and long-range (greater than 12.0 cm) pairs are connected by medium-wide cyan lines and thin orange lines.

Figures 45 to 55 (following 11 pages). Atomic decompositions for the remaining 11 participants of the NASA-C study. The figures are labeled with the participants' 3-letter codes, which match the codes of the figures in Appendix 3. Graphical conventions are the same as in Figure 44.

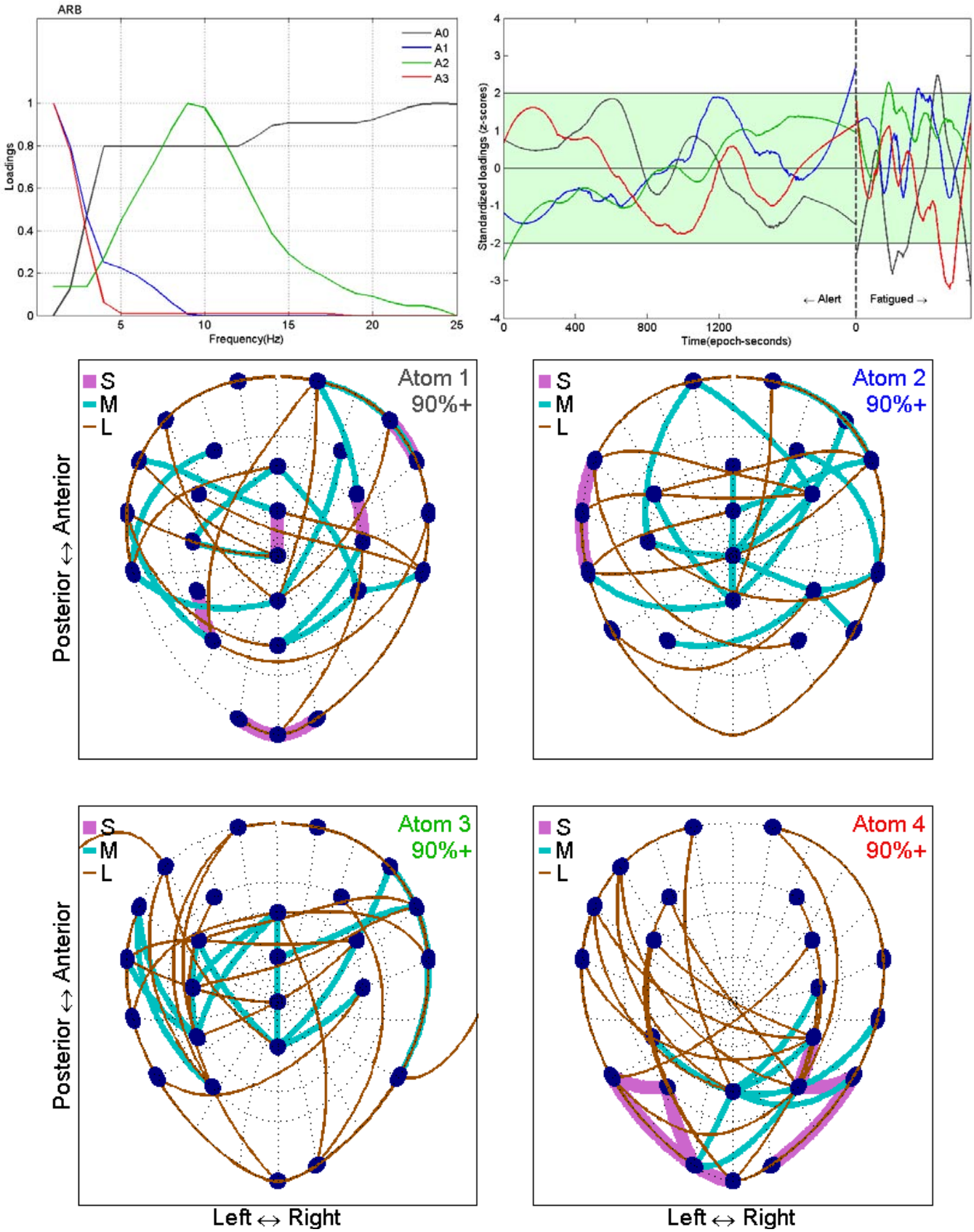

Figure 44. Coherence analyses for participant ARB. Graphing conventions are explained in Figure 44.

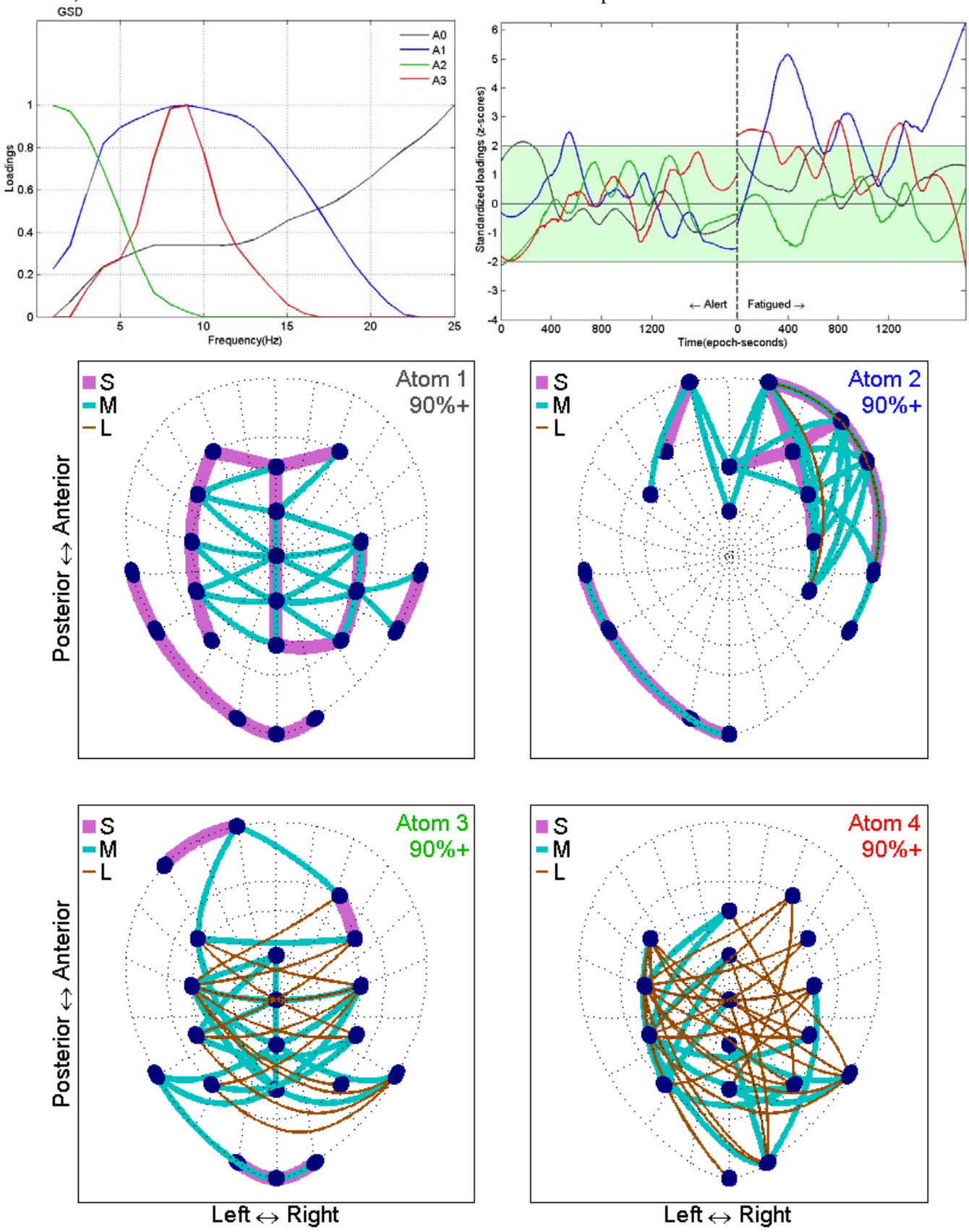

Figure 45. Coherence analyses for participant GSD. Graphing conventions are explained in Figure 44.

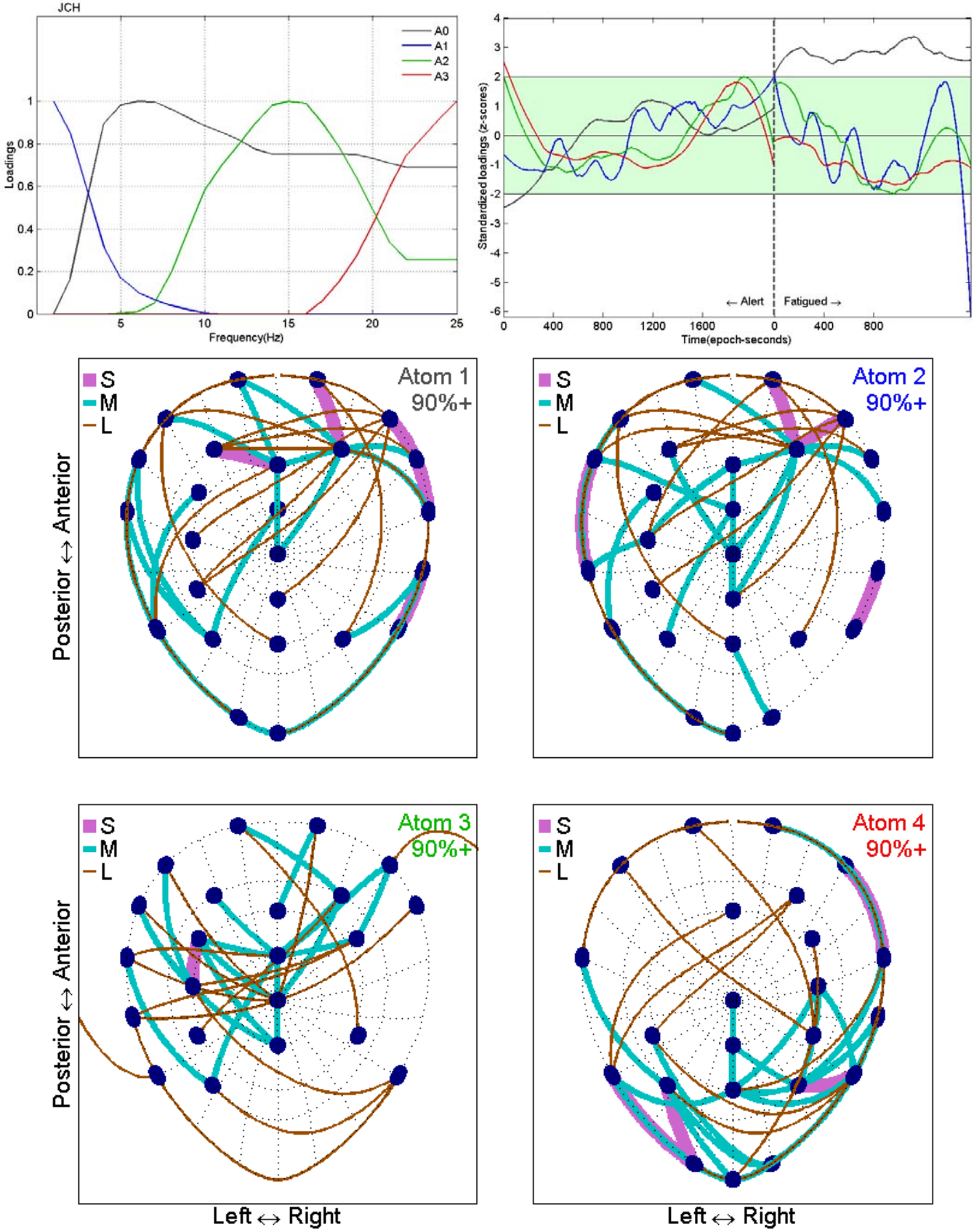

Figure 46. Coherence analyses for participant JCH. Graphing conventions are explained in Figure 44.

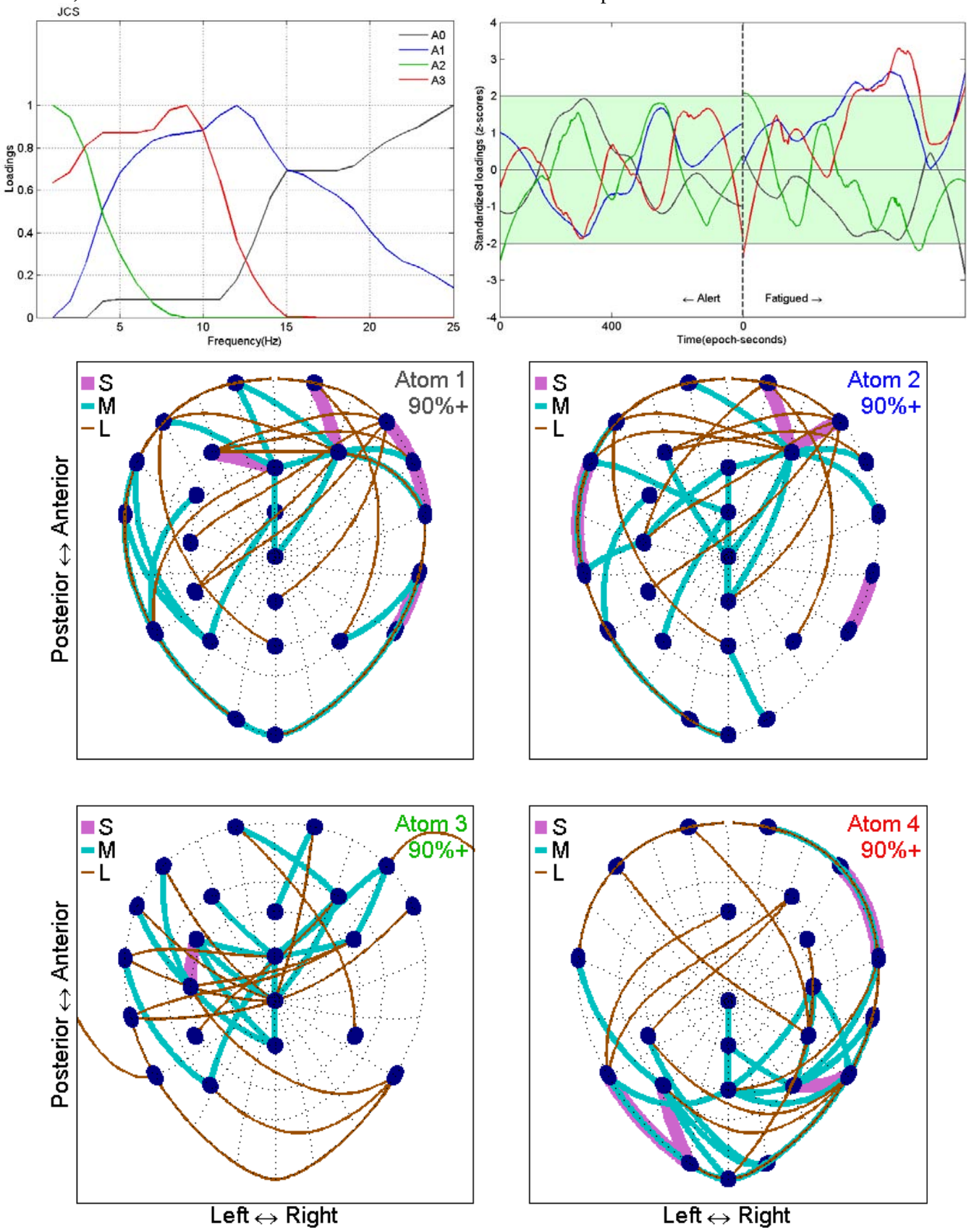

Figure 47. Coherence analyses for participant JCS. Graphing conventions are explained in Figure 44.

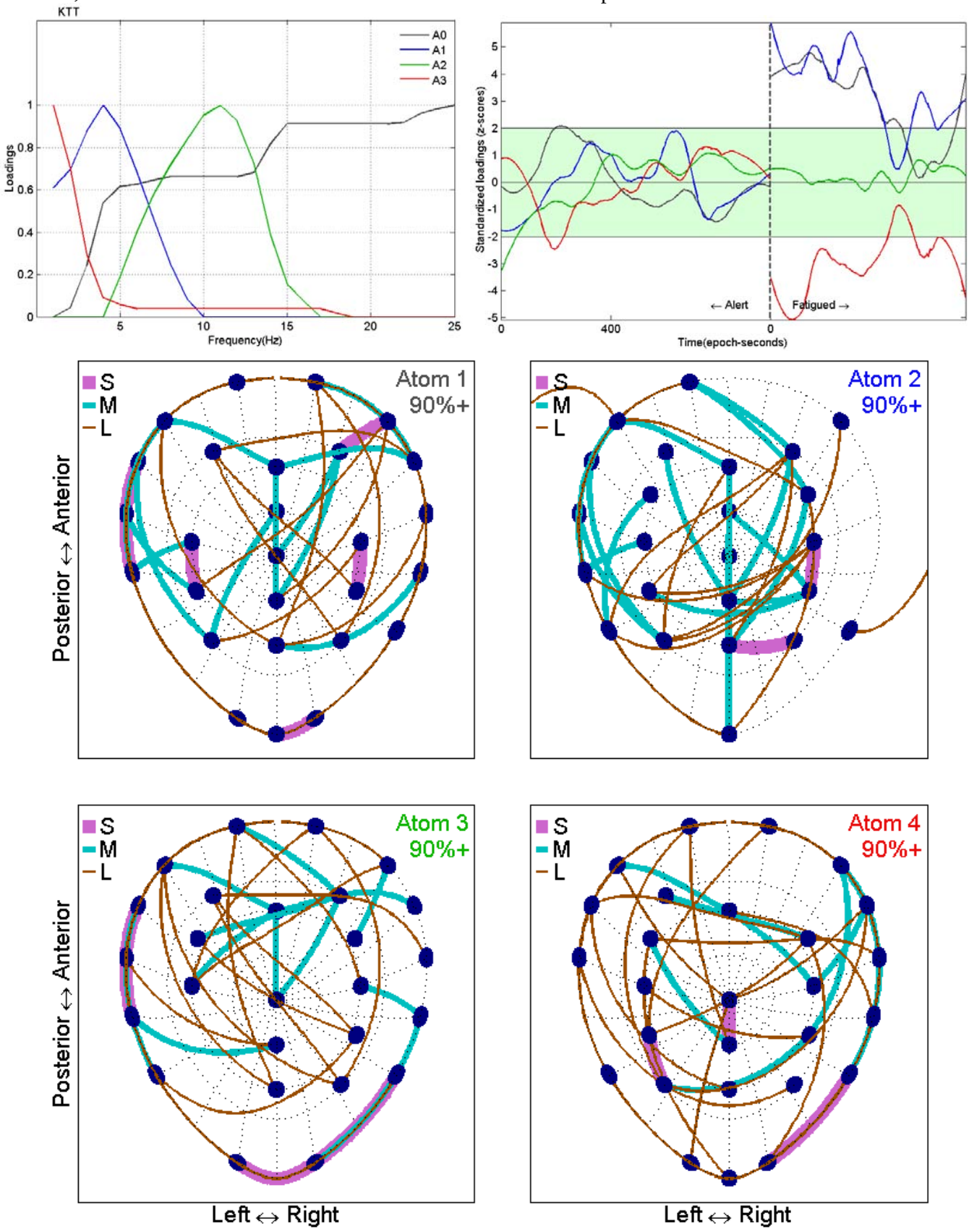

Figure 48. Coherence analyses for participant KTT. Graphing conventions are explained in Figure 44.

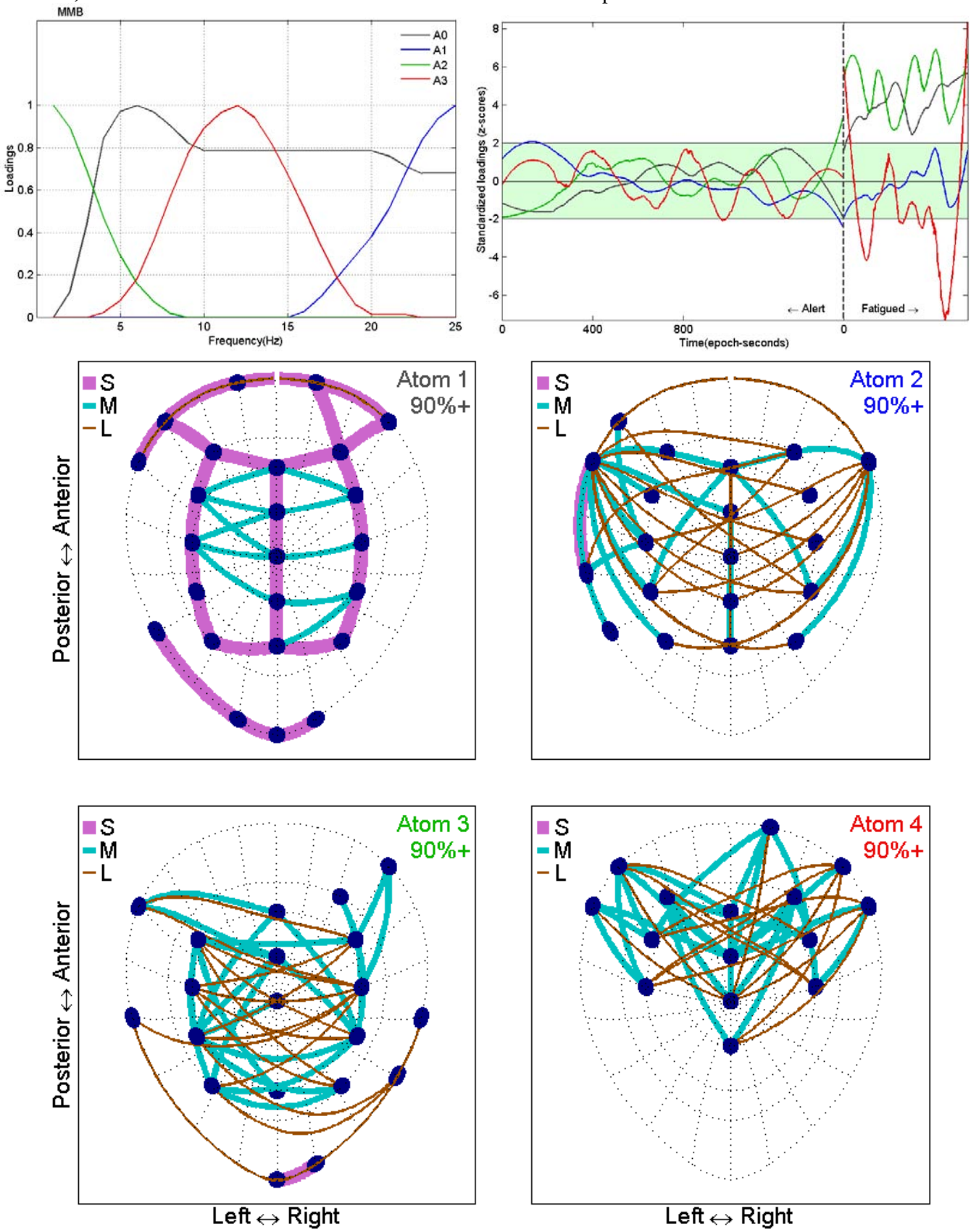

Figure 49.Coherence analyses for participant MMB. Graphing conventions are explained in Figure 44.

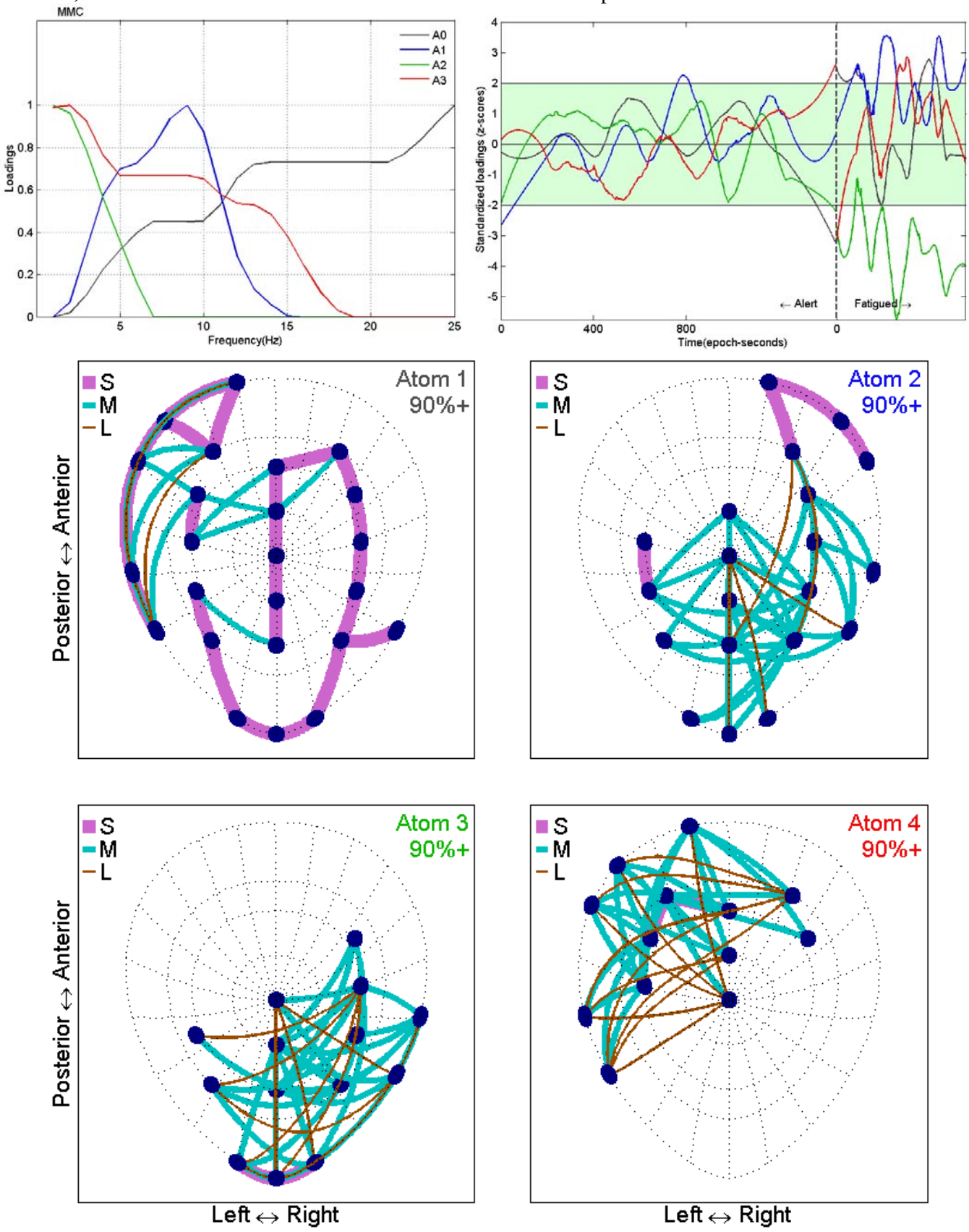

Figure 50. Coherence analyses for participant MMC. Graphing conventions are explained in Figure 44.

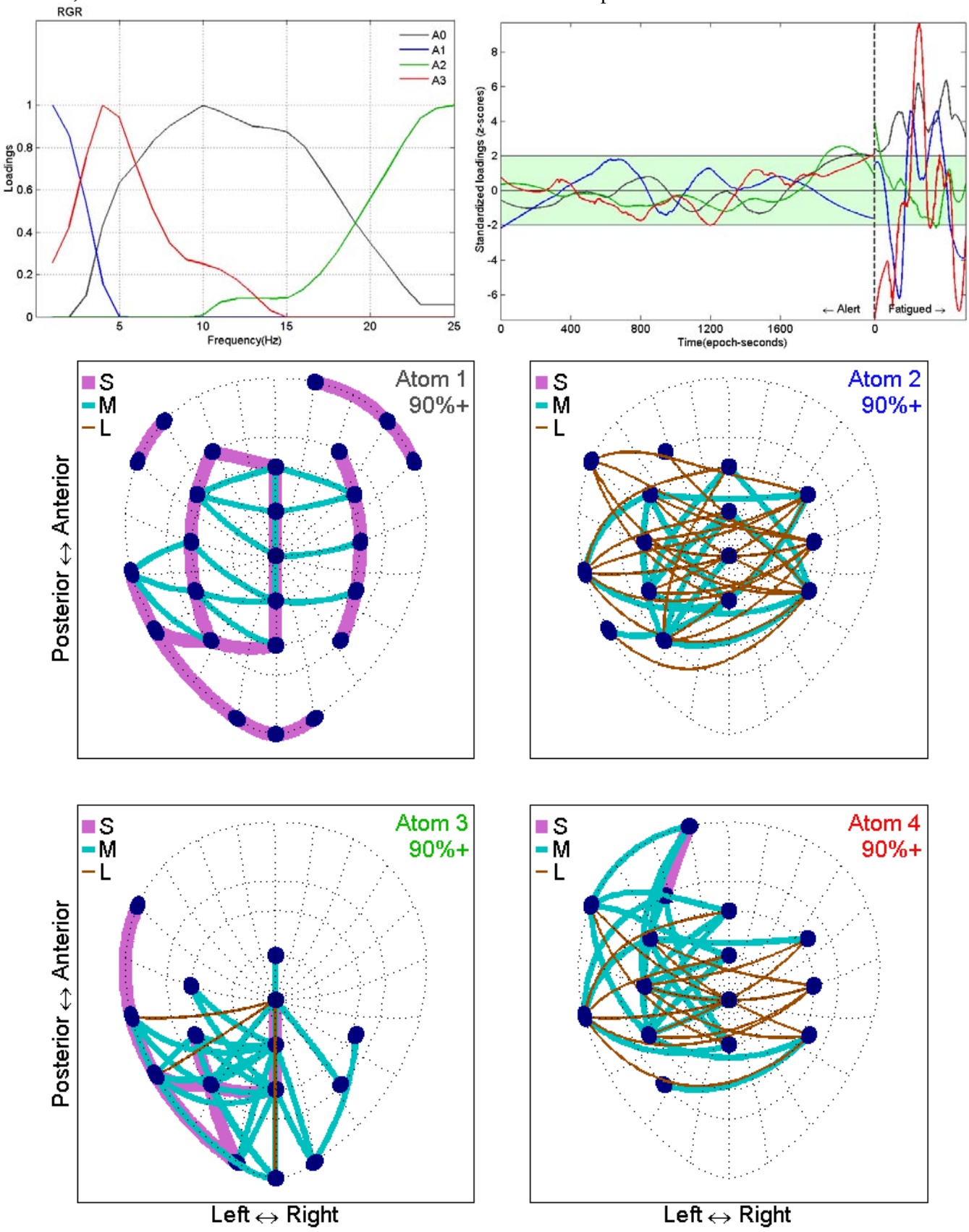

Figure 51. Coherence analyses for participant RGR. Graphing conventions are explained in Figure 44.

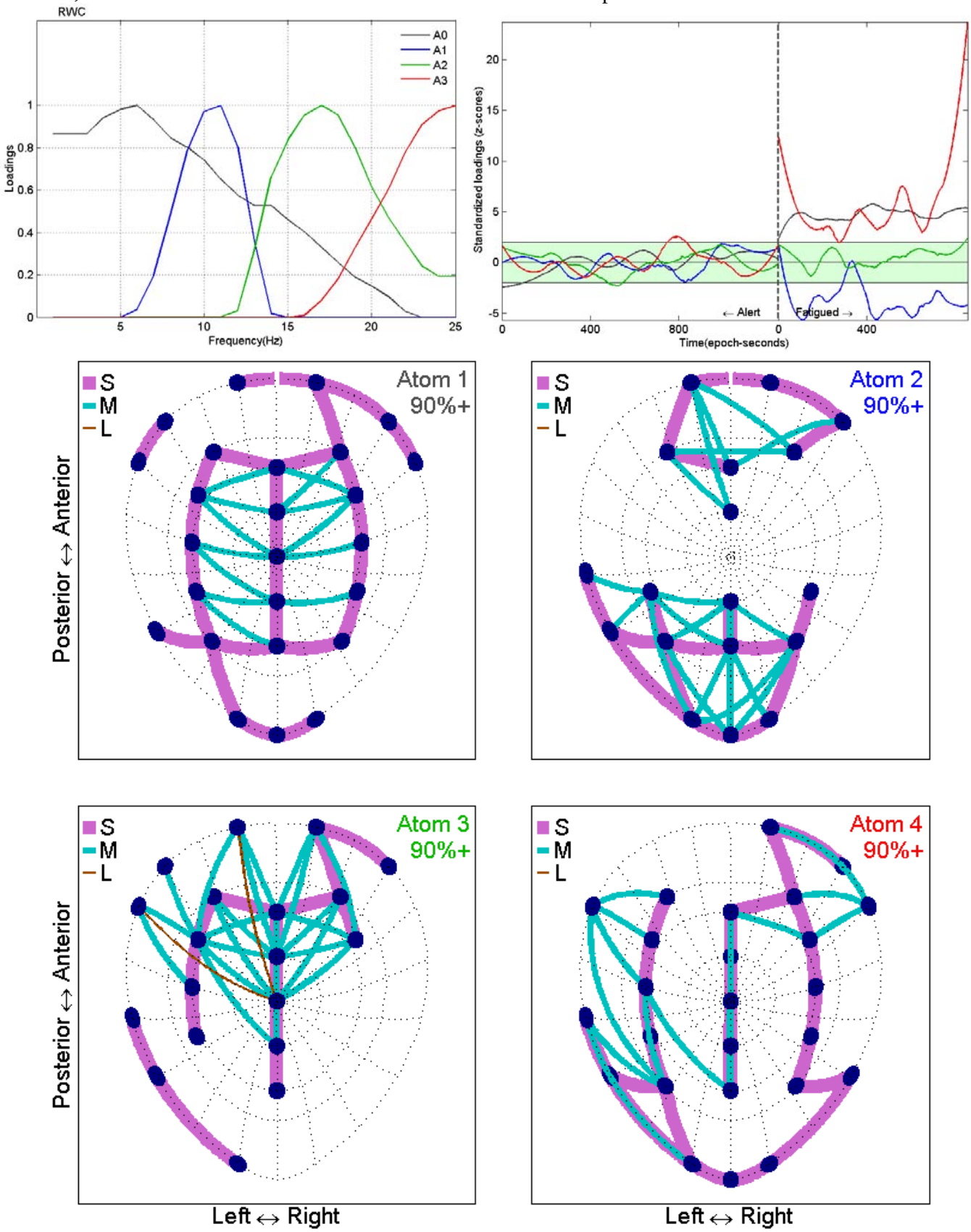

Figure 52. Coherence analyses for participant RWC. Graphing conventions are explained in Figure 44.

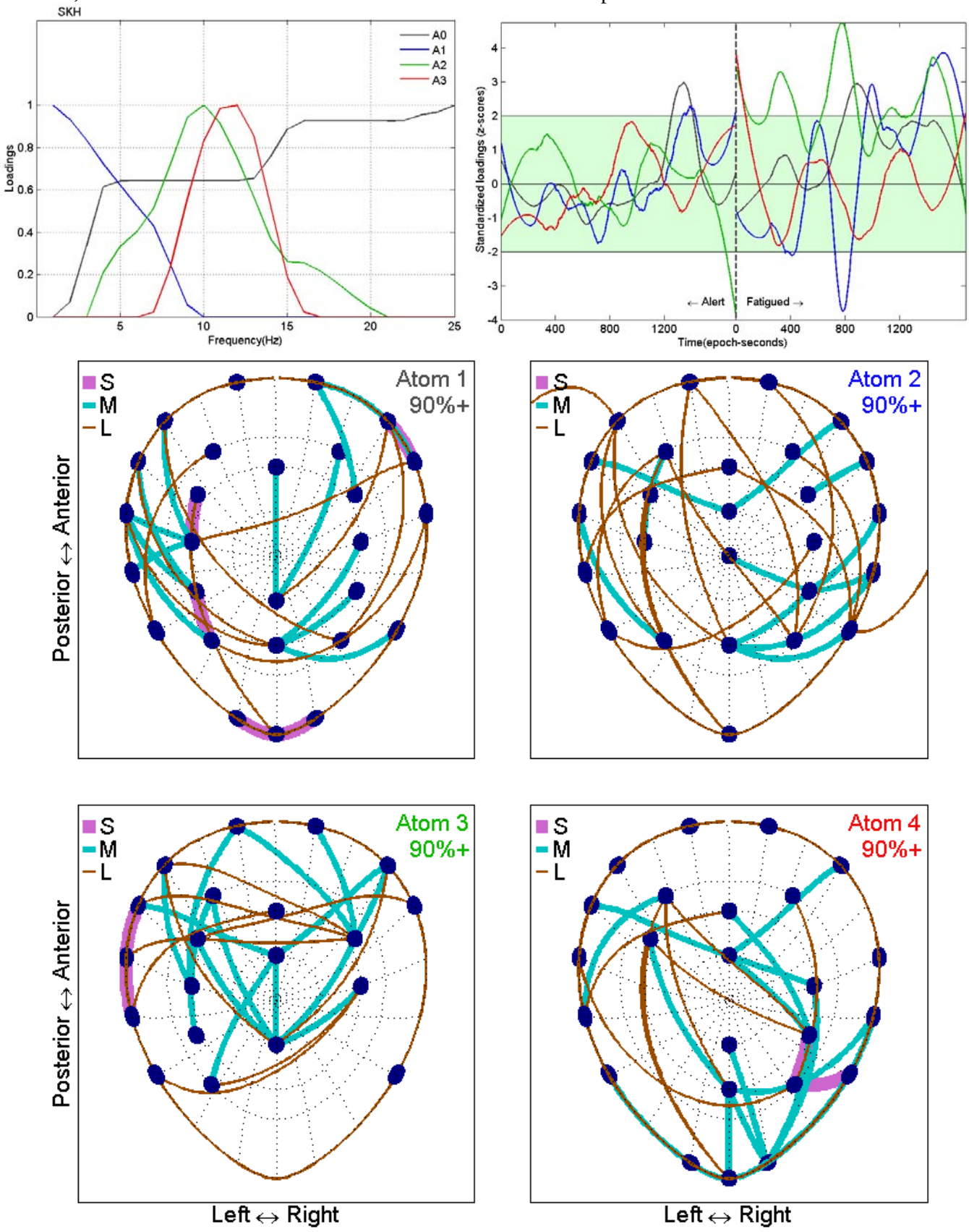

Figure 53. Coherence analyses for participant SKH. Graphing conventions are explained in Figure 44. 44.

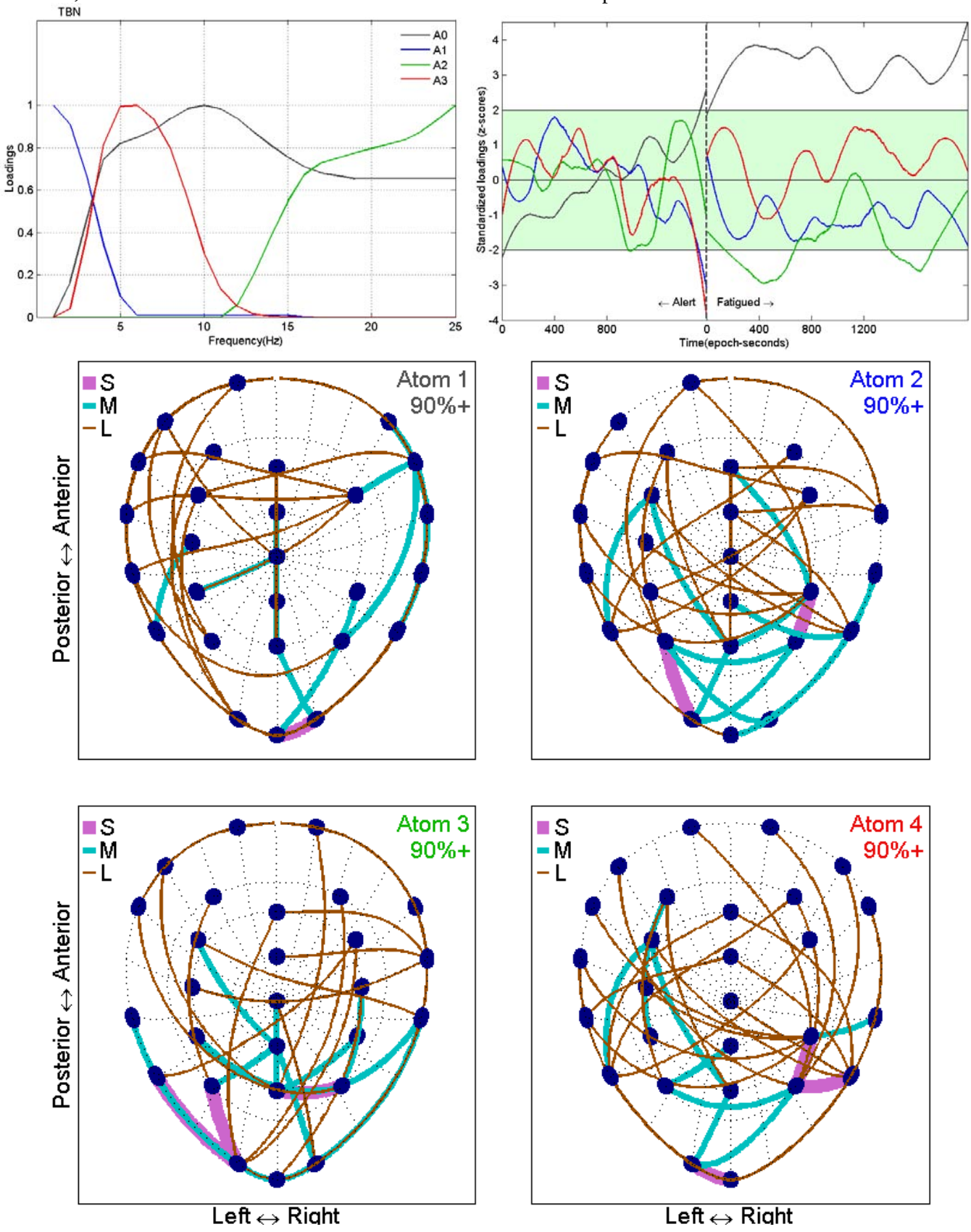

Figure 54. Coherence analyses for participant TBN. Graphing conventions are explained in Figure 44.

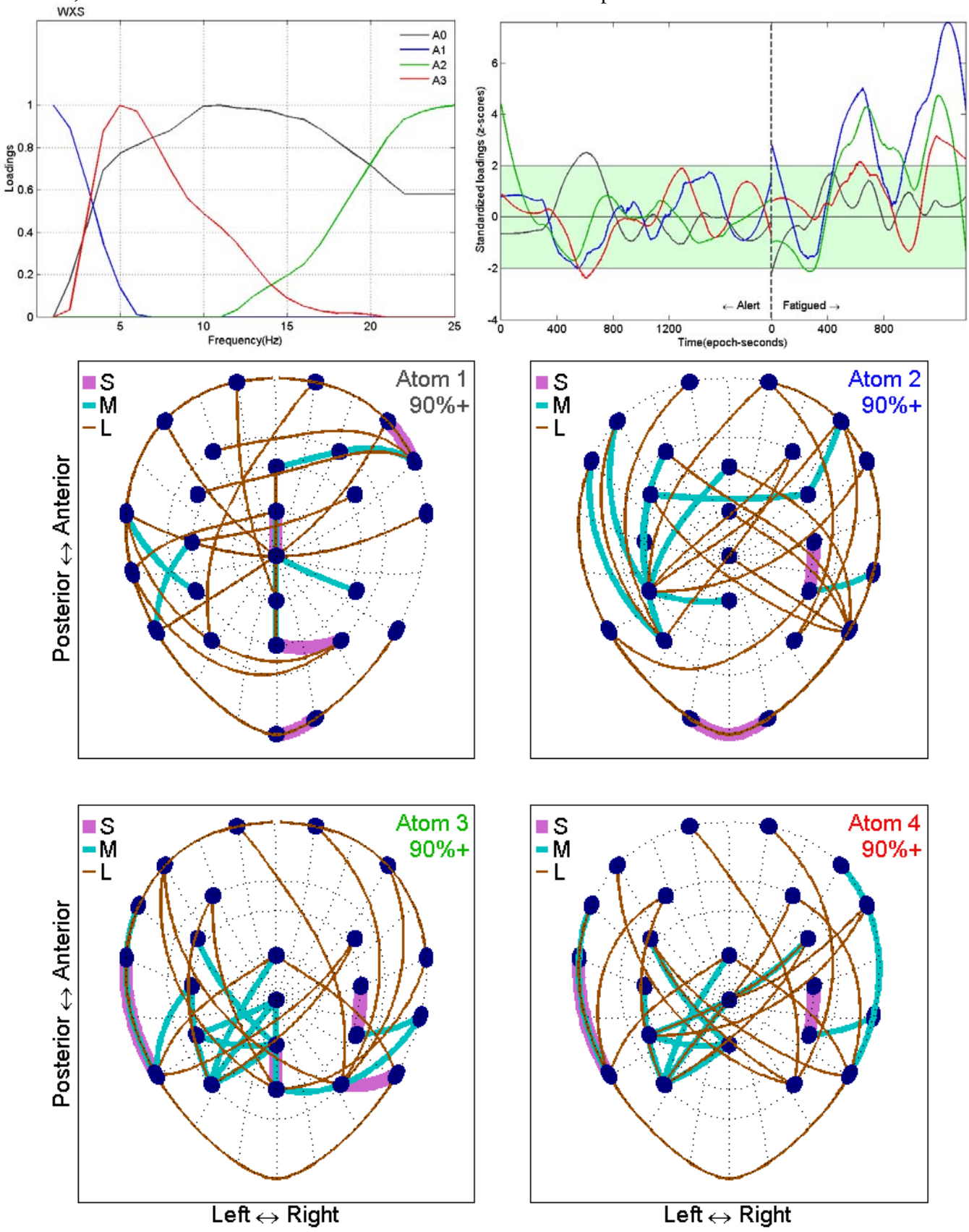

Figure 55. Coherence analyses for participant WXS. Graphing conventions are explained in Figure 44.

12 References

[1] Wearable Physiological Sensor Suite for Early Detection of Cognitive Overload. US Army Phase II STTR Contract No. W911NF-05-C-0112.

[2] *Remote Neurological Measurement and Sensing.* US Army Phase II SBIR Contract No. W91ZLK-04-P-0235.

[3] Dorneich, M., Whitlow, S., Ververs, P. M., Mathan, S., et al. (2004). *DARPA improving warfighter information intake under stress - Augmented Cognition: Concept validation experiment analysis report for the Honeywell Team*. DARPA technical report (contract no. DAAD16-03-C-0054).

[4] Trejo, L.J., Matthews, R., & Allison, B.Z. (2007). Experimental Design and Testing of a Multimodal Cognitive Overload Classifier. In D.D. Schmorrow, D.M. Nicholson, J.M. Drexler, & L.M. Reeves (Eds.), *Foundations of Augmented Cognition,* (4th ed., pp. 13-22). Strategic Analysis, Inc., Arlington

[5] Trejo, L. J., Knuth, K., Prado, R., et al. (2007). EEG-based estimation of mental fatigue: Convergent evidence for a three-state model. In D.D. Schmorrow, L.M. Reeves (Eds.): *Augmented Cognition, HCII 2007*, LNAI 4565, pp. 201–211, 2007. Berlin: Springer-Verlag.

[6] Trejo, L. J., Kochavi, R., Kubitz, K., Montgomery, L. D., Rosipal, R., & Matthews, B. (2006, January). EEG-based estimation of mental fatigue. Available on line at: http://publications.neurodia.com/Trejo-et-al-EEG-Fatigue-2006-Manuscript.pdf.

[7] Berka, C., Levendowski, D. J., Lumicao, et al. (2007). EEG correlates of task engagement and mental workload in vigilance, learning, and memory tasks. *Aviation, Space, and Environmental Medicine*, **78 (5)**, B231-B244.

[8] Trejo, L. J. (2008, January). Ninth Quarterly Report. *Wearable Physiological Sensor Suite for Early Detection of Cognitive Overload.* Army Phase II SBIR Contract No. W911NF-05-C-0112. San Diego: QUASAR, Inc.

[9] Nunez, P. L., Srinivasan, R., Westdorp, A. F., et al. (1997). EEG coherency I: statistics, reference electrode, volume conduction, Laplacians, cortical imaging, and interpretation at multiple scales. *Electroencephalography and clinical Neurophysiology*, **103**, 499–515.

[10] Bro, R (1996). Multiway calibration. Multilinear PLS. *Journal of Chemometrics*, **10**, 47-61.

[11] Morup, M (2005). Analysis of Brain Data - Using Multi-Way Array Models on the EEG. Master's thesis. Informatics and Mathematical Modelling, Technical University of Denmark, Lyngby, Denmark.

[12] Prinzel, L.J., Parasuraman, R.J., Freeman, F.G., et al. (2003). Three experiments examining the use of electroencephalogram, event-related potentials, and heart-rate variability for real-time human-centered adaptive automation design. NASA-TP-2003-212442.

[13] Trejo, L. J., Raj, A., Prinzel, L. J., and Trevino, R. C. (2005-2006). *Embedded real-time advisory system for crew-automation reliability.* Human and Robotic Technology Program, Exploration Systems Mission Directorate, NASA Ames Research Center.

[14] Raj, A., Trejo, L., Higgins, J., Kochavi, R. & Matthews, B. (2006). Embedded Real Time Assistant Task Performance. *Habitation 2006*, Orlando, FL.

[15] St. John, M., Kobus, D. A., Morrison, J. G., & Schmorrow, D. (2004). Overview of the DARPA augmented cognition technical integration experiment. International. *Journal of Human-Computer Interaction*, **17**, 131-149.

[16] Wallerius, J., Trejo, L. J, Matthews, R., Rosipal, R., and Caldwell, J. A. (2005). Robust feature extraction and classification of EEG spectra for real-time classification of cognitive state. 11th International Conference on Human Computer Interaction and 1st International Conference on Augmented Cognition, July 22-27, Las Vegas, NV.

[17] Real-time Non-Invasive Monitoring of C2ISR Cognitive Performance Using Off-Body Sensors**.** **USAF** SBIR Phase II Contract FA8650-06-C-6611.

[18] Integrated Adaptive Aiding System for UAV Control and Related Applications (2008). US Air Force Phase I SBIR Project AF073-013-0674.

[19] Rosipal, R. & Trejo, L. J. (2001). Kernel partial least squares in reproducing kernel Hilbert space. *Journal of Machine Learning Research*, **2**, 97-123.

[20] Trejo, L. J., Matthews, B., and Rosipal, R. (2006). Brain-computer interfaces for 1-D and 2-D cursor control: designs using volitional control of the EEG spectrum or steady-state visual evoked potentials. *IEEE Trans. Neural Syst. Rehabil. Eng*., **14**, 225-229.

[21] Rosipal, R., Trejo, L. J., and Matthews, B. (2003, August). Kernel PLS-SVC for Linear and Nonlinear Classification. In *Proceedings of the Twentieth International Conference on Machine Learning* (ICML-2003), 640-647. Washington, DC.

[22] Nunez, P.L., Silberstein, R.B., Carpentar, M.R., Srinivasan, R., Wijesinghe, R.S., Tucker, D.M., Cadusch, P.J. and Wu, X. (1999). EEG coherency. II: Comparisons of multiple measures of EEG coherency differences between resting and cognitive states, *Clinical Neurophysiology*, **110**, 469-486.

[23] Gevins, A., Smith, M.E., McEvoy, L., & Yu, D. (1997). High-resolution EEG mapping of cortical activation related to working memory: Effects of task difficulty, type of processing, and practice. *Cerebral Cortex*, **7**, 374-385.

[24] Klimesch, W. (1999) EEG alpha and theta oscillations reflect cognitive and memory performance: a review and analysis. *Br. Res. Rev.* **29**, 169–195.

[25] Miwakeichi, F., Martinez-Montes, E., Valdes-Sosa, P. A., Nishiyama, N., Mizuhara, H., Yamaguchi, Y., (2004). Decomposing EEG data into space-time-frequency components using Parallel Factor Analysis. *Neuroimage*, **22**, 1035-45.

[26] Mørup, M., Hansen, L. K. Hermann, C. S., Parnas, J. & Arnfred S. M. (2006). Parallel Factor Analysis as an exploratory tool for wavelet transformed event-related EEG, *Neuroimage*, **29**, 938-947.

[27] Martínez-Montes, E., Valdés-Sosa, P.A., Miwakeichi, F., Goldman, R. I., & Cohen, M. S. (2004). Concurrent EEG/fMRI analysis by multiway Partial Least Squares. *Neuroimage*, **22**, 1023-1034.

[28] Trejo, L. J., Kramer, A. F., & Arnold, J. (1995). Event-related potentials as indices of display-monitoring performance. *Biol. Psychology*, **40**, 33-71.

[29] Gevins, A., Smith, M.E., Leong, H., McEvoy, L., Whitfield, S., Du, R., et al. (1998). Monitoring working memory load during computer-based tasks with EEG pattern recognition methods. *Human Factors*, **40**, 79-91.

[30] Rosipal, R., Trejo, L.J. & Nunez, P.L. (2009). Application of Multi-way EEG Decomposition for Cognitive Workload Monitoring. In Vinzi V.E, Tenenhaus M., Guan R. (eds.), *Proceedings of the 6th International Conference on Partial Least Squares and Related Methods*, Beijing, China, pp. 145-149.

[31] Sharbrough F., Chatrian G.-E., Lesser R.P., Lüders, H., Nuwer M., Picton T.W. (1991). American Electroencephalographic Society Guidelines for Standard Electrode Position Nomenclature. *J. Clin. Neurophysiol.* **8,** 200-202.

[32] Thomson, D. J. (1982). Spectrum estimation and harmonic analysis. *Proceedings of the IEEE*, **70**, 1055–1096.

[33] The original prime contractor granted PDT a non-exclusive license to use the data until October 2010, with the provision that any publication of the results by PDT would be subject to their review.

[34] Thayer, R. E. (1986). Activation-Deactivation Adjective Check List: Current overview and structural analysis. *Psychological Reports, 58*, 607-614.

[35] Stern, R.A. (1997). Visual Analogue Mood Scales. Odessa, FL: Psychological Assessment Resources.

[36] Compumedics USA, El Paso, TX.

[37] Snyder, John P. & Voxland, Phillip M. (1994). *An Album of Map Projections*. U.S.G.S. Professional Paper 1453. Denver: U.S. Government Printing Office, 1989. Reprinted 1994 with corrections.